Leukocyte attraction and transmigration in type 1 diabetes: Neutralization of CXCR3 and JAM-C reduces the severity of disease

Dissertation

zur Erlangung des Doktorgrades

der Naturwissenschaften

Vorgelegt beim Fachbereich

Chemische und Pharmazeutische Wissenschaften

der Johann Wolfgang Goethe-Universität

in Frankfurt am Main

von

Selina Christen

aus Chur

Frankfurt am Main, 2010

D30

vom Fachbereich

Chemische und Pharmazeutische Wissenschaften der

Johann Wolfgang Goethe-Universität als Dissertation angenommen.

Dekan: Prof. Dr. D. Steinhilber

1. Gutachter: Prof. Dr. Th. Dingermann

2. Gutachter: PD Dr. U. Christen

Datum der Disputation:

TO MY FAMILY

1 Table of Contents

2 Summary

Type 1 diabetes (T1D) is a chronic T cell-mediated autoimmune disorder that results in the destruction of insulin-producing pancreatic ß cells leading to life-long dependence on exogenous insulin. Attraction, activation and transmigration of inflammatory cells to the site of ß-cell injury depend on two major molecular interactions. First, interactions between chemokines and their receptors expressed on leukocytes result in the recruitment of circulating inflammatory cells to the site of injury. In this context, it has been demonstrated in various studies that the interaction of the chemokine CXCL10 with its receptor CXCR3 expressed on circulating cells plays a key role in the development of T1D. Second, once arrived at the site of inflammation adhesion molecules promote the extravasation of arrested cells through the endothelial cell layer to penetrate the site of injury. Here, the junctional adhesion molecule (JAM) JAM–C expressed on endothelial cells is involved in the process of leukocyte diabedesis. It was recently demonstrated that blocking of JAM-C efficiently attenuated cerulein-induced pancreatitis in mice.

In my thesis I studied the influence of the CXCL10/CXCR3 interaction on the one hand, and of the adhesion molecule JAM-C on the other hand, on trafficking and transmigration of antigen-specific, autoaggressive T cells in the RIP-LCMV mouse model. RIP-LCMV mice express the glycoprotein (GP) or the nucleoprotein (NP) of the lymphocytic choriomeningitis virus (LCMV) as a target autoantigen specifically in the ß cells of the islets of Langerhans and turn diabetic after LCMV-infection.

In my first project I found that pharmacologic blockade of CXCR3 during development of virus-induced T1D results in a significant delay

but not in an abrogation of overt disease. However, neither the frequency nor the migratory properties of islet-specific T cells was significantly changed during CXCR3 blockade.

In the second project I was able to demonstrate that JAM-C was upregulated around the islets in RIP-LCMV mice after LCMV infection and its expression correlated with islet infiltration and functional ß-cell impairment. Blockade with a neutralizing anti-JAM-C antibody slightly reduced T1D incidence, whereas overexpression of JAM-C on endothelial cells did not accelerate virus-induced diabetes.

In summary, our data suggest that both CXCR3 as well as JAM-C are involved in trafficking and transmigration of antigen-specific autoaggressive T cells to the islets of Langerhans. However, the detection of only a moderate influence on the onset of clinical disease during CXCR3 or JAM-C blockade reflects the complex pathogenesis of T1D and indicates that several different inflammatory factors need to be neutralized in order to achieve a stable and persistent protection from disease.

3 Zusammenfassung

Type 1 Diabetes (T1D) ist eine chronische T Zell-vermittelte Autoimmunerkrankung, welcher die Zerstörung der ß Zellen der Langerhans'schen Inseln im Pankreas zugrunde liegt. Da die ß Zellen für die Insulinproduktion verantwortlich sind, führt dies zu einem absoluten Insulin-Mangel. Es wird angenommen, dass die Kombination von genetischer Veranlagung und Umweltfaktoren, wie Infektionen durch Pathogene oder Xenobiotika, die Entstehung von Autoimmunerkrankungen herbeiführen kann. Eine Entzündung in den ß Zellen, wird durch eine Rekrutierung von aktivierten Leukozyten, wie T Zellen, B Zellen und dentritische Zellen, ausgelöst. Für die Rekrutierung, Aktivierung und Transmigration von Leukozyten sind Interaktionen zwischen Oberflächenrezeptoren von zirkulierenden Leukozyten und endothelialen Entzündungsfaktoren oder Adhäsionsmolekülen verantwortlich. Obschon viel über die Immunpathogenese von T1D bekannt ist, gibt es immer noch Unklarheiten mit welchen Mechanismen und Interaktionen die antigen-spezifischen T Zellen zu den ß Zellen gelangen und wie sie durch die Endothelzellschicht der Inselzellen wandern.

In meinem Projekt habe ich mich mit Hilfe des RIP-LCMV Maus-Modell für T1D mit dem Thema der gerichteten Zellwanderung und Extravasation detaillierter auseinandergesetzt. Unter der Kontrolle des Ratten-Insulinpromotors (RIP) exprimieren transgene RIP-LCMV-Mäuse das Glycoprotein (GP) oder das Nucleoprotein (NP) des lymphozytären Choriomeningitis Virus (LCMV) spezifisch in den ß Zellen. In den RIP-LCMV Mäusen werden die Antigene (GP/NP) als körpereigen erkannt. Da die antigen-spezifischen Vorläufer T Zellen die GP oder NP Moleküle ‚tolerieren' oder ‚ignorieren' werden die ß Zellen nicht zerstört und die

transgenen Mäuse entwickeln keinen T1D. Eine Infektion von RIP-LCMV Mäusen mit LCMV hingegen verursacht eine Entzündung im Pankreas, die zu einer Anlockung und Aktivierung von Leukozyten und antigen-spezifischen Vorläufer T Zellen führt. Die aktivierten LCMV-spezifischen T Zellen eliminieren nicht nur das Virus sondern beginnen auch die auf den ß Zellen exprimierten (viralen) Zielantigene anzugreifen. Dieser autoimmune Vorgang verursacht die Zerstörung der ß Zellen und endet in T1D in nahezu 100% der infizierten RIP-LCMV-Mäuse.

3.1 Blockierung von CXCR3 während T1D

Die virusinduzierte Entzündung wird begleitet durch den Ausstoß von Chemokinen, die mit Rezeptoren, welche von Leukozyten exprimiert werden, interagieren und die eine gerichtete Zellwanderung zu der beschädigten (virusinfizierten) Stelle vermitteln. In diesem Zusammenhang konnte gezeigt werden, dass das Chemokin CXCL10 eine wesentliche Rolle in der Anlockung von autoaggressiven T Zellen zu den Langerhans'schen Inseln spielt. In unserem RIP-LCMV Maus-Modell beeinflusst die Neutralisation oder die Überexprimierung von CXCL10 die Entwicklung von virusinduziertem T1D signifikant. Der Rezeptor CXCR3, welcher mit CXCL10 interagiert, wird vorwiegend durch die aktivierten T_H1-typ T Zellen exprimiert. Es konnte gezeigt werden, dass in CXCR3-defizienten RIP-LCMV Mäusen die Entwicklung des T1D signifikant verzögert ist. Ferner wurden in einem Patienten mit T1D preproinsulin-spezifische CD8^{+} T Zell Klone gefunden, die CXCR3 auf ihrer Oberfläche exprimierten. Diese CD8^{+} T Zellen konnten tatsächlich menschliche ß Zellen zerstören.

Da in mehreren Studien nachgewiesen wurde, dass die Interaktion von CXCL10 mit CXCR3 eine wichtige Rolle in Autoimmunerkrankungen spielt, haben wir den CXCR3 Rezeptor mit einem Antagonist,

NIBR2130, blockiert und dessen Einfluss auf die Entstehung von virusinduziertem T1D im RIP-LCMV Maus-Modell untersucht.

Die pharmakologische Blockade von CXCR3 während der Entwicklung des T1D führte zu einem milden aber dennoch signifikant verlangsamten Auftreten der Erkrankung. Die Blockade von CXCR3 war allerdings nur vorübergehend wirksam. Die behandelten Mäuse entwickelten einen T1D sobald die Antagonisttherapie abgesetzt wurde. Die Blockierung von CXCR3 hatte keine offensichtliche Auswirkung auf die Pathogenese des T1D. Weder die Funktion der ß Zellen noch die Frequenz und das Migrationsverhalten der Insel-spezifischen aggressiven und regulatorsichen T Zellen wurden durch die Therapie signifikant beeinträchtigt. Unsere Resultate zeigen, dass eine Blockade eines wichtigen Chemokinrezeptors nur zu einem moderaten therapeutischen Effekt führt. In Anbetracht der gegebenen Komplexität der T1D Pathogenese einerseits und des Chemokin/Zytokin-Netzwerks andererseits, müssten wohl mehrere zentrale Entzündungsfaktoren blockiert werden, um eine verbesserte therapeutische Wirkung zu erreichen.

3.2 Der Einfluss von JAM-C auf T1D

Im ersten Teil meiner Arbeit habe ich mich mit der gerichteten Zellwanderung von Leukozyten auseinandergesetzt. Im zweiten Teil der Arbeit habe ich einen weiteren Schritt in der Immunpathogenese des T1D, nämlich die Transmigration der zirkulierenden Zellen durch die Endothelzellschicht, analysiert. Viele verschiedene Adhäsionsmoleküle (Selektine, Integrine und Immunglobulinsuperfamillien Proteine) werden durch Endothelzellen exprimiert und sind in das Rollen, die Aktivierung, die Adhäsion, und dem parazellulären oder transzellulären Durchwandern von Leukozyten involviert. Das junktionale

Adhäsionsmolekül C (JAM-C) ist an der parazellulären Transmigration von Leukozyten beteiligt. Es konnte gezeigt werden, dass JAM-C in verschiedenen inflammatorischen Krankheiten, wie Peritonitis, Arthritis oder Pankreatitis in Mäusen eine wichtige Rolle spielt. In einem Maus-Modell für akute Pankreatitis ausgelöst durch die Injektion von Cerulein, konnte eine erhöhte JAM-C Expression im Pankreas beobachtet werden. Ferner wurde mit Hilfe eines neutralisierenden Antikörpers JAM-C blockiert und dabei konnte die Pankreatitis reduziert werden. Die Immunpathogenese im Cerulein-Modell entspricht nicht exakt der des T1D im Menschen. Dennoch wurde in diesem Maus-Modell nachgewiesen, dass die Blockade von JAM-C im Pankreas zu einer reduzierten Zellwanderung und Extravasation von Leukozyten führte. Dies hatte eine Verminderung der lokalen Entzündung der Inselzellen zur Folge.

Aufgrund dieser Erkenntnisse haben wir die Rolle von JAM-C im virusinduzierten T1D im RIP-LCMV Maus-Modell untersucht. Wir haben einerseits JAM-C mit einer Antikörperbehandlung blockiert und andererseits JAM-C auf den Endothelzellen überexprimiert. Nachdem RIP-LCMV Mäuse mit LCMV infiziert wurden, konnten wir eine erhöhte Expression von JAM-C beobachten. Diese Zunahme korrelierte gut mit dem Ausmaß der Leukozyteninfiltration und der ß Zell-Zerstörung. Die Neutralisation von JAM-C resultierte in einem leicht reduzierten und teilweise revertierten T1D. Dennoch konnte nur eine moderate Auswirkung auf die Frequenz und das Migrationsverhalten der Insel-spezifischen T Zellen festgestellt werden. Die Überexprimierung von JAM-C hatte hingegen keinen Einfluss auf die Entwicklung der Krankheit.

Unsere Beobachtungen zeigen, dass JAM-C in der Pathogenese des T1D eine eher untergeordnete Rolle zukommt. Die Funktion von JAM-C

wird bei einer Blockade möglicherweise von anderen Adhäsionsmolekülen kompensiert. Somit ist die Infiltration der Langerghans'schen Inseln durch aggressive T Zellen auch bei JAM-C Neutralisierung weiterhin gewährleistet.

4 List of abbreviations

APECED	Autoimmune polyendocrinopathy-candidiasis-ectodermal dystrophy
APC	Antigen presenting cells
B cells	B lymphocytes
CAMs	Cell adhesion molecules
CTLA-4	T lymphocyte-associated antigen 4
CTLs	Cytotoxic T lymphocytes
DC	Dendritic cell
DM	Diabetes mellitus
EAE	Experimental autoimmune encephalomyelitis
Foxp3$^+$	Transcription factor forkhead box P3$^+$
GAD65	Glutamic acid decarpoxylase
GFP	Green fluorescent protein
GP	Glycoprotein
IA-2	Insulinoma antigen-2
ICAMs	Intercellular adhesion molecules
ICCS	Intracellular cytokine stain
IFN-γ	Interferon γ
Ig	Immunoglobulin
IL-	Interleukin-
IP-10	IFN-γ-inducible protein 10
I-TAC	Interferon-inducible T cell alpha chemoattractant
JAMs	Junctional adhesion molecules
LCMV	Lymphocytic choriomeningitis virus
LFA-1	Leukocyte function-associated antigen1
LT-α	Lymphotoxin-α
LSD	Lysergic acid diethylamine
Mac-1	Macrophage-1 antigen
MHC	Major histocompatibility complex
MIG	Monokine induced by IFN-γ
MIP	Mouse insulin promoter
NCAM	Neural-cell adhesion molecule
NOD	Nonobese diabetic mouse
NP	Nucleoprotein
PDLN	Pancreatic draining lymph nodes
PECAM-1	Platelet-endothelial-cell adhesion molecule
pfu	Plaque forming units
Poly(I:C)	Polyinosinic-polycytidylic acid

PP	Pancreatic polypeptide
PSGL1	P-selectin glycoprotein ligand 1
PTPN22	Protein tyrosine phosphatase, non-receptor type 22
RIP	Rat insulin promoter
T cells	T lymphocytes
T1D	Type 1 diabetes mellitus
TCR	T cell antigen receptor
TGF-ß	Tumor growth factor ß
T_H cells	CD4$^+$ T helper cells
TLR	Toll-like receptor
TNF-α	Tumor necrosis factor α
T_{reg}	Regulatory T cells
VCAM-1	Vascular-cell adhesion molecule 1
VLA-4	Very late antigen 4
VNTR	Variable number tandem repeat

5 List of figures

INTRODUCTION

6 Introduction

6.1 Overview of the immune system

In the battle against pathogenic invaders such as viruses, bacteria, fungi, protozoa and parasites many defensive mechanisms have evolved, which finally resulted in the complex immune system of vertebrates.

The immune system can be divided into two distinct parts: the *innate immune system*, which reacts to pathogens in a non-antigen-specific manner, and the *adaptive immune system*, which is able to exert an antigen-specific response against pathogens. These two systems work together to generate an effective immune response.

6.1.1 Innate immune system

The innate immune system is composed of a number of barriers representing the first line of defense against infections. Innate immune responses include anatomic, physiologic, endocytic or phagocytic and inflammatory barriers. As anatomic barriers, the skin and the mucous membranes act as a first line of defense by preventing entry of most pathogens into the body. Physiological barriers include body temperature, low pH, and chemical mediators such as lysozymes, interferons and the complement. The white blood cells, such as blood monocytes, neutrophils, natural killer cells and tissue macrophages provide the phagocytotic and endocytotic barriers, by engulfing and digesting microorganisms. Moreover in response to microbes, they secrete inflammatory factors, such as chemokines and cytokines that mediate many cellular reactions of the innate immunity and can activate the adaptive immune system (1).

6.1.2 Adaptive immune system

The adaptive immune system is characterized by its antigen specificity. It can be divided into humoral and cell-mediated responses. B lymphocytes, T lymphocytes and antigen presenting cells (APC) are the primary cells involved.

The adaptive immune system is able to recognize and selectively respond to foreign antigens. Several characteristics of the adaptive immune system enable it to respond to a large variety of pathogens and toxins without attacking the organism's own cells. One of those characteristics is the generation of recognition molecules that can be enormously diverse. Another one is the antigen-specificity that enables the immune system to distinguish subtle differences among antigens. Third, the development of immunological memory enables the immune system to respond more rapidly and more effectively to a second encounter with an antigen. The last characteristic is the self and non-self recognition that enables the immune system to distinguish between foreign and self and to respond only to non-self antigens during the process of antigen presentation. An aberrant immune response to self-antigens can be severe and can lead to the development of autoimmune diseases (1).

6.1.3 T Lymphocytes

T cells originate from pluripotent hematopoietic stem cells in the bone marrow that migrate to the thymus, where they mature to different subsets of T cells. T cells recognize antigens with their T cell receptor (TCR) only when the antigen is associated with major histocompatibility complexes (MHCs) expressed by antigen presenting cells. During the maturation of T cells within the thymus the cells undergo distinct phases that are marked by the status of T cell

receptor gene rearrangement and the expression of T cell receptors. About five percent of the T cells rearrange the γ and the δ chain and develop into γ:δ CD3+ T cells. The majority of thymocytes rise to α:ß T cells that have to pass positive and negative selection. Only approximately two percent of all these thymocytes survive the selection processes and mature to immunocompetent T cells. During positive selection T cells that interact via their TCRs with self-MHC molecules are rescued from programmed cell death. In contrast, in negative selection the T cells that bind self-antigen associated with self-MHC molecules in a high-avidity manner are eliminated to maintain self-tolerance. Once T cells have passed the two-step selection process so called central tolerance they become mature T cells expressing either CD4 or CD8 co-receptors and can enter the periphery.

Naïve CD8+ T cells interact with peptides presented via MHC class I molecules that are expressed on virtually all nucleated cells (2). Upon activation naïve CD8+ T cells differentiate into CD8+ cytotoxic T cells that can specifically lyse target cells by realising cytotoxic granules. In addition, they are able to produce interferon-γ (IFN-γ), tumor necrosis factor-α (TNF-α) and lymphotoxin-α (LT-α). IFN-γ inhibits viral replication, increases expression of MHC class I molecules and enhances the activity of macrophages (1).

Naïve CD4+ T cells interact with peptides presented via MHC class II molecules that are expressed on B cells, dendritic cells, macrophages, and activated T cells (2). CD4+ T cells secrete large quantities of cytokines in response to antigen-specific activation. On the basis of their cytokine production and their function they can be subdivided into different subsets, such as T-helper type 1 (T_H1), T_H2, T_H17 or T regulatory (T_{reg}) cells.

T$_H$1 cells develop in response to Interleukin 12 (IL-12) and IFN-γ and produce IL-2 and IFN-γ, which enhances cellular immunity, activates macrophages and enables them to destroy intracellular microorganisms. They also can stimulate B cells producing antibodies and are important for autoimmunity and anti-tumor response. T$_H$2 cells mature in response to IL-4 and produce IL-4, IL-5, IL-10 and IL-13, which enhance humoral immunity by activating naïve B cells and inducing immunoglobulin class switching, and are important for extracellular defence. The recently discovered T$_H$17 cells differentiate from naïve CD4$^+$ T cells that have been activated in the presence of transforming growth factor-ß (TGF-ß) and IL-6, and after differentiation they secrete IL-6, IL-17, IL-22, and TNF-α. It also could be shown that the secretion of IL-23 by APCs maintains T$_H$17 cells survival. T$_H$17 cells has been implicated in different autoimmune diseases, but could also be linked to providing protection in certain infections (2, 3). T$_{reg}$ cells are Foxp3$^+$ (transcription factor forkhead box P3$^+$) and are thought to participate in maintenance of peripheral tolerance and prevention of autoimmunity by suppressing other T cell responses. Two major groups of T$_{reg}$ cells are identified so far. The first group are naturally occurring CD4$^+$CD25$^+$ T$_{reg}$ cells that develop in the thymus and are able to produce TGF-ß and the second group differentiates in the periphery from naïve CD4$^+$ T cells after TGF-ß, retinoic acid and IL-2 induction (4).

6.2 Autoimmunity

Autoimmunity develops when central and/or peripheral tolerance are overcome, tolerance to self-antigens is broken and autoreactive cells or antibodies are present. In autoimmune diseases those antibody and T cell responses become activated and cause clinical relevant damage.

The development of autoimmune diseases, such as rheumatoid arthritis, multiple sclerosis, Grave's disease, autoimmune hepatitis and T1D, are triggered by a combination of genetic predisposition and environmental factors (1).

6.2.1 Genetic susceptibility factors

It is known that some individuals are genetically predisposed to autoimmunity and that there are several genetic susceptibility factors that influence the development of autoimmune diseases.

The most important genetic susceptibility factor is the MHC haplotype that is involved in the processes of the central tolerance within the thymus where MHC alleles are involved in shaping the T cell repertoire (MHC restriction). In addition, MHC haplotypes are also important in peripheral tolerance where the ability of T cells to respond to a particular antigen depends on the MHC genotype (5). Another susceptibility factor is the autoimmune regulator (AIRE) that encodes a transcription factor that enables tissue-restricted self-antigens to be expressed by thymic epithelial cells. A defect in the gene AIRE leads to a breakdown of negative selection and to a severe autoimmune disease called autoimmune polyendocrinopathy candiasis ectodermal dystrophy (APECED) (1, 6). It could also be shown that cytolytic T lymphocyte-associated antigen 4 (CTLA-4) and Protein tyrosine phosphatase, non-receptor type 22 (PTPN22) are genetic susceptibility factors involved in autoimmunity. CTLA-4 is a key negative regulator for T cell activation that limits the proliferative response of activated T cells to antigen whereas PTPN22 is involved in the negative control of T-cell activation and in T-cell development (7).

6.2.2 Environmental factors

The discordance found in homozygotic twins and the observed overall north-south geographical gradient of autoimmune diseases in the northern hemisphere suggest that environmental factors play a role in autoimmunity as well. Moreover the detection of higher prevalence of autoimmunity in more industrialized countries compared to countries with lower living standards ("hygiene hypothesis") emphases the idea of an involvement of environmental factors. In addition to drugs and toxins perhaps the most important environmental factors in association with autoimmune diseases are microbial and viral infections. It is still a matter of debate if single pathogen infections directly initiate autoimmune disease or rather modulate autoimmunity in an antigen-specific and/or antigen-nonspecific (bystander inflammation) manner. In concordance with the hygiene hypothesis it has been demonstrated that infections by some pathogens can protect from autoimmunity (8).

There are a lot of animal models available in which the influence of microbial and viral infections on autoimmunity can be tested, but there are difficulties to determine a direct epidemiological association between infections and various autoimmune disorders in human. One of the reasons might be that viral infections can be cleared years before the time of diagnosis (hit-and-run events). Further, infections might be latent and nearly undetectable. In addition, viral infections can also ameliorate disease for example by stimulation of T_{regs} or hyperactivation of aggressive T cells (9).

6.2.3 Virus-induced autoimmunity

In spite of central and peripheral tolerance mechanisms some autoreactive B and T cells escape the tolerance mechanisms and are

present in all individuals. Even though autoantigens of these autoreactive lymphocytes are present they are not able to initiate autoimmune disease by their-selves. Often the required additional activation is provided by viral infections. Two possible mechanisms are proposed for such virus-induced activation of autoreactive lymphocytes and subsequent autoimmunity. First, a virus-induced inflammation might induce leukocyte activity and attraction to the side of injury in an antigen-independent nonspecific manner. Second, the production of cytokines and chemokines of bystander cells can lead to activation of autoreactive T cells. This bystander activation can further expand such low-affinity autoreactive cells that have escaped negative selection or can awake anergic autoaggressive T cells (9, 10).

In the other pathway virus can break self-tolerance by sharing similar epitopes with the host that leads to a cross-reactive immune response. This mechanism is called molecular mimicry (11). Two of the best examples of molecular mimicry in autoimmune diseases are rheumatic fever and Guillain-Barré syndrome. In rheumatic fever individuals can develop an autoimmune disease due to infection with *Streptococcus pyogenes*, where its dominant epitope shares structural similarity to the lysoganglioside of the host. This cross-reactivity can lead to antibody-mediated autoimmunity (12). In Guillain-Barré syndrome the infection with *Campylobacter jejuni* that shares a structural homology of the lipo-oligo-saccharide with peripheral nerve GM1 ganglioside can cause autoimmune disorders affecting the peripheral nervous system (13). In both cases convincing mouse models that support the role of molecular mimicry have been established. In the RIP-LCMV model for T1D, (see chapter: The RIP-LCMV Model for T1D) molecular identity seems to be required to induce autoimmune disease. Briefly, infection of transgenic RIP-LCMV mice, which express LCMV-proteins in the

pancreas, with LCMV itself (molecular identity) results in autoimmunity and the development of type 1 diabetes. In contrast, infection of RIP-LCMV mice with Pichinde virus that shares an epitope that is cross-reactive with a LCMV protein epitope (molecular mimicry) is not sufficient to establish autoimmune disease (14). Overall, the evidence that molecular mimicry alone can induce autoimmune diseases remains controversial and it may need several sequential or coinciding environmental challenges to induce autoimmunity.

In summary, any genetic susceptible individual might be repeatedly exposed to infections without developing autoimmunity. But induction of disease might be possible if bystander activation, molecular mimicry as well as virus persistence coincide and the threshold for autoimmune diseases is exceeded ("fertile field" hypothesis) (9, 15). A dynamic and complex interaction between genetic and environmental factors is likely to be involved in the initiation and abrogation of autoimmune disease.

6.3 Diabetes overview

Diabetes mellitus (DM) is a group of disorders of multiple etiologies characterized by chronic hyperglycemia with disturbances of carbohydrate, fat and protein metabolism resulting from defects in insulin secretion, insulin action, or both.

Based upon etiology, diabetes can be divided into four main groups. In T1D the absolute insulin deficiency occurs due to an autoimmune-associated destruction specifically of the insulin-producing ß cells in the islets of Langerhans, whereas in type 2 diabetes the relative insulin deficiency happens due to decreased effect of insulin in the target tissues or due to secretory defects of insulin with or without insulin resistance. In the gestational diabetes the glucose intolerance results

in hyperglycemia of variable severity with onset or first recognition during pregnancy. Finally the forth group includes other specific types of diabetes such as specific genetic defects of ß cell function, diseases of the exocrine pancreas, endocrinopathies and infections (16).

6.3.1 Anatomy and function of the pancreas

The pancreas is a gland organ in the digestive and endocrine system of vertebrates with lobular architecture and it can be divided into three parts, the head, the body and the tail.

The pancreas is located across the back of the abdomen, behind the stomach. The head of the pancreas is attached to the small intestine whereas the tail of the organ extends slightly upward and ends near the spleen.

The exocrine tissue within the pancreas is considered to be a compound gland that produces digestive enzymes and an alkaline fluid (called pancreatic juice), and secretes them through a system of exocrine ducts into the small intestine. The islet cells of Langerhans that are crisscrossed by a dense network of capillaries compose the endocrine part of the pancreas and are scattered throughout the pancreas (17). Discovered 1869 by a pathologic anatomist Paul Langerhans, the islets of Langerhans constitute about 1-2% of the mass of a human pancreas and are most numerous in the head (18).

There are four main cell types in the islets that can be classified by their secretion of hormones in the bloodstream. Mostly prominent are the ß cells that secrete insulin and thus lower the glucose levels. Contrary to ß cells, α cells secrete glucagon that induces the release of glucose into the blood stream resulting in an increase of blood glucose levels. δ cells produce somatostatin and inhibit insulin, glucagon, and pancreatic polypeptide (PP) secretion. Lately, PP cells

are a very few numbers that secrete pancreatic polypeptide, which inhibits intestinal motility, pancreatic exocrine and bile secretion and stimulates gastric leader cells. Human islets show different architecture compared with rodent islets. In human, ß, α, δ, and PP cells are distributed throughout the whole islets whereas in rodents, ß cells form the core of the islets and α, δ, and PP cells form the mantle of the islets (17, 19).
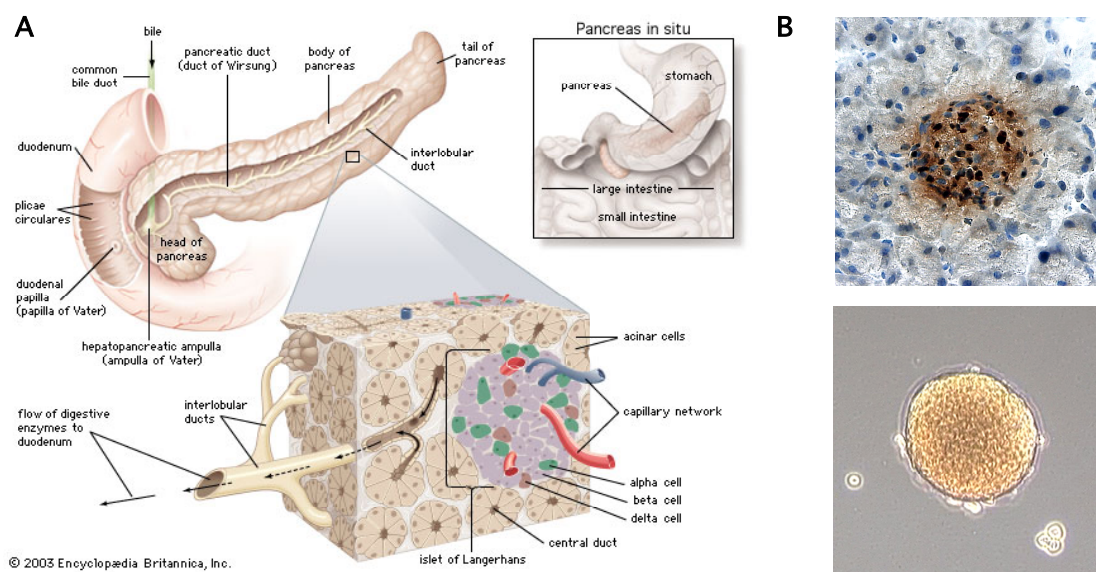
Figure 1: Composition of the pancreas.

(A) The pancreas is divided into three parts: the head attached to the small intestine, the body, and the tail that ends near the spleen. The islet cells are distributed throughout the pancreas, and are most frequent in the head. Islets are composed of ß, α, δ and PP cells. (B) An immunohistological staining of insulin of a murine islet cell and a fresh isolated islet cell after 7 days of culturing. (Adapted from Encyclopaedia Britannica, Inc 2003)

6.3.2 Type 1 diabetes

Type 1 *diabetes mellitus* (T1D) occurs in 5% to 10% of all cases of diabetes, affects primarily children and results from T cell-mediated destruction of pancreatic ß cells. As also observed for other autoimmune diseases a north to south decrease in T1D incidence has been reported. For example the incidence seen in Finland (40 cases per 100,000/year) is extremely high compared with extremely low rates in

Venezuela (0.1 cases per 100,000/year) (20). However, the incidence of T1D is also highly variable among different ethnic and racial populations as in Estonia that borders Finland has only an incidence rate of about one quarter of its neighbor. Moreover, some 'hot-spots' in warm climates such as Sardinia with almost as high rate as in Finland have also been reported (21). These observations indicate that not only geographic position plays a role but probably the combination of genes and environment (see chapters: Genetic susceptibility factors and Environmental factors).

As mentioned above, T1D is a multifactoral autoimmune disease thought to originate from the combination of susceptibility genes with environmental factors. Susceptibility and protection from T1D is associated with the major histocompatibility complex (MHC) HLA class II DR and DQ molecules. The HLA DR3/4-DQ8 heterozygous genotype is the genotype associated with the highest risk for T1D. Whereas DQB1*0602 are associated with protection from T1D in multiple populations (22). Further non-HLA loci genes are associated with T1D susceptibility. For instance, the insulin gene (VNTR), where short forms of a variable number tandem repeat in the insulin promoter are associated with susceptibility to disease, longer forms provide protective effects. In addition, PTPN22 as well as CTLA-4 are also reported to be implicated in T1D susceptibility (23).

Besides climatic influences viral infection, early infant diet and toxins also serve as modifiers of disease pathogenesis. Viruses, such as rubella, coxackie virus and enteroviruses have been reported to play a role in etiology of T1D. It could be shown that patients suffering from T1D harbored higher levels of coxsackievirus-specific antibodies compared with control population. Moreover infection of coxsakie B virus, isolated from diabetic patient, enhanced T1D onset in nonobese

diabetic (NOD) mice (24). Not only viruses have been reported to modulate the course of T1D there is also a report existing that maternal intake of Vitamin D in food during pregnancy can protect against islet autoimmunity in offspring (25). It is supposed that active vitamin D3 modifies dendritic cell action and T cell differentiation following shifting the balance to regulatory T cells.

The detection of autoantibodies against islet antigens in the blood is highly predictive of the development of T1D. The three principal autoantibodies react with glutamic acid decarpoxylase (GAD65) (26), insulin (27) and insulinoma antigen-2 (IA-2) (28) and can be present in some individuals for decades prior until up to 80% of ß cells are destroyed and T1D develops (29).

Insulitis in human samples contained CD8^{+} and CD4^{+} T cells, B cells and macrophages, with a predominance of CD8^{+} T cells (29). It is proposed that development of islet autoimmunity primary requires genetic predisposition and a critical repertoire of autoreactive T cells against islet antigens. Furthermore, a local event such as viral infection or APC dysfunction could via molecular mimicry or bystander effects activate such autoreactive T cells and afford their migration to the target organ. Following secretion of various cytokines such as IL-1ß, TNF-α and nitric oxide as well as cytotoxic T cells finally cause the destruction of ß cells leading to the outcome of disease (2).

There are several prevention strategies to enhance regulatory responses and dampen aggressive anti-islet activities. As an antigen non-specific intervention the T cell depletion with an anti-CD3 antibody could be shown to have encouraging outcome. In two different phase I/II intervention trials with anti-CD3 antibodies a remission or a reduced insulin requirement out to 18 months could be reached (30, 31). Moreover, an islet-antigen specific DNA vaccine that induces T_{reg} cells

has demonstrated striking efficacy in recent-onset diabetes in NOD mice (32). However, an even more promising attempt would be to combine the non-specific and antigen-specific intervention mentioned above. Indeed there are *in vivo* studies showing success in prolonging the onset of T1D in mice using a so called combination-therapy (33). However, it will need more time and research to establish such a combination-therapy in humans and to ensure that there are no side effects. Besides different prevention strategies islet transplantation is one of the most promising treatments for diabetes so far. The landmark for islet transplantation was done in 1999 where 7 patients underwent isolated islet transplantation and achieved insulin independence for at least one year. The treatment protocol used was a corticosteroid-free immunosuppression regimen, known as Edmonton protocol (34). However, many of the patients required more than one infusion of islets from two donor pancreata. One of the most serious problems is the impairment and loss of the islet function over time. Infused islet cells are new targets for the autoaggressive processes of the autoimmune disease. After islet transplantation hypoglycemic episodes can be avoided but T1D is still not cured (35). Anyway, until now the best way to keep the disease under control is a livelong controlled injection of insulin (32).

6.4 Mouse models for T1D

The two most frequently used mouse models for T1D are the spontaneous nonobese diabetic (NOD) mouse that was discovered 1980 (36) and the inducible RIP-LCMV mouse model established in two different laboratories by Michael Oldstone (37) and Hans Hengartner/Rolf Zinkernagel in 1991 (38).

6.4.1 Classification and morphology of the lymphocytic choriomeningitis virus

Lymphocytic choriomeningitis virus (LCMV) is a member of the genus Arenavirus in the family of Arenaviridae and is normally carried by rodents. The LCMV genome consists of two negative-sense single-stranded RNA segments, a short (S) and large (L) segment, with approximate size of 3.4 and 7.2 kb, respectively (39, 40). Each RNA species contains two genes encoded in opposite orientation (ambisensed RNA). The S RNA encodes for the two major structural proteins of LCMV, namely the nucleoprotein NP and the glycoprotein precursor (GP-C). The two virion glycoproteins GP-1 and GP-2 derive by posttranslational cleavage of GP-C. Tetramers of GP-1 and GP-2 are present on the surface of the virion and mediate virus interaction with the host cell surface receptors. The NP, the most abundant viral protein in virus-infected cells, is present within the virion and encapsulates viral RNA. The L RNA segment encodes for the non-glycosylated L protein, which is presumably the viral RNA dependent RNA polymerase and for the RING finger Protein (Z) (40, 41).

LCMV is a model virus often used in research of viral immunity. One of its advantages is that it induces a tremendous (i.e. easily measured) immune response. The LCMV infection of mice leads to the generation of a strong cytotoxic T lymphocyte (CTL) response and therefore the immune response peaks 6 to 8 days after infection. That makes it relatively easy to detect individual components of the immune response (42, 43).

6.4.2 The RIP-LCMV Model for T1D

As mentioned previously (see chapter: Mouse models for T1D) two different groups created separate transgenic mouse lines in which either the glycoprotein (GP) or the nucleoprotein (NP) are expressed as defined target antigen in pancreatic ß cells under the control of the rat insulin promoter (RIP) (37, 38). In these mice both target antigens are considered as 'self' and the mice are ignorant or tolerant to these antigens (Figure 2.1). Therefore, these RIP-LCMV mice do not show islet-cell infiltration, ß cell dysfunction, hyperglycaemia, or spontaneous activation of autoreactive (anti-LCMV) lymphocytes. However, LCMV infection triggers autoimmune diabetes within 10-14 days in the RIP-LCMV-GP mice and 1-6 months in the RIP-LCMV-NP mice in a two-step manner. First, upon infection of the pancreas the innate immune system is initiated, resident macrophages or dendritic cells are activated and release pro-inflammatory cytokines, such as IFN-γ, TNF-α, and IL-1. Moreover, activated ß cells and endothelial cells release chemokines, such as CXCL10, resulting in an attraction of activated lymphocytes as well as the first autoaggressive T cells in an non-specific manner (Figure 2.2). In a second stage, over time an antigen-specific immune response evolves and attacks target antigens expressed by virus and ß cells. After clearance of the virus the only viral antigen available is expressed by ß cells. Therefore, some LCMV-specific T cells kill ß cells in a perforin dependent manner leading to an increase in islet- as well as LCMV-antigen presentations by professional APCs. Finally, this increase results in further expansion and proliferation of autoaggressive T cells and together with the bystander inflammation the destruction of most ß cells and overt diabetes follows (Figure 2.3-4).

As mentioned earlier (see chapter: Autoimmunity), in these mouse models molecular identity rather than molecular mimicry is responsible for the induction of T1D (11, 44, 45).

Anyway, in this RIP-LCMV mouse model the onset of diabetes depends on the autoreactive CD8$^+$ and CD4$^+$ T cells. As mentioned above, LCMV-infection of RIP-LCMV-GP and RIP-LCMV-NP mice results in a different diabetes onset. It is believed that this difference is due to the distinct expression pattern of the transgene. The RIP-LCMV-GP mice (fast-onset) express the LCMV-GP transgene exclusively in the ß cells and not in the thymus. Therefore, GP-specific CD8$^+$ T cells are not negatively selected in the thymus and after LCMV infection the high systemic numbers of autoaggressive CD8$^+$ T cells are able to induce diabetes without the help of CD4$^+$ T cells. In contrast, in the RIP-LCMV-NP mice (slow-onset) the LCMV-NP transgene is expressed in the ß cells as well as in the thymus resulting in the deletion of high-affinity NP-specific T cells. The low-affinity NP-specific CD8$^+$ T cells in the periphery are not sufficient to induce diabetes after LCMV infection. For this reason they need the assistance of CD4$^+$ T cells to induce T1D (46).

Hence, the RIP-LCMV mouse model is an attractive tool to study the mechanisms of T1D. Its advantages compared with other mouse models, such as the NOD mice, are the clearly defined initiation point (LCMV-infection) that enables to study the precise kinetics of disease, the organ (islet) restricted disease and the presence of well-characterised target antigens (GP, NP). Moreover, there are tools available to easily visualize these target antigens by MHC class I-peptide tetramers in flow cytometry or directly on quick frozen sections (47).
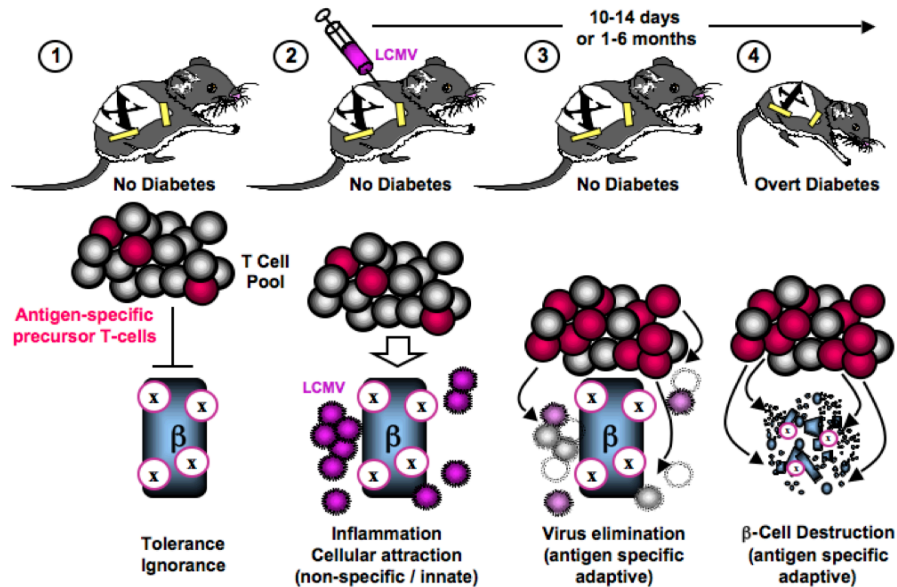
Figure 2: RIP-LCMV mouse model.

(1) Transgenic RIP-LCMV mice are tolerant or ignorant to their glycoprotein (GP) or nucleoprotein (NP) of lymphocytic choriomeningitis virus (LCMV) expressed by their ß cells. (2) LCMV infection causes local non-specific inflammation and chemokines and cytokines attract and activate leukocytes as well as LCMV-specific precursor lymphocytes by bystander activation. (3) Specific anti-LCMV lymphocytes are activated and expanded reacting against the target antigen GP or NP expressed by the virus or the ß cells. After virus elimination the ß cells express the only remaining target antigen. (4) Finally, this results in increased destruction of ß cells and subsequently overt diabetes. (Adapted from Urs Christen)

6.5 Chemokines

6.5.1 Chemokines overview

Chemokines and cytokines have been implicated in several autoimmune diseases, homeostasis, development, host defense mechanisms, and pathogen infections and can have both beneficial and exacerbating effects. In microbial or viral infections chemokines and cytokines play a pivotal role in attraction and activation of leukocytes with the aim of controlling the invading pathogen. Mainly resident macrophages or endothelial cells release chemokines upon activation by cytokines, like IFN-γ and TNF-α. The chemokines released coordinate both the timing and location of invading cell populations as well as the composition of these infiltrating immune competent cells (44, 45).

35

Chemokines are small molecules (~ 8-14 kDa) divided into two major subfamilies on the basis of the arrangement of the N-terminal cysteine residues, CC chemokines with two adjacent cysteines and CXC chemokines with the equivalent two cysteine residues that are separated by a single amino acid. Chemokines interact with a subset of G protein-coupled seven-membrane-spanning receptors that are expressed by their target cells, such as a variety of leukocytes (45, 48, 49).

6.5.2 The role of cytokines in T1D

In T1D, the immune response is characterized by type 1 cytokines (IFN-γ and IL-2) that are thought to enhance autoimmune processes and have mainly pro-diabetic influences, type 2 cytokines (IL-4, IL-5, IL-10, and IL-13) and TGF-ß secreted by CD4$^+$CD25$^+$ T$_{reg}$ cells that have supposable more regulatory functions (44, 50). Although a recent study has shown an upregulation of T$_H$17 immunity in peripheral blood T cells from children with T1D (51), to date is not entirely clear how T$_H$17 cytokines (IL-17, and IL-22) are involved in T1D (see chapter: T Lymphocytes).

Several studies investigated the role of the two major pro-inflammatory cytokines IFN-γ and TNF-α in mouse models for T1D. In the RIP-LCMV transgenic IFN-γ-deficient mice the incidence of disease was drastically reduced (52), whereas TNF-α plays a dual role depending on the time of expression. The early expression of TNF-α in the RIP-LCMV mouse model led to enhancement of the frequencies of diabetic mice, whereas late expression reversed the auto-destructive process (53).

6.5.3 The role of CXCL10 and CXCR3 in T1D

The CXCR3 chemokine receptor is the only receptor known so far that binds the three chemokines CXCL9 (MIG or monokine induced by IFN-γ), CXCL10 (IP-10 or IFN-γ-inducible protein 10 of 10 kDa), and CXCL11 (I-TAC or interferon-inducible T cell alpha chemoattractant). Upon stimulation with TNF-α and IFN-γ the CXCR3 ligands are mainly expressed by macrophages, fibroblasts, endothelial cells, and keratinocytes but are also expressed by normal T cells, thymocytes, and activated T cell hybridomas (50, 54).

CXCL10 is thought to be involved in various inflammatory pathologies by attracting leukocytes to the sites of infection or injury. Moreover, CXCL10 plays a role in inhibition of angiogenesis, wound healing, and antiviral response. CXCL10 is highly expressed early after infection with several viruses, such as HIV, LCMV, adenovirus, and mouse hepatitis virus (55, 56). Due to their unspecific paracrine nature CXCR3 chemokines activate T cells as well as autoreactive T cells ('bystander activation') and thereby direct the anti-viral response towards the more aggressive T_H1-type T cell dominance that can lead to an autoaggressive immune defense and finally might end in autoimmune disease. In fact, several evidences suggest a pivotal role of CXCL10 in the course of T1D in the RIP-LCMV mouse model. First, neutralization of CXCL10, but not CXCL9, resulted in decreased cellular infiltration and abrogated T1D by inhibiting the expansion and migration of antigen-specific T cells into the islets (56). Second, in both the RIP-LCMV and NOD mice, expression of CXCL10 during the ongoing autoaggressive immune response, outside the pancreas attracted antigen-specific cells out of the pancreas and abrogated disease. This inflammation outside the pancreas was achieved by an infection of a

virus that predominantly accumulates in the pancreatic draining lymph nodes (PDLN). The autoaggressive cells then migrated along a CXCL10 gradient to the PDLN and once arrived the hyper-activated cells underwent apoptosis (14). Third, transgenic mice that express CXCL10 specifically in the ß cells of Langerhans have spontaneous islet infiltration but do not develop spontaneous diabetes indicating that this bystander activation is not sufficient to induce disease. Nevertheless, if these mice are crossed with RIP-LCMV mice the islet-specific CXCL10 expression lead to an enhancement of antigen-specific T cell migration to the pancreas and to an acceleration of T1D after LCMV-infection (57).

As mentioned above, the receptor known for CXCL10 is CXCR3, which is a G protein-coupled seven-membrane-spanning glycoprotein that is internalized upon activation. This internalization leads to calcium influx and intracellular activation of signaling cascade that includes kinases and finally often cytoskeleton rearrangement and cell movement. CXCR3 is expressed by natural killer cells, B cells, plasmacytoid and myeloid dendritic cells, and predominantly expressed by activated T_H1-type T cells (58, 59). CXCR3-deficient mice crossed with RIP-LCMV mice showed a significant delay but no abrogation of the development of virus-induced diabetes (60). In another study neither CXCR3-deficient mice nor a pharmacologic blockade of CXCR3 with an antagonist in rats had an effect on cardiac allograft survival (61).

6.6 Adhesion molecules

6.6.1 Rolling, adhesion and transmigration - the families of adhesion molecules

Leukocyte extravasation from the blood to site of injury or infection is essential in the development of an inflammatory response. This event is strictly controlled by a multistep action of chemokines and adhesion molecules (62, 63).

In the leukocyte adhesion cascade that includes tethering, rolling, activation and arrest, adhesion strengthening, crawling and finally paracellular or transcellular migration is mediated by a lot of different cell adhesion molecules (CAMs) such as selectins, integrins, cadherins and cell adhesion molecules of the immunoglobulin superfamily (Figure 3) (64-66):

6.6.1.1 Selectins (P-, E- or L-selectin)

Selectins are a family of heterophilic CAMs that bind glycosylated ligands such as P-selectin glycoprotein ligand 1 (PSGL1) and are the adhesion molecules expressed on inflamed endothelial cells that interact with a leukocyte during the rolling process. Under conditions of blood flow they are able to capture leukocytes in a high dissociation/association rate allowing the leukocytes to role and to sense chemoattractants on the endothelial wall (Figure 3). L-selectin is expressed by most leukocytes whereas E- and P-selectins are synthesized by inflamed endothelial cells. In addition, P-selectin can also be expressed by activated platelets (64, 66, 67). After treatment of NOD mice with an antibody neutralizing L-selectin insulitis was reduced and the severity of T1D was decreased (68). However, if the

mice were treated during an ongoing diabetogenic response, the blockade of L-selectin could only marginally delay the disease (69).

6.6.1.2 Integrins (LFA-1, Mac-1, VLA-4)

Integrins are heterodimers of α and ß subunits that are particularly expressed by leukocytes and mediate leukocyte adherence to the vascular endothelium or other cell-cell interactions. During rolling, after leukocytes have bound to the chemokines present on endothelial surfaces, the constitutively expressed integrins get activated and improve their affinity and/or avidity for their ligands expressed on the endothelium. These processes finally lead to rolling arrest and firm adhesion (Figure 3) (1, 64, 66). The importance of integrins in T1D is illustrated by an adoptive transfer experiment in NOD mice, where neutralization of the integrin VLA-4 (very late antigen 4) resulted in a complete reduction of T1D (68).

6.6.1.3 Immunoglobulin (Ig) superfamily (ICAMs, VCAM-1, PECAM-1, JAMs)

The Ig superfamily CAMs (IgSF CAMs) are calcium-independent transmembrane glycoproteins that are either homophilic or heterophilic. Member of the IgSF CAMs include the intercellular adhesion molecules (ICAMs), vascular-cell adhesion molecule 1 (VCAM-1), platelet-endothelial-cell adhesion molecule (PECAM-1), neural-cell adhesion molecule (NCAM) and junctional adhesion molecules (JAMs). Most Ig superfamily CAMs play a role in paracellular transmigration whereas ICAM-1 is involved in transcellular migration as well.

ICAM-1 is constitutively expressed in low concentrations on endothelial cells and on several leukocytes. However, upon inflammation ICAM-1 is highly upregulated on endothelial cells only. ICAM-1 can bind LFA-1 (leukocyte function-associated antigen1) and MAC-1 (Macrophage-1

antigen) of activated leukocytes and plays an important role in rolling arrest and firm adhesion (Figure 3) (63, 70).

VCAM-1 is mainly expressed on vascular endothelium and only after cytokine stimulation of endothelial cells. Like ICAM-1 it also mediates adhesion of leukocytes to the vascular endothelium (67, 70). In an adoptive transfer model of diabetes in NOD mice neutralization of ICAM-1 had only a marginal effect on the onset of T1D, whereas blocking antibody against VCAM-1 delayed the onset of disease (71).

PECAM-1, also called CD31, support homophilic interactions and is expressed by leukocytes, platelets and endothelial cells (63, 64). In vitro, antibodies against PECAM-1 were demonstrated to inhibit monocyte and neutrophil migration, but not lymphocyte migration (63). It also could be shown that PECAM-1 knockout mice did not show a diminished inflammatory response, demonstrating that PECAM-1 is compensable for transmigration in vivo (64, 72).

Besides endothelial cells CD99 is expressed by erythrocytes and most leukocytes. It supports homophilic interactions and also acts in diabedesis downstream of PECAM-1 (Figure 3) (64, 72).

Junctional adhesion molecules (JAMs) are expressed at cell junctions in epithelial and endothelial cells as well as by leukocytes and platelets. Several reports suggest that JAM proteins are important for a variety of cellular processes, including tight junction assembly, platelet activation, angiogenesis, virus binding and leukocyte transmigration (Figure 3) (for more information see chapter: Junctional adhesion molecules) (73).

6.6.1.4 Cadherins (VE-cadherin)

Cadherins are calcium-dependent adhesion molecules that are involved in tissue organization and endothelial cell-contact stability (67). VE-

cadherin is highly expressed at adherens junctions and is linked to the cell cytoskeleton via catenins. It also plays its role in leukocyte transmigration (72).
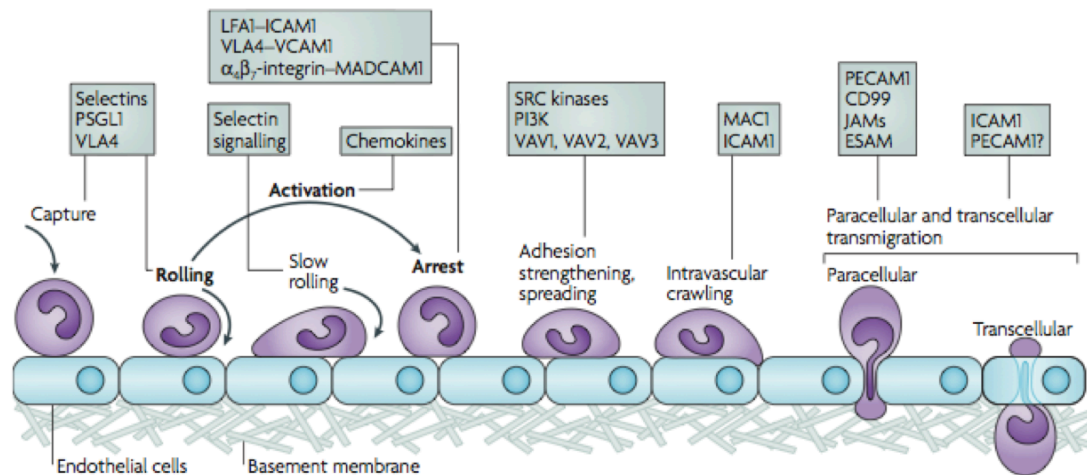
Figure 3: Adhesion molecules and their role in the leukocyte adhesion cascade.

Capturing and rolling is mediated by selectins, activation is caused by chemokines and arrest is mediated by the interaction of integrins with ICAM-1 or VCAM-1. Current knowledge suggests that leukocytes can transmigrate by two different pathways: the transcellular migration that is mediated by ICAM-1 and the paracellular migration in which a lot of different adhesion molecules, such as PECAM-1, CD99 and JAMs, are involved. (Adapted from K. Ley, Nature Reviews 2007)

6.7 Junctional adhesion molecules

6.7.1 Junctional adhesion molecule family and its origin

Junctional adhesion molecules are members of the larger CTX protein (Cortical Thymocyte marker for Xenopus) family, in which ancestral precursors may be the origin of T cell and B cell immune receptors. Several of these CTX proteins have also been described as receptors for various viruses like reovirus and adenovirus (74, 75). JAMs consist of a family of three closely related CTX proteins, JAM-A, JAM-B, and JAM-C and four members of another CTX subfamily ESAM, CAR, JAM-4, and JAML (72).

6.7.2 Structure and biochemical properties

The classical JAM proteins are type 1 transmembrane proteins that have an N-terminal signal peptide, an extracellular domain consisting of two extracellular Ig-like domains, a single transmembrane domain and a short cytoplasmic tail that contains phosphorylation sites that may serve as substrates for PKA, PKC and Casein Kinase II. In addition, they have a class II PDZ-binding motif at the C-terminal end that appears to facilitate interactions with tight junctions-associated scaffold proteins such as ZO-1, PAR3, AF-6 and MUPP1 (Figure 4a) (73).

6.7.3 Tissue expression and cellular localization

In general, if expressed on endothelial or epithelial cells the classical JAM proteins are found at tight junctional complexes, where they participate in maintenance and assembly of junctions.

JAM-A can be found on the surface of endothelial cells and epithelial cells of various tissues, including the heart, liver, pancreas, kidney, brain, lymph nodes, intestine, lungs, placenta and vascular tissue. The expression of JAM-A could also been shown on platelets, monocytes, neutrophils, a subset of lymphocytes and on antigen-presenting cells, such as macrophages and dendritic cells (62, 64, 74).

JAM-B is expressed by endothelial cells and is specifically enriched in certain vessels, such as high endothelial venules and lymphatics. Recently JAM-B expression could be shown on peripheral mouse leukocytes, such as conventional dendritic cells (76).

JAM-C is highly expressed on high endothelial venules and lymphatics and is found on fibroblasts and human epithelial cells. In addition, JAM-C is expressed by human platelets, monocytes, neutrophils, natural killer cells, dendritic cells, B cells and a subset of T cells but has not yet been detected on mouse leukocytes (62, 77, 78).

6.7.4 Properties, interaction and ligands

JAM proteins have been implicated in a variety of physiology and pathologic processes involving cellular adhesion. All three JAMs can support homophilic as well as heterophilic interactions. Moreover, JAM-A can interact with LFA-1, whereas JAM-B can support heterophilic interactions with JAM-C and VLA-4. Besides interaction with JAM-B, JAM-C can also bind the leukocytes integrins Mac-1 and CD11c (Figure 4b) (62, 79).
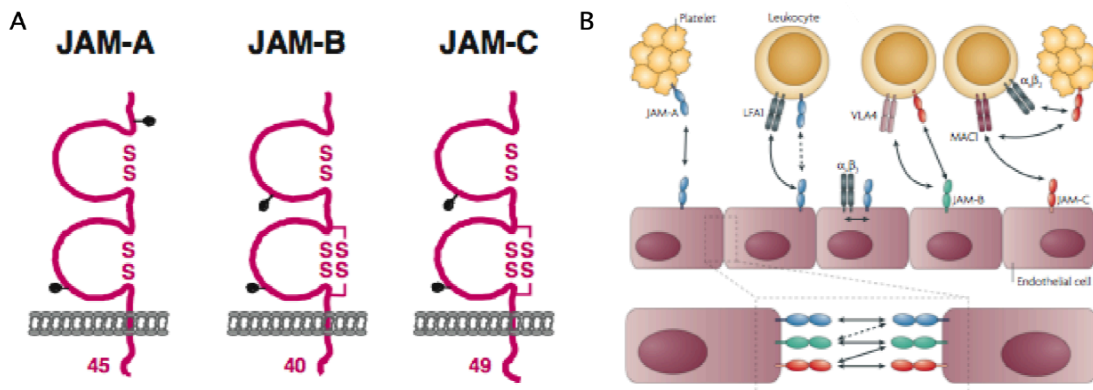
Figure 4: Structure of classical junctional adhesion molecules (JAMs) and their ligands.

(A) All three JAMs have an extracellular domain with two Ig-like domains, a single transmembrane sequence, and a short cytoplasmic tail that contains a PDZ binding motif. (B) The JAMs can support heterophilic as well as homophilic interactions. JAM-A interact with the integrin lymphocyte function-associated antigen 1 (LFA-1), JAM-B interacts with JAM-C or very late antigen 4 (VLA-4), and JAM-C moreover interacts with Mac-1 and CD11c. (Adapted from K. Ebnet, J. of Cell Science 2004 and C. Weber, Nature Reviews 2007)

6.7.5 The role of JAM-C in various diseases and pancreatitis

Since JAM-C has been discovered and characterized ten years ago many different investigations have proven the importance of JAM-C in various diseases. JAM-C is implicated in cell polarity formation in myelinated peripheral nerves and spermatid differentiation (80, 81), in angiogenesis and tumor growth in mice (82), in vascular permeability

(83), and leukocyte adhesion and transmigration (84). The role of JAM-C in various diseases has been analyzed *in vitro* and *in vivo* in numerous imaging studies and animal models for several diseases. In inflammatory pathologies such as peritonitis and arthritis treatment of mice with a JAM-C neutralizing antibody reduced the accumulation of neutrophils at the side of inflammation (85, 86). In JAM-C knockout mice pulmonary dysfunction and reduced IgG memory could be found (76, 87). Moreover, the blockade of JAM-B/JAM-C interaction reduced the initial monocyte numbers in the lung of mice following intranasal LPS challenge. However, this reduction of abluminal monocytes was not due to a lower transmigration rate of the cells but rather due to increased reverse transmigration (88).

A very interesting study analyzed the role of JAM-C in cerulein-induced pancreatitis in mice. JAM-C expression in the pancreas was increased after cerulein-treatment of mice. Additional treatment of mice with a JAM-C neutralizing antibody led to reduced leukocyte infiltration, acinar cell necrosis and oedema. On the other hand, if transgenic mice overexpressing JAM-C were treated with cerulein the leukocyte accumulation at site of injury, tissue damage as well as oedema were increased (89).

These results indicate that JAM-C plays a pivotal role in various inflammatory diseases and its expression in the pancreas contributes to the development of acute pancreatitis by abetting leukocyte extravasation.

AIMS

7 Aims of the study

The goal of my project was to investigate the mechanisms involved in attraction, activation and transmigration of lymphocytes to the target site of injury in type 1 diabetes.

Aim 1

Analysis of the impact of the chemokine receptor CXCR3 antagonist NIBR2130 on the development of T1D in the RIP-LCMV mouse model

Aim 2

Characterization of the influence of the adhesion molecule JAM-C on the development of virus-induced T1D

7.1 Strategy

As previously described (see chapter: Introduction) T1D results from the autoimmune destruction of insulin-producing ß cells in the pancreas. Attraction, activation and transmigration of inflammatory cells, such as T cells, B cells and dendritic cells are prerequisite to ß cell-injury. Such processes include several molecular interactions between receptors expressed on circulating cells and chemokines or adhesion molecules expressed on endothelial cells. Thus, our strategy was to directly block the interaction of either the key chemokine CXCL10 with its receptor CXCR3 or of the adhesion molecule JAM-C with its ligand MAC-1.

7.2 Aim 1: Inhibition of CXCR3 during T1D

Generally, it is believed that autoimmune disease is caused by the combination of genetic predisposition with environmental triggers, such as pathogen infection or xenobiotics (see chapter: Introduction). In the RIP-LCMV mouse model the target antigens are considered as 'self' and antigen-specific precursor T cells are ignorant or tolerant to these antigens. T1D is initiated by LCMV-infection that leads to an unspecific inflammation in the pancreas resulting in the attraction and activation of leukocytes including LCMV-specific precursor lymphocytes to the site of injury. Along with virus elimination, activated LCMV-specific T cells attack target antigens expressed by transgenic ß cells resulting in a progressive destruction of ß cell-mass and subsequently overt diabetes. The initial virus-induced inflammation is triggered by the release of chemokines. Directed migration is mediated by the interaction between chemokines and their corresponding receptors expressed on different leukocytes. This interaction is crucial for the activation and migration of leukocytes to the site of injury. In this context it was shown that the chemokine CXCL10 that binds to the chemokine receptor CXCR3 plays a pivotal role in attracting autoaggressive T cells to the islets of Langerhans in T1D. Neutralization or overexpression of CXCL10 significantly influenced the development of virus-induced T1D in the RIP-LCMV mouse model (56, 57)(see chapter: Introduction).

As previously described the main receptor of CXCL10 is CXCR3, a G protein-coupled seven-membrane-spanning glycoprotein predominantly expressed by activated Th1-type T cells (see chapter: Introduction). It was shown that CXCR3-deficient mice crossed with RIP-LCMV mice showed a significant delay in the development of T1D (60). Moreover,

it has also be demonstrated that a preproinsulin specific autoreactive CXCR3 expressing CD8^{+} T cell clone, derived from a type 1 diabetes patient, was able to kill human pancreatic ß cells (90).

Due to the fact that CXCL10/CXCR3 interaction seems to play a significant role in autoimmune diseases we investigated the impact of the inhibition of CXCR3 with the small molecule CXCR3 antagonist NIBR2130 on the outcome of virus-induced T1D in the RIP-LCMV mouse model.

Figure 5: Working hypothesis – Project 1

A: Immunopathogenesis in the RIP-LCMV model:

(A1) LCMV-infection of the pancreas leads to the release of pro-inflammatory cytokines, such as TNF-α, by resident antigen presenting cells. (A2) Subsequently, activated endothelial cells as well as ß cells release chemokines, such as CXCL10 that is one of the earliest chemokine expressed in high local concentrations after LCMV-infection. (A3) Through binding to its receptor CXCR3, CXCL10 predominantly attracts activated aggressive Th1-type T cells, which migrate into the inflamed tissue. (A4) Activated T cells transmigrate through the endothelial cell layer and penetrate the ß cells. (A5) Infiltrating LCMV-specific T cells start destroying some transgenic β cells expressing LCMV proteins in a perforin dependent manner. At a later stage professional antigen presenting cells, such as dendritic cells, migrate to pancreatic draining lymph nodes and present LCMV and other islet antigens leading to further proliferation and expansion of the autoaggressive T-cell repertoire and subsequently increased infiltration of autoaggressive T cells to the islets. (A6) Finally, islet antigen-specific, aggressive T cells together with unspecific bystander factors destroy most of the remaining β cell-mass resulting in overt diabetes.

B: Blockade of CXCL10-CXCR3 interaction by NIBR2130

(B1 and B2) The same events as in figure A1 and A2. (B3) Through binding to the CXCR3 receptor the CXCR3 antagonist, NIBR2130, inhibits the interaction between CXCL10 and CXCR3. (B4) Subsequently the attraction of T cells is blocked resulting in a diminished migration of autoaggressive T cells into the islets of Langerhans. NIBR2130 treated RIP-LCMV mice should therefore display reduced incidence and severity of T1D.
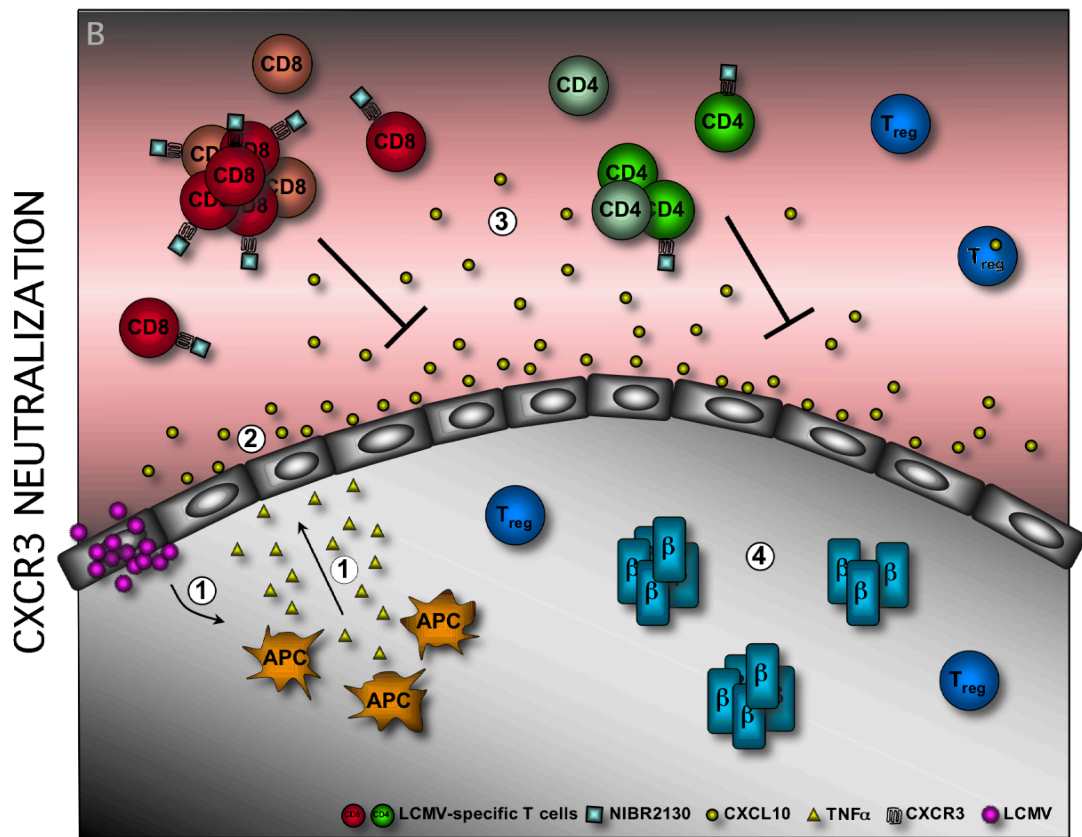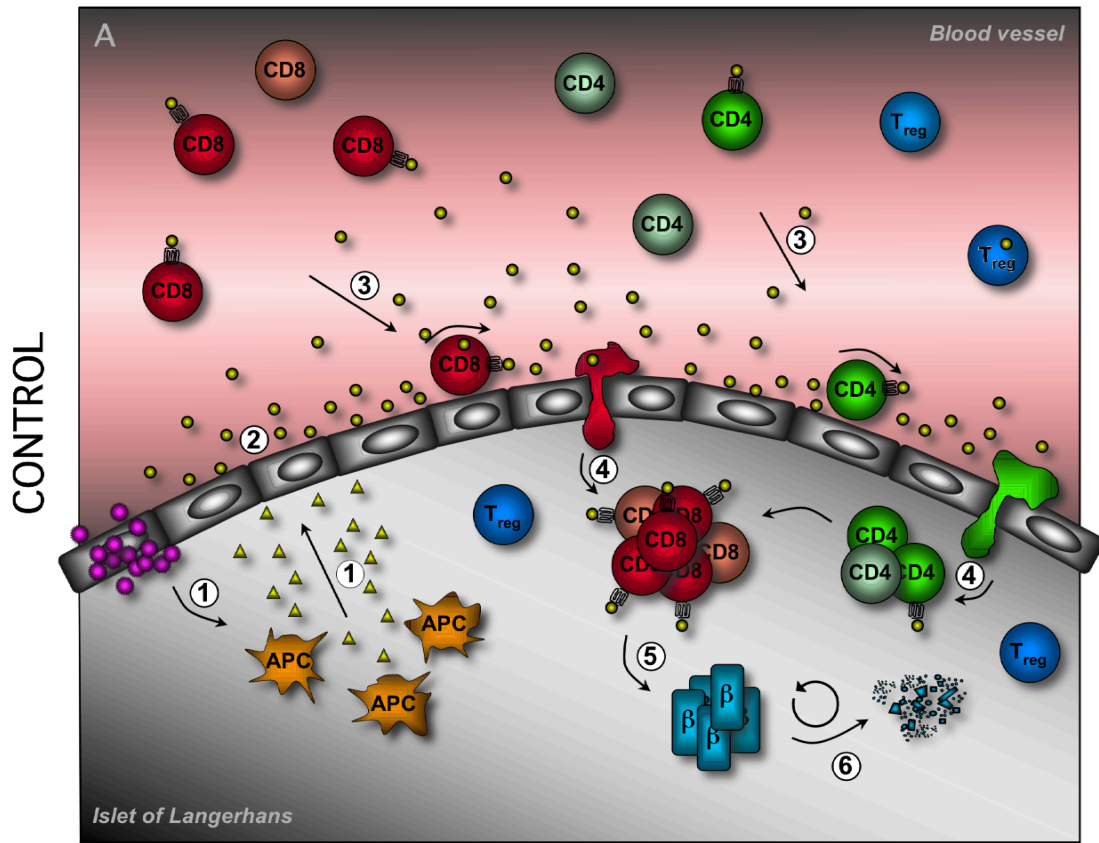
7.3 AIM 2: JAM-C and its influence on T1D

Once arrived at the site of inflammation, namely the islets of Langerhans, the leukocytes have to extravasate through the endothelial cell layer to penetrate the islets. Thereby many different adhesion molecules such as selectins, integrins and immunoglobulin-superfamily proteins are involved in leukocyte rolling, activation and arrest, adhesion strengthening, crawling and finally paracellular or transcellular migration (62). As mentioned previously, it has been shown that JAM-C plays a crucial role in several inflammatory diseases such as peritonitis, arthritis and cerulein-induced pancreatitis (85, 86, 89) (see chapter: Introduction). In the cerulein-induced acute pancreatitis mouse model an increase of JAM-C expression in the pancreas could be observed. Further, blockade of JAM-C with a neutralizing antibody resulted in reduced pancreatitis (89). Although, the immunopathogenic processes involved in the destruction of ß cells in the cerulein mouse model is different than in human T1D, the outcome of this study shows that blockade of JAM-C results in a reduced leukocyte extravasation through the endothelium, which finally leads to a diminished local inflammation of islets (89).

Therefore in the second part of the project, I investigated whether JAM-C expression has an influence on virus-induced T1D in the RIP-LCMV mouse model. First, T1D development was analyzed in RIP-LCMV mice administered with a neutralizing antibody to block JAM-C. Second, RIP-LCMV mice have been crossed with mice overexpressing JAM-C on endothelial cells.

Figure 6: Working hypothesis – Project 2

A: JAM-C neutralization:

(A1) LCMV-infection of the pancreas leads to the release of pro-inflammatory cytokines, such as TNF-α, by resident antigen presenting cells. (A2) Subsequently, activated endothelial cells as well as ß cells release chemokines, such as CXCL10. Blockade of JAM-C with a neutralizing antibody prevents the interaction between Mac-1, expressed on attracted aggressive T cells and JAM-C expressed on endothelial cells surrounding islets. (A3 and A4) Subsequently, transmigration of aggressive T cells is reduced and complete destruction of the ß cell-mass is prevented.

B: JAM-C overexpression:

(B) The same events as in figure 1A except that due to the overexpression of JAM-C on endothelial cells the transmigration of activated T cells through the endothelial cell layer of islets is increased. This might lead to increased ß cell-destruction and accelerated T1D.
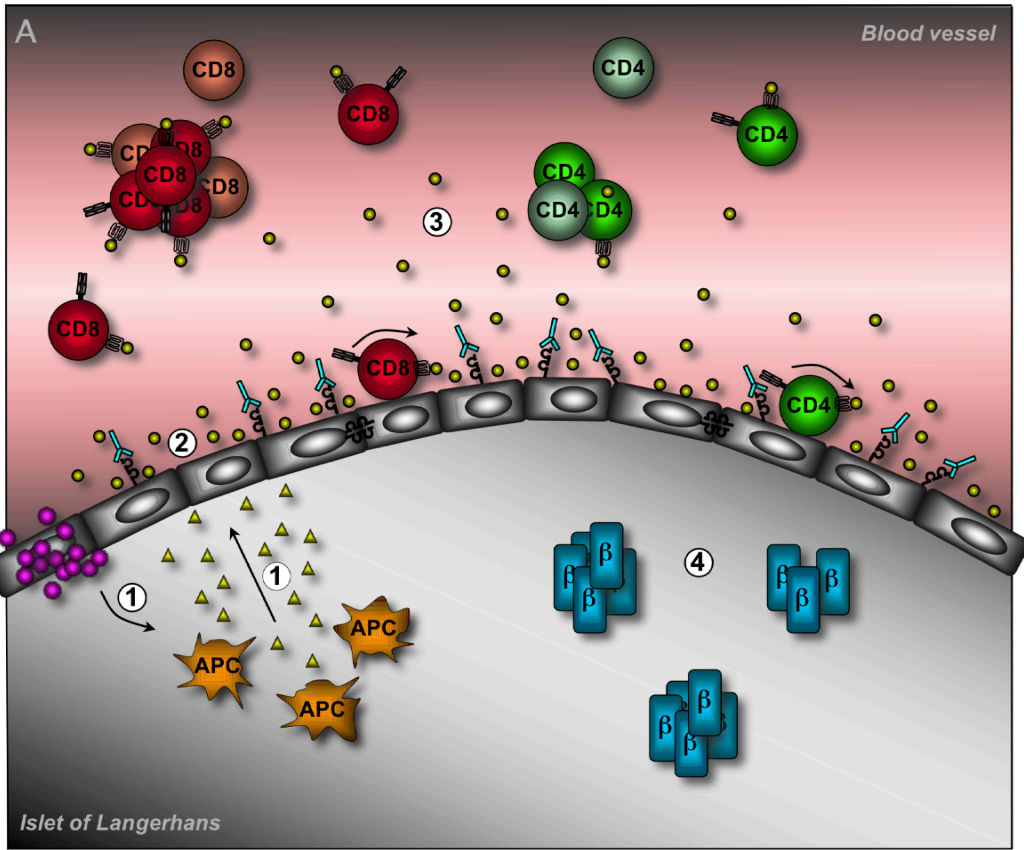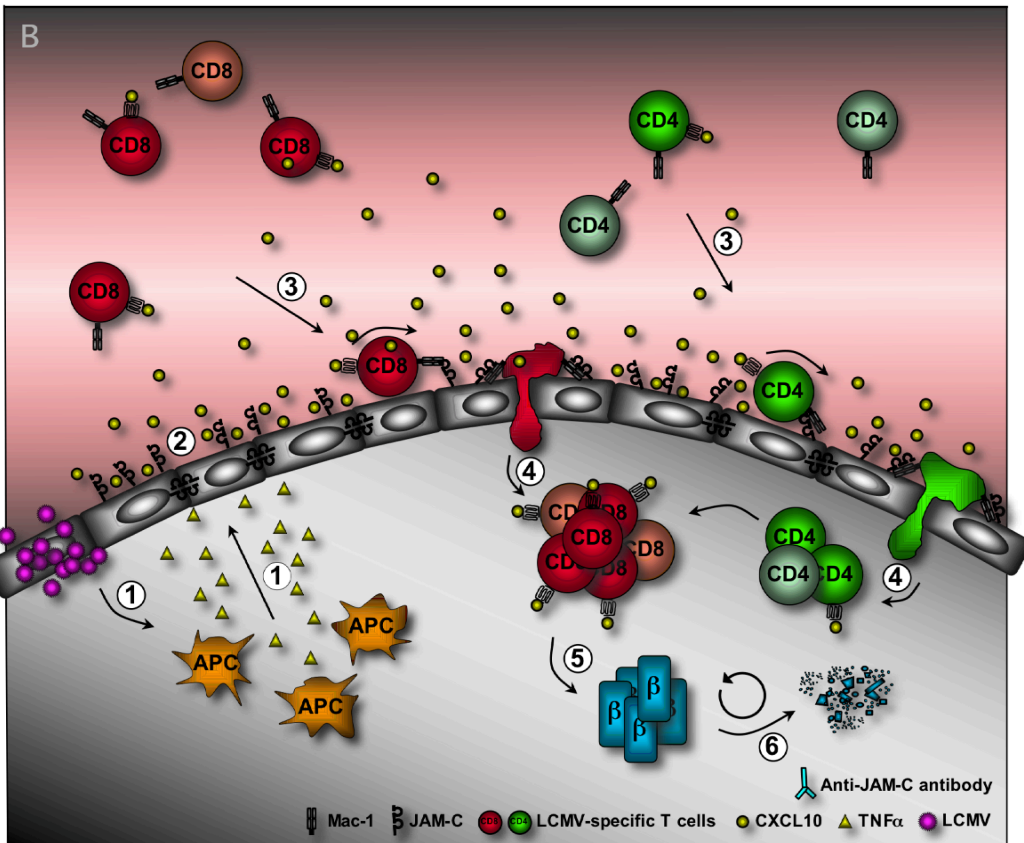
RESULTS

8 Results

8.1 Project 1: CXCR3 and its role in T1D

In the first part of my project I investigated the influence of the inhibition of CXCR3 with the CXCR3 antagonist NIBR2130 on the outcome of T1D.

8.1.1 Implantation of osmotic pumps guarantees a constant delivery of sufficient NIBR2130

To ensure a constant blockade of CXCR3 a model 2002 osmotic pump from Alzet (Cupertino, CA) releasing 0.5 μl/h NIBR2130 or buffer alone was implanted under the skin of mice for 4 weeks. The concentration in the pumps used was 16.7 mg/ml, which corresponds to 200 μg NIBR2130 per day. Due to its maximal capacity of 250 μl the pumps had to be exchanged after two weeks. This approach provided a continuous and constant delivery of the antagonist as demonstrated by the blood concentration of NIBR2130 (Figure 7A and Figure 8A). Blood levels reached concentrations of 250 to 500 ng/ml. It has been demonstrated before that the half maximal inhibitory concentration (IC_{50}) for NIBR2130 is 85.2 ng/ml (91). In our study we found a continuous NIBR2130 blood concentration, which was approximately 3 to 6 times higher than the IC_{50} of this compound. Thus, implantation of osmotic pumps reliably delivers NIBR2130 at a concentration that is sufficient for CXCR3 blockade.
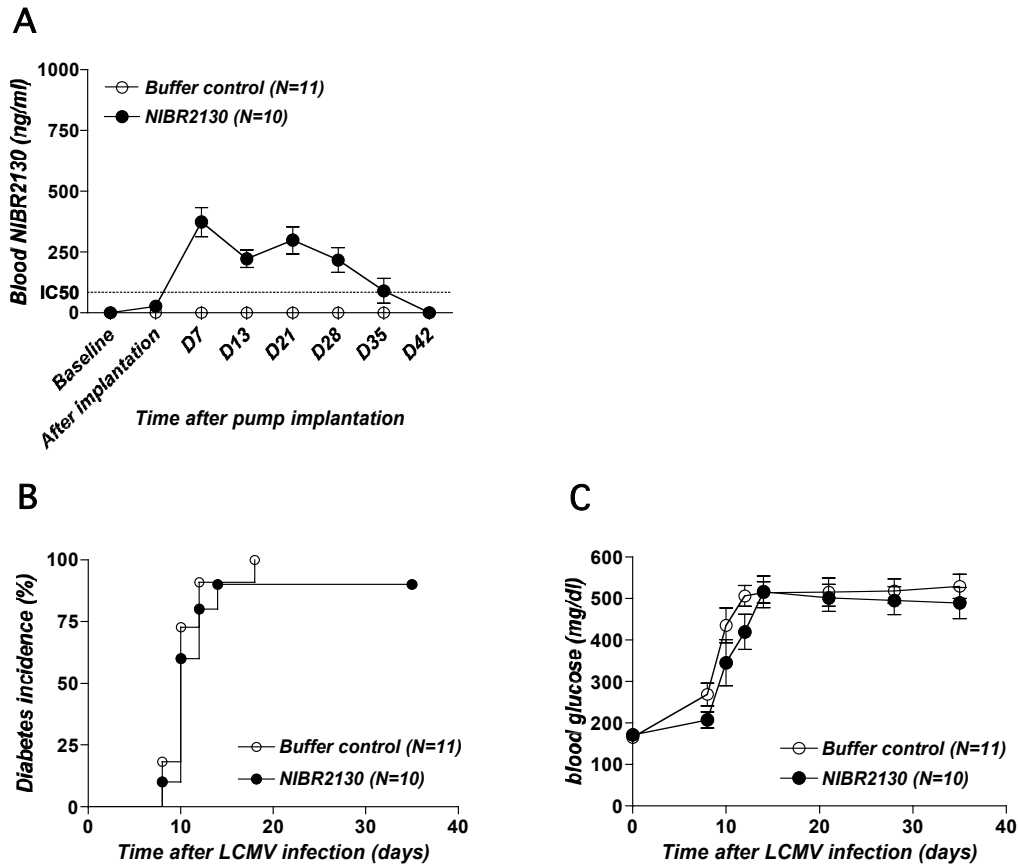
Figure 7: Inhibition of CXCR3 in RIP-LCMV-GP mice has no influence on T1D.

(A) Osmotic pumps were filled with NIBR2130 or buffer implanted under the skin of RIP-LCMV-GP mice and exchanged after two weeks. The delivery of the antagonist was verified by the measurement of the blood concentration of NIBR2130 at different times as indicated. Dotted line displays the IC_{50} of NIBR2130 (B and C) Antagonist-treated and untreated RIP-LCMV-GP mice were infected with a single dose of 5 x 10^4 pfu LCMV on day zero, and blood glucose was measured at days indicated (values >300 mg/dl were considered diabetic). Data are the mean ± SEM of 10-11 mice per group.

8.1.2 Inhibition of CXCR3 significantly delays the outcome of disease in RIP-LCMV-NP mice

Next I investigated how blockade of the CXCR3-CXCL10 interaction influences the development of autoimmune diabetes. Osmotic pumps filled with NIBR2130 or buffer were implanted into RIP-LCMV-GP and RIP-LCMV-NP mice for 4 weeks. One day after pump implantation the mice were infected with 5 x 10^4 pfu LCMV and blood glucose was measured on days indicated. No significant reduction in blood glucose

56

levels and diabetes incidence or onset were detected in RIP-LCMV-GP mice (fast-onset diabetes) treated with NIBR2130 compared to control mice (Figure 7B and C).
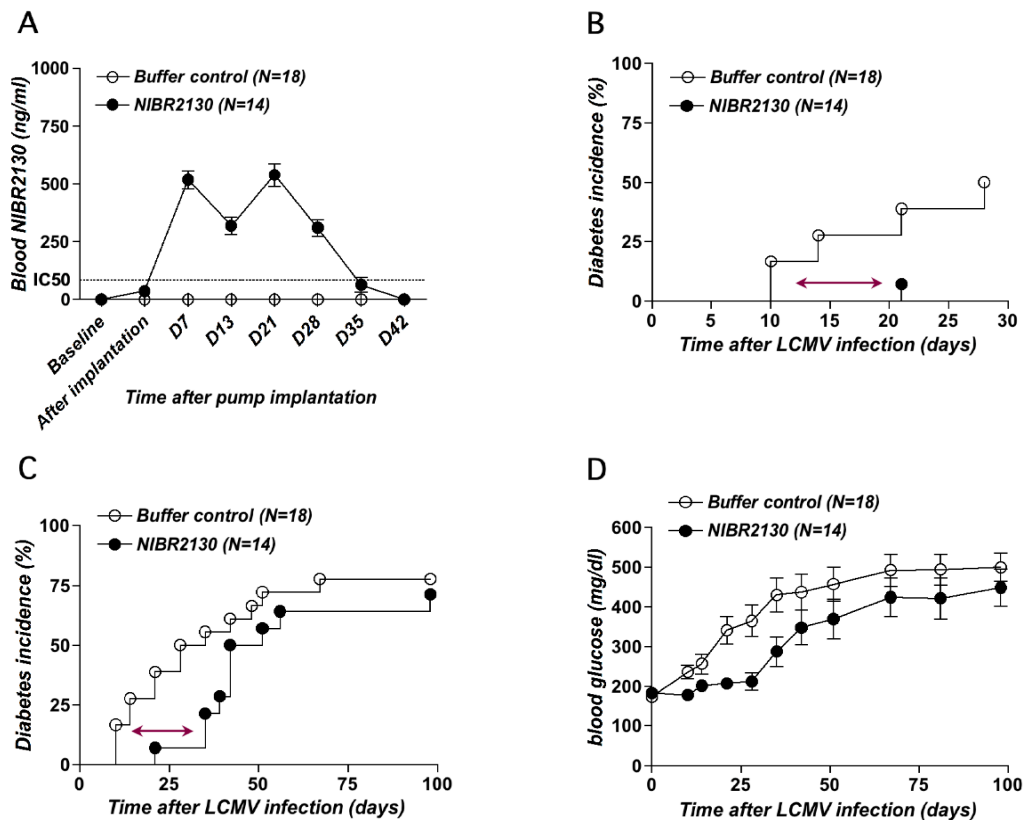
Figure 8: Inhibition of CXCR3 in RIP-LCMV-NP mice significantly delays the outcome of T1D.

(A) Osmotic pumps were filled with NIBR2130 or buffer and were implanted under the skin of RIP-LCMV-NP mice and exchanged after two weeks. The delivery of the antagonist was verified by the measurement of the blood concentration of NIBR2130 at different times as indicated. Dotted line displays the IC_{50} of NIBR2130 (B-D) Antagonist-treated and untreated RIP-LCMV-NP mice were infected with a single dose of 5×10^4 pfu LCMV on day zero, and blood glucose was measured at days indicated (values >300 mg/dl were considered diabetic). Note, in (B) the same data as in (C) are shown except that the incidence is only shown until day 28 post LCMV-infection to give an improved view of the significant delay in the development of T1D. Data are the mean ± SEM of 14-18 mice per group.

In contrast, onset of diabetes was significantly delayed in the antagonist-treated RIP-LCMV-NP (slow-onset of diabetes) mice compared to control animals (Figure 8C and D). Interestingly, the majority of NIBR2130-treated mice turned diabetic around day 35

after LCMV-infection (Figure 8C), which is immediately after the pumps have been removed and the antagonist concentration has dropped to baseline level (Figure 8A). Thus, it seems that only a continuous delivery of the CXCR3 antagonist NIBR2130 inhibits the development of virus-induced T1D.

These experiments indicate that a continuous blockade of CXCR3 might have an influence on virus-induced diabetes by delaying the incidence of disease in the slow-onset but not in the more aggressive fast-onset diabetes model.

8.1.3 Inhibition of CXCR3 has no effect on ß cell function

To investigate the impact of the neutralization of CXCR3 on ß cell function within islets NIBR2130-treated and control mice infected with LCMV were analyzed by glucose tolerance experiments. At day 28 after LCMV-infection mice that have not turned diabetic by that time were challenged with a single i.p. injection of 1.5 mg/g body weight glucose and the efficiency of regulating the blood glucose to normoglycemia was assessed over time. Both the NIBR2130 treated and the control mice showed increased blood glucose values of ~ 300 mg/dl at 10 minutes after glucose injection. The blood glucose levels declined similarly in NIBR2130-treated and control mice, with an approximate half-life of 20 minutes (Figure 9A). When the same assay was performed at day 49 post LCMV-infection NIBR2130-treated mice showed a slight but not significantly accelerated down-regulation of blood glucose compared to untreated control mice (Figure 9B).
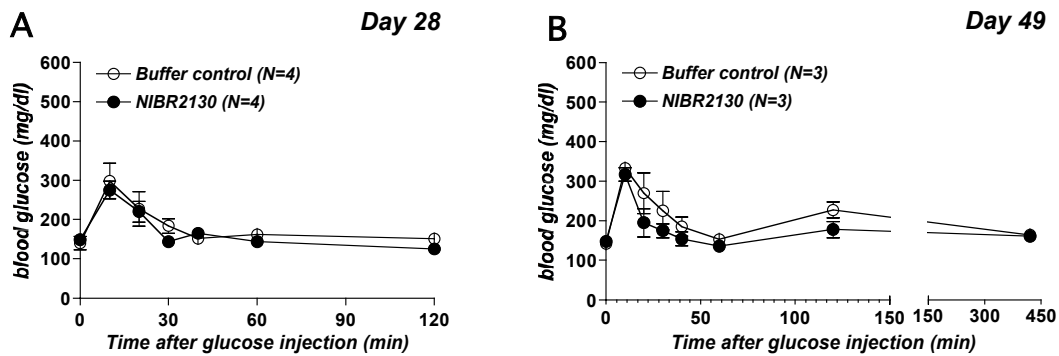
Figure 9: Inhibition of CXCR3 has no positive effect on impaired ß cell function.

Glucose tolerance assay. (A and B) At day 28 (A) and 49 (B) after 5 x 10^4 pfu LCMV-infection groups of 3-4 NIBR2130-treated and untreated RIP-LCMV-NP mice were challenged with a single i.p. injection of 1.5 mg/g body weight glucose, and blood glucose was measured at different time points as indicated. Data are the mean ± SEM of 3-4 non-diabetic mice per group.

8.1.4 Inhibition of CXCR3 has no influence on islet infiltration in virus-induced T1D

In order to identify the immunological mechanisms responsible for the significant delay in the onset of T1D, cellular infiltration of different leukocytes into the islets of Langerhans was analyzed by immunohistochemistry and an infiltration score was applied for statistical analysis. One possibility might be a decreased infiltration rate of aggressive islet-antigen-specific T cells. An alternative explanation for the delayed disease onset might be an increased recruitment of T_{regs}. Therefore, we compared protected, non-diabetic RIP-LCMV-NP mice treated with NIBR2130 with diabetic control mice (three mice per group) at day 28 after 5 x 10^4 pfu LCMV-infection. Pancreas sections were stained for insulin production as well as cellular infiltration by CD8+ T cells, T_{regs}, NK cells and CXCR3 expressing cells (Figure 10A). All mice assessed showed a similar reduction of insulin production as well as a similar infiltration pattern of the different immune cells analyzed. No difference between NIBR2130-treated and

untreated animals was observed. Interestingly, in NIBR2130-treated mice the amount of cells expressing CXCR3 within the infiltrations of islets was the same as in control mice (Figure 10A). Moreover, independently of the disease pattern islets from both mouse groups showed similar infiltration rates (Figure 10B). Some morphologically viable islet cells with insulin expression were found in both mouse groups. Nevertheless, most islets were already infiltrated and more than 30% of all islets analyzed had heavy intra-insular infiltration and/or remained as 'islet-scars'. Moreover, cells infiltrating islets were predominantly of the CD8$^+$ phenotypes and the amount of T$_{regs}$ within islets was not increased in the NIBR2130-treated mice compared with control animals. Approximately 10 T$_{regs}$ per mm^2 area of infiltration were found in both mouse groups analyzed (Figure 10C). These observations indicate that the observed delay in the onset of T1D is not due to a decreased infiltration rate or a redistribution of specific T cell subsets such as T$_{regs}$.

8.1.5 Neutralization of CXCR3 has no significant influence on the functional activity of LCMV-specific lymphocytes

CD8$^+$ T cells specific for the NP$_{396}$ peptide and the assistance of CD4$^+$ T cells are required to cause diabetes in RIP-LCMV-NP mice. Therefore, the functional activity of antigen-specific T cells after CXCR3 neutralization was assessed by staining for intracellular cytokines (ICCS) produced by T cells after *ex vivo* stimulation.
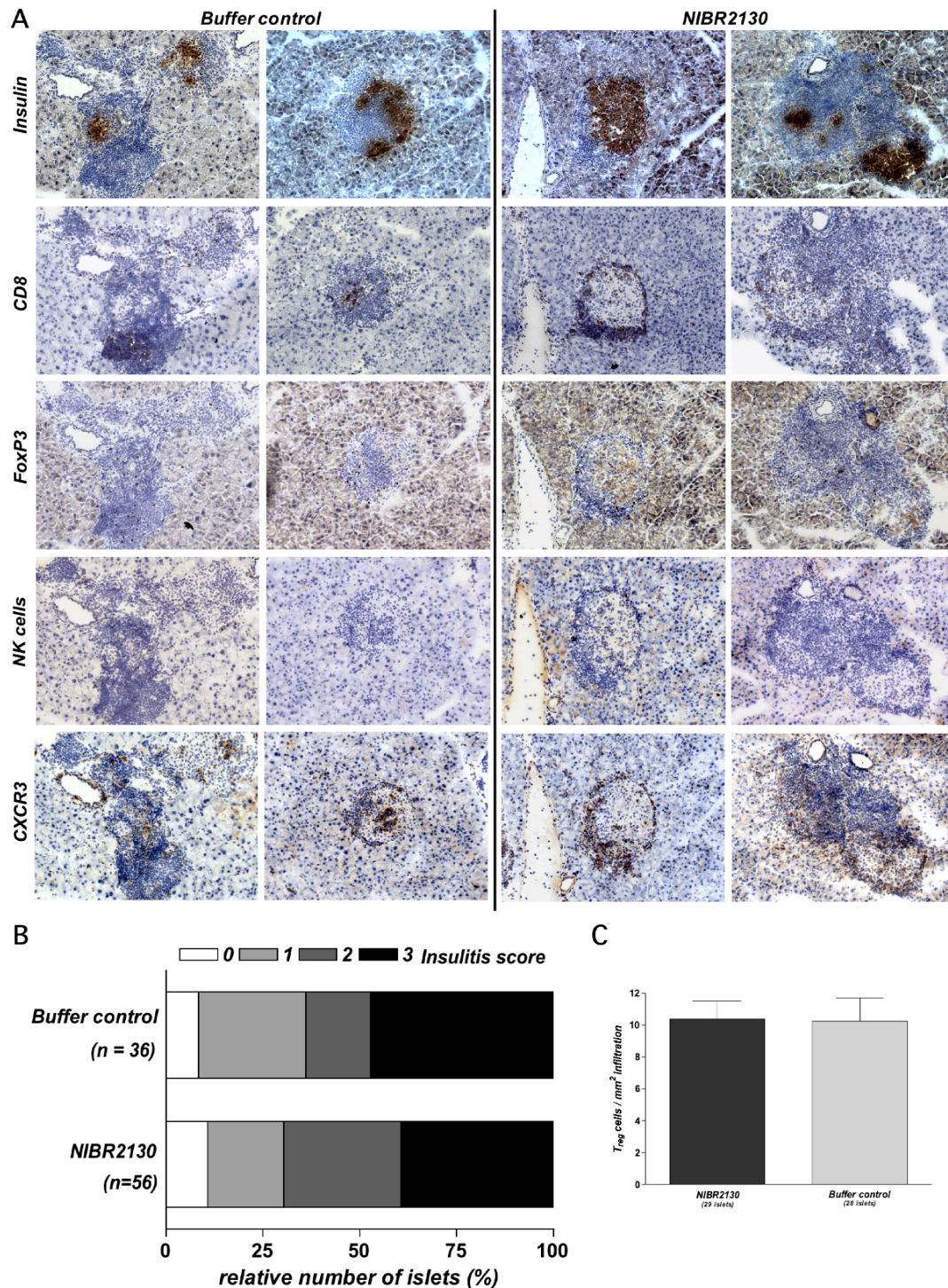
Figure 10: Inhibition of CXCR3 has no impact on different cell types infiltrating islets.

(A) Pancreas sections of NIBR2130-treated and untreated RIP-LCMV-NP mice at day 28 after LCMV-infection were probed for insulin production and infiltrations by $CD8^+$ T cells, T_{regs}, NK cells and CXCR3 expressing cells. (B) Insulitis score was obtained from sections of 3 mice per group (n=36, islets analyzed). Scoring system: 0, no infiltration; 1, some peri-insular infiltration; 2, heavy peri-insular infiltration with some intra-insular infiltrates; 3, heavy intra-insular infiltration and/or islet scars. (C) Evaluation of the amount of T_{regs} per mm^2 area of islet infiltration. Data are the mean ± SEM of 3 mice per group.

The different T cell subsets were overnight *ex vivo* stimulated with the immunodominant LCMV-NP$_{396}$ or LCMV-GP$_{33}$ peptide presented on MHC class I H-2D^b and with the LCMV-GP$_{61}$ peptide presented on MHC class II H-2IA^b molecules. Therefore, mice were treated with NIBR2130 by subcutaneously implanted osmotic pumps one day before 5 x 10^4 pfu of LCMV-infection in RIP-LCMV-NP mice. At day 7 and day 28 post-infection splenocytes as well as lymphocytes from pancreatic draining lymph nodes (PDLN) were isolated and different T cell subsets were analyzed for intracellular IFN-γ production after over night stimulation with NP$_{396}$, GP$_{33}$ or GP$_{61}$ peptides. On day 7 post-infection in the spleen of untreated control mice, approximately 7% and 2-3% of CD8$^+$ T cells were GP$_{33}$- and NP$_{396}$-specific, respectively. Moreover, a slight reduction was observed for both GP$_{33}$- and NP$_{396}$-specific CD8$^+$ T cells in the spleen as well as in the PDLN of NIBR2130-treated mice compared to control animals (Figure 11B). In contrast, only a few GP$_{61}$-specific CD4$^+$ T cells were found in both mouse groups (Figure 11C). On day 28 after LCMV-infection, no difference between NIBR2130-treated and control mice was found for the NP$_{396}$-specific CD8$^+$ T cells in the spleen as well as in the PDLN, whereas an increase of GP$_{33}$-specific CD8$^+$ T cells in the spleen was detected in antagonist-treated mice compared with control animals (Figure 11D). In spite of minimal differences in the presence of IFN-γ producing LCMV-specific T cells in NIBR2130-treated compared to control mice these data indicate that the neutralization of CXCR3 has no significant effect on the functional activity of LCMV-specific T cells in the spleen as well as in the PDLN during both the acute, anti-viral phase (day 7) as well as the memory, autoimmune phase (day 28) (Figure 11).
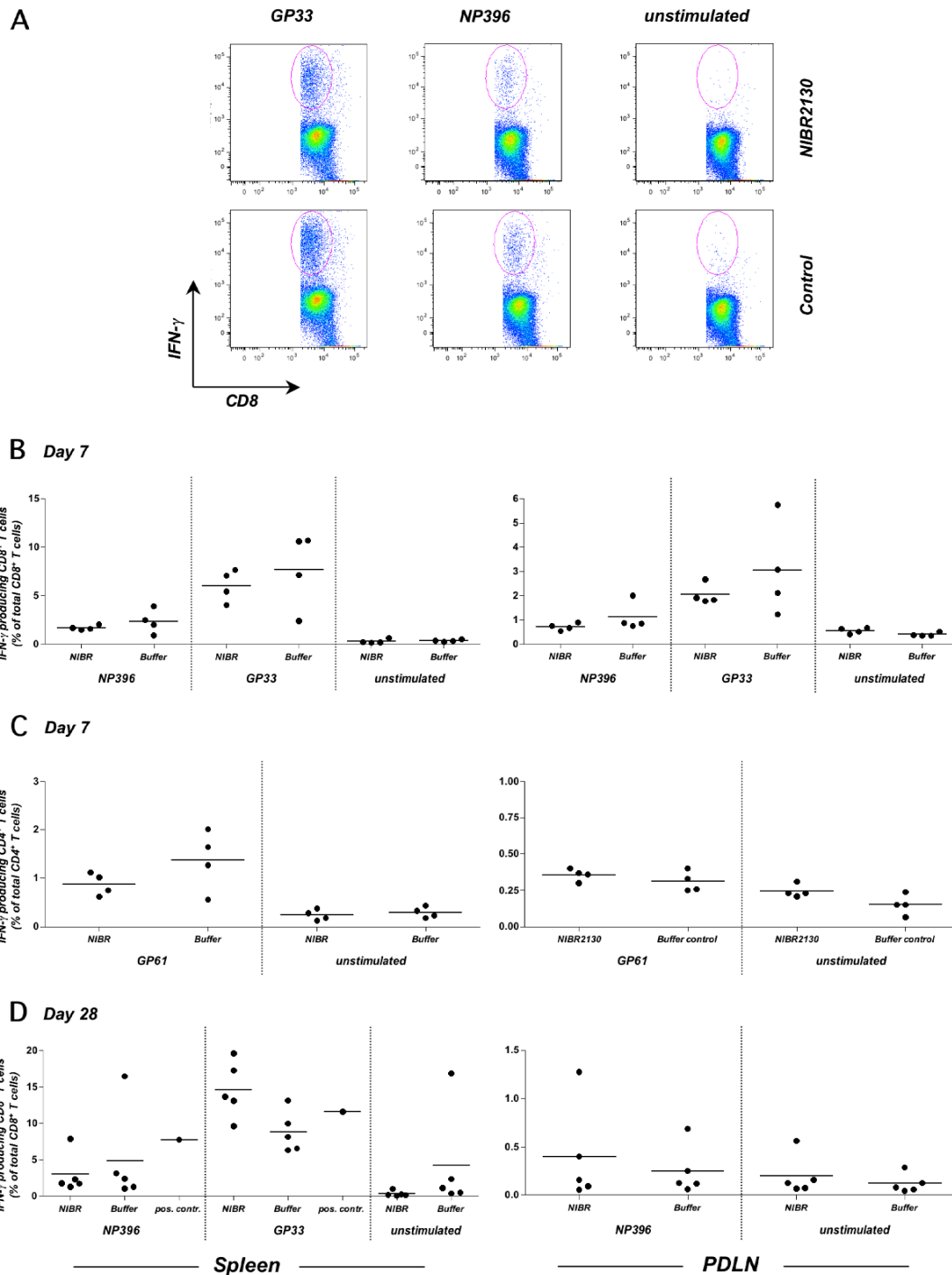
Figure 11: Inhibition of CXCR3 has no significant influence on the functional activity of LCMV-specific T cells.

(A) Representative dot plots of splenocytes of an NIBR2130-treated (upper panel) and untreated (lower panel) control mouse 7 days post-infection stained for surface CD8 and intracellular IFN-γ (left side, GP_{33} stimulated; middle, NP_{396} stimulated; right side, unstimulated) (B-D) The presence of GP_{33}-, NP_{396}- and GP_{61}-specific T cells on day 7 and 28 after LCMV-infection in the spleen and PDLN of NIBR2130-treated and untreated RIP-LCMV-NP mice was analyzed by ICCS (IFN-γ) after o/n *in vitro* stimulation with GP_{33}, NP_{396} or GP_{61} peptide. Data are the mean of 4-6 mice per group. (B and D) GP_{33}-, NP_{396}- specific CD8+ T cells. (C) GP_{61}-specific CD4+ T cells.

8.2 Project 2: JAM-C and its role in T1D

In this part of the project the influence of JAM-C on rolling and transmigration of leukocytes in T1D was characterized.

8.2.1 LCMV-infection results in an upregulation of JAM-C around the islets of Langerhans

To assess the kinetics of JAM-C expression pancreata from RIP-LCMV-GP mice were harvested at day 0, 4, 7, 10, 14, and 28 after i.p. infection with 1×10^4 pfu LCMV and analyzed by immunohistochemistry or immunofluorescence staining. JAM-C was upregulated around the islets predominantly at days 10 and 14 after LCMV-infection (Figure 12 left panel and Figure 13A). Interestingly, islet infiltration was most pronounced at the time of strongest JAM-C expression (Figure 12 and Figure 13A right panel). At day 10 to 14 post-infection most islets of LCMV-infected RIP-LCMV-GP mice showed massive peri- and intra-islet $CD8^+$ T cell infiltrations (Figure 12 right panel and Figure 13A right panel). The presence of high numbers of T cells in and around the islets resulted in the destruction of islet cells and impaired ß cell function that finally led to overt disease (Figure 12 middle panel).

For immunofluorescence stainings the constitutively expressed adhesion molecule, CD31, was used as an endothelial cell marker and the colocalization of JAM-C and CD31 was characterized by confocal microscopy (Figure 13B). Endothelial cells from pancreatic blood vessels are double-stained with JAM-C and CD31 (Figure 13A and B). As seen previously (Figure 12) a significant increase in fluorescence intensity of JAM-C expression was detected at day 10 to 14 after LCMV-infection (Figure 13C).
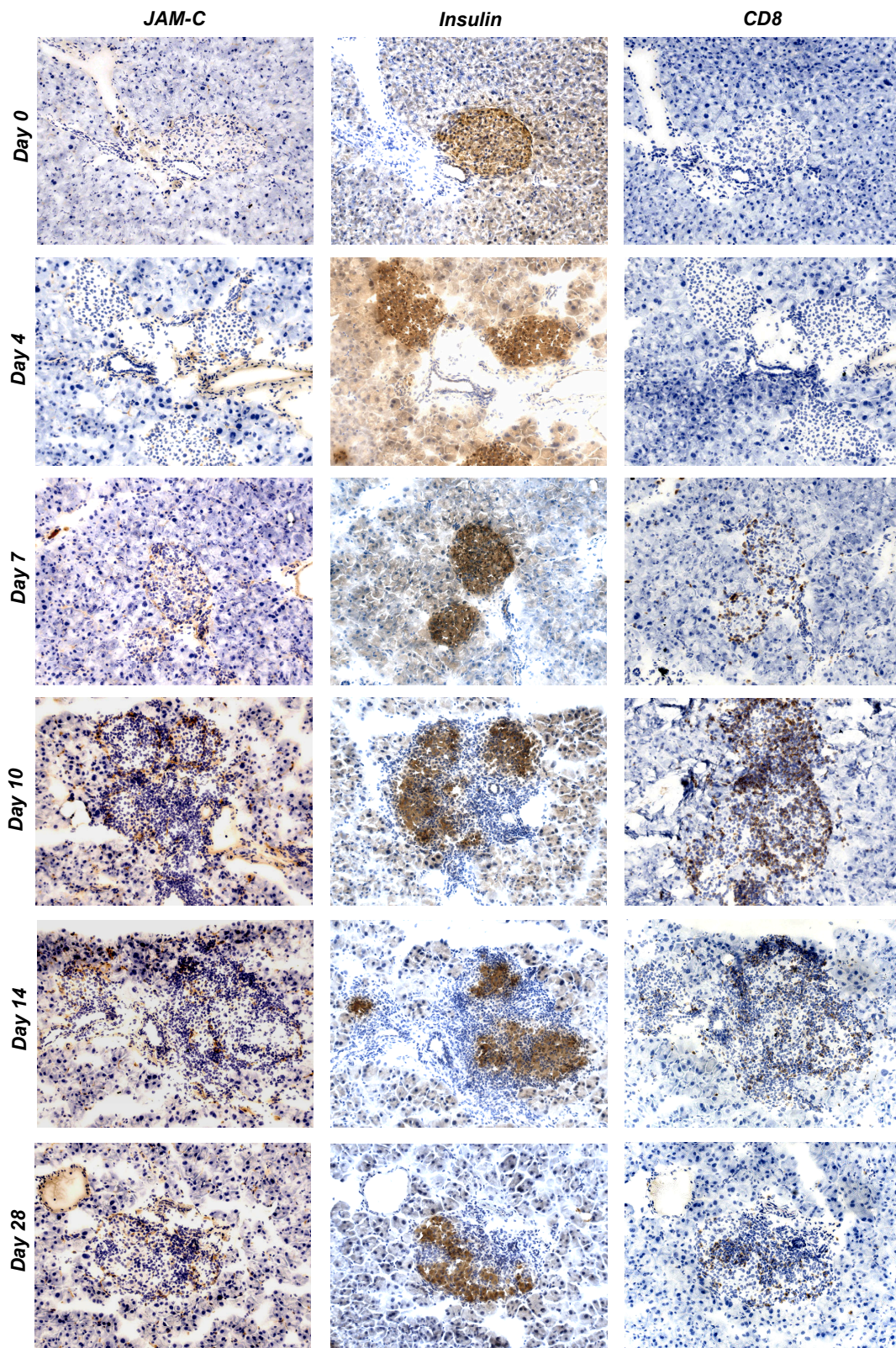
Figure 12: JAM-C expression correlates with islet infiltration and functional impairment.

Pancreas sections of RIP-LCMV-GP mice were probed for JAM-C expression, insulin production and CD8+ T cell infiltrations at different times after LCMV-infection.

For this analysis a histogram showing the average light intensity of the individual fluorescence channels in the image was performed. In comparison to day 0, days 2, 7, 21 and 28 showed significant differences with a p-value $p < 0.05$, whereas day 14 ($p = 0.0015$) and day 10 ($p = 0.0001$) showed a highly significant increase in the fluorescence intensity (Figure 13C). Additionally, these stainings confirmed the observation made in Figure 12 concerning the overlap between the increase of JAM-C expression and the peak of CD8$^+$ T cell infiltration (Figure 13A).

These experiments indicate that JAM-C is upregulated in the pancreas upon LCMV-infection and might therefore play a role in the immunopathogenesis of T1D in the RIP-LCMV model.

8.2.2 JAM-C blockade: Neutralization of JAM-C results in a decreased T1D incidence

Because JAM-C expression was upregulated around the islets at day 10 to 14 post LCMV-infection, at the peak of islet infiltration, the influence of JAM-C expression on the pathogenic processes of T1D particularly islet infiltration of autoaggressive T cells resulting in ß cell-destruction, was assessed. JAM-C was blocked with a neutralizing anti-JAM-C antibody that disrupts murine JAM-B/-C interactions (79). In RIP-LCMV-GP mice anti-JAM-C antibody (100 μg each injection) was administered i.p. one day before 1 x 10^4 pfu LCMV-infection and then at days 1, 2, 5, 8, 11, and 14 post-infection. Anti-JAM-C antibody-treated as well as control RIP-LCMV-GP mice displayed a similar initial diabetes incidence of more than 60% within the first 21 days after LCMV-infection.
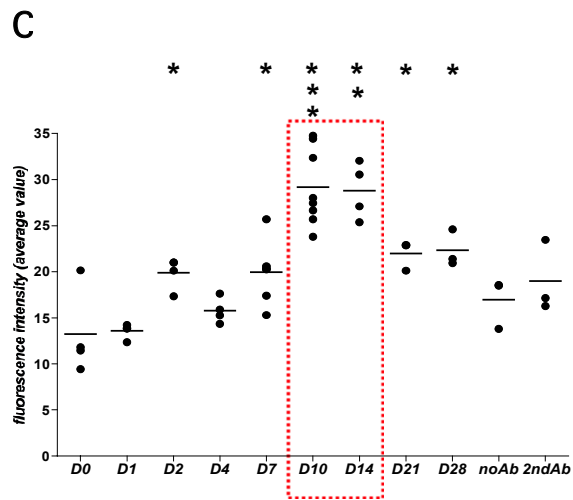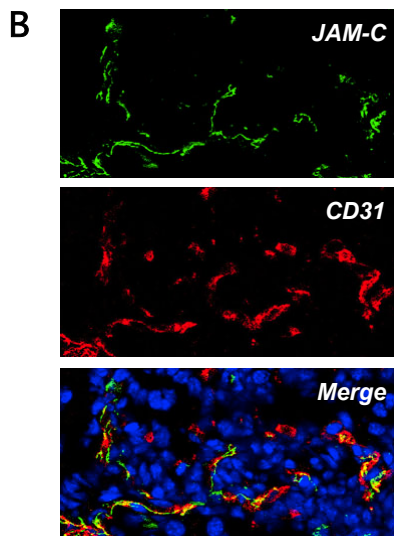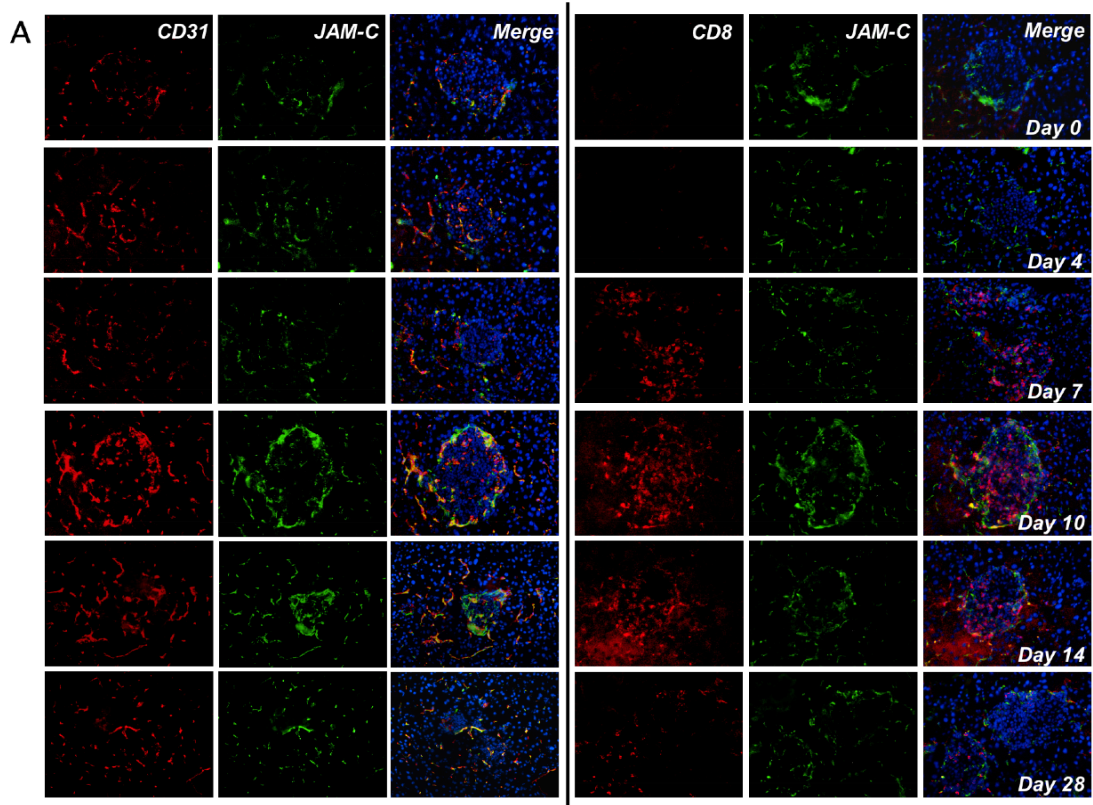
Figure 13: Expression of JAM-C after LCMV-infection.

(A) Pancreas sections of RIP-LCMV-GP mice at different times after LCMV-infection were analyzed for CD31 (red, left) and JAM-C (green) expression and CD8$^+$ T cell infiltrations (red, right) in the islets of Langerhans. (B) Colocalization analyzed for JAM-C (green) and CD31 (red) expression. (C) Evaluation of fluorescence intensity of JAM-C expression at different times after LCMV-infection. Bars representing mean of 3-8 islets each time point and statistical significance of the fluorescence intensity relative to day 0 were determined using the unpaired t test (*, $p < 0.05$; **, $p < 0.005$; ***, $p < 0.0005$).

Interestingly, neutralization of JAM-C lead to a reversion of T1D two months after LCMV-infection in that only 30% of the anti-JAM-C antibody-treated mice remained diabetic compared to 60% of diabetic control animals. Reverting mice remained non-diabetic throughout the whole observation period (Figure 14A). In RIP-LCMV-NP mice anti-JAM-C antibody (100 μg each injection) was administered i.p. one day before 1 x 10^4 pfu LCMV-infection and then at days 1, 3, 7, 11, 14, 18, 22, 26, 29, and 34 post-infection.
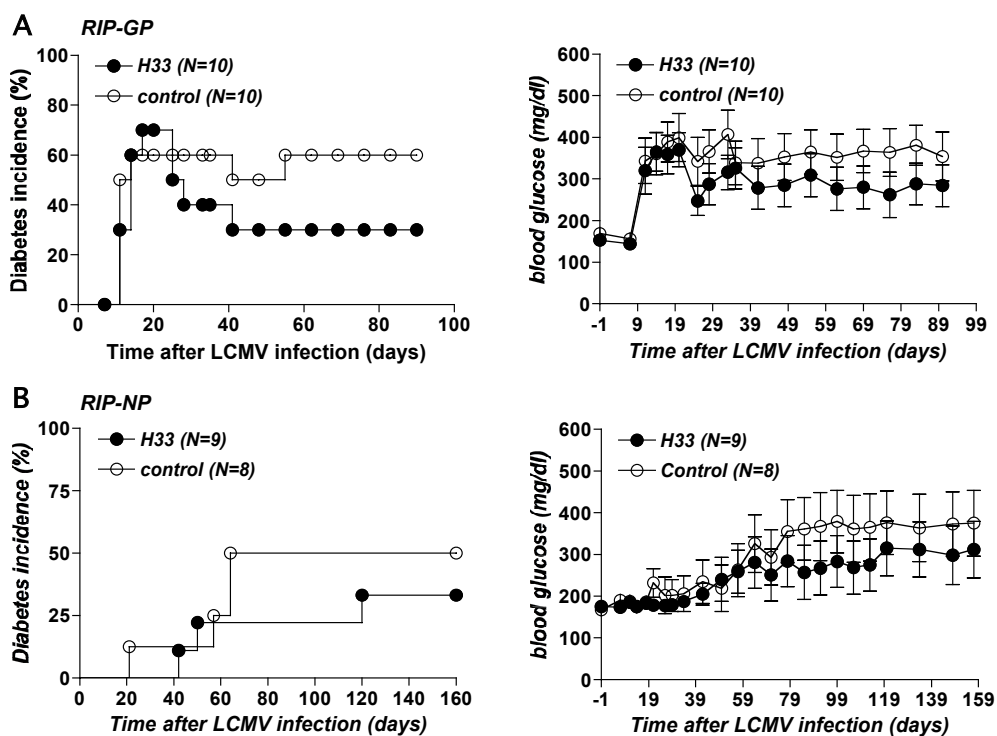
Figure 14: Neutralization of JAM-C reduces the development of T1D.

RIP-LCMV-GP (A) and RIP-LCMV-NP (B) mice were infected with LCMV. Mice were treated with 100 μg of anti-JAM-C mAb (H33) (closed circles) or were left untreated (open circles). Blood glucose was measured at weekly intervals (values >300 mg/dl were considered diabetic). Data are the mean ± SEM of 8-10 mice per group.

In the RIP-LCMV-NP mice the incidence of diabetes in JAM-C antibody-treated mice was slightly delayed and reduced to 30% compared to an incidence of 50% in control mice (Figure 14B). The rather high variation (SEM) in blood glucose values seen in the RIP-LCMV-GP as well

as in the RIP-LCMV-NP mice is due to the fact that some mice are already diabetic with blood glucose levels of up to 600 mg/dl and other are still in a non-diabetic region of <200 mg/dl. In addition, islet infiltration in RIP-LCMV-NP mice treated with JAM-C neutralizing antibody and control-treated animals was compared at the end point (six months after LCMV-infection). For semi-quantitative assessment of the islet infiltration, an infiltration score was applied and statistical evaluation was performed after double blind analysis of the data. No significant difference in islet infiltration was found in antibody-treated mice compared to control animals (Figure 15).

Nevertheless, the blocking studies in RIP-LCMV mice indicate that JAM-C plays a role in the pathogenesis of T1D, since neutralization of JAM-C resulted in a reversion of T1D in the fast-onset RIP-LCMV-GP model and a reduction of disease in the slow-onset RIP-LCMV-NP mouse line.
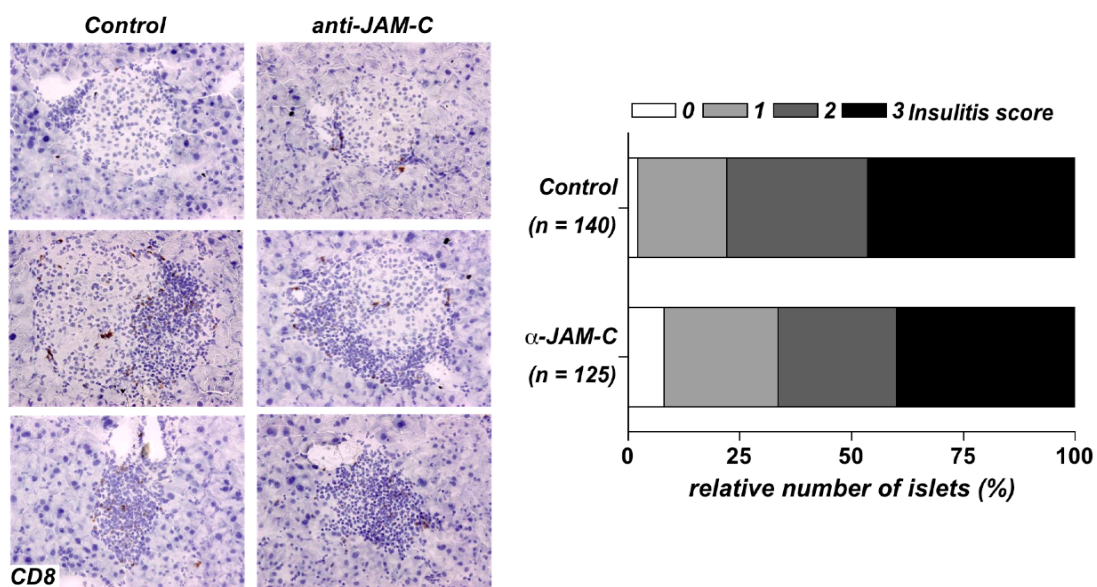
Figure 15: Neutralization of JAM-C has no influence on insulitis six months after LCMV-infection in RIP-LCMV-NP mice.

Insulitis score was determined in pancreas sections of 8-9 RIP-LCMV-NP mice per group that have been stained for CD8+ T cells (brown) (n=140, islets analyzed). Scoring system: 0, no infiltration; 1, some peri-insular infiltration; 2, heavy peri-insular infiltration with some intra-insular infiltrates; 3, heavy intra-insular infiltration and/or islet scars.

8.2.3 JAM-C blockade: The frequency of LCMV-specific T cells is not reduced after neutralization of JAM-C

Due to the fact that the blockade of JAM-C resulted in a reduction of the development of T1D the influence of JAM-C neutralization on the functional activity of LCMV-specific T cells was analyzed. Therefore, anti-JAM-C antibody (100 μg each injection) was administered i.p. one day before 1 x 10^4 pfu LCMV-infection and then at days 1, 3, 7, 11, 14, 18, 22 and 26 post-infection. At day 7 and 28 post-infection lymphocytes from the spleen and the PDLN were isolated and stained for CD8, CD4 and IFN-γ after overnight stimulation with the immunodominant LCMV-peptides NP$_{396}$, GP$_{33}$, and GP$_{61}$. At day 7 post-infection a slight reduction of GP$_{33}$-specific CD8$^+$ T cells, which in RIP-LCMV-NP mice reflect the anti-viral response rather than the autoimmune reaction, was observed in the spleen and PDLN of anti-JAM-C antibody-treated mice compared to control animals. In contrast, a slight increase in GP$_{33}$-specific CD8$^+$ T cells was found in the anti-JAM-C antibody-treated mice compared to control animals during the autoimmune phase on day 28 after LCMV-infection. The autoimmune response represented by NP$_{396}$-specific CD8$^+$ T cells showed similar appearance of IFN-γ producing CD8$^+$ T cells upon NP$_{396}$ *ex vivo* stimulation in the spleen as well as PDLN from both mouse groups at day 7 as well as day 28 (Figure 16A). As negative control a wildtype C57BL/6 mouse was included into all experiments. As previously mentioned in the RIP-LCMV-NP mice the LCMV-NP transgene is expressed in the ß cells as well as in the thymus resulting in the deletion of high-affinity NP-specific T cells. This leads to low-affinity NP-specific CD8$^+$ T cells in the periphery being not sufficient to induce

diabetes after LCMV-infection. For this reason they need the assistance of CD4$^+$ T cells to induce T1D and due to that fact the functional activity of GP$_{61}$-specific CD4$^+$ T cells was assessed. At both time points approximately 1% of CD4$^+$ T cells were found to be GP61-specific in all groups. In particular, no difference between anti-JAM-C antibody-treated and control animals was found at either day 7 or day 28 after LCMV-infection (Figure 16B). Finally, those results indicate that the neutralization of JAM-C resulting in a reduction in the outcome of virus-induced diabetes is not due to a decreased presence of LCMV-specific T cells.
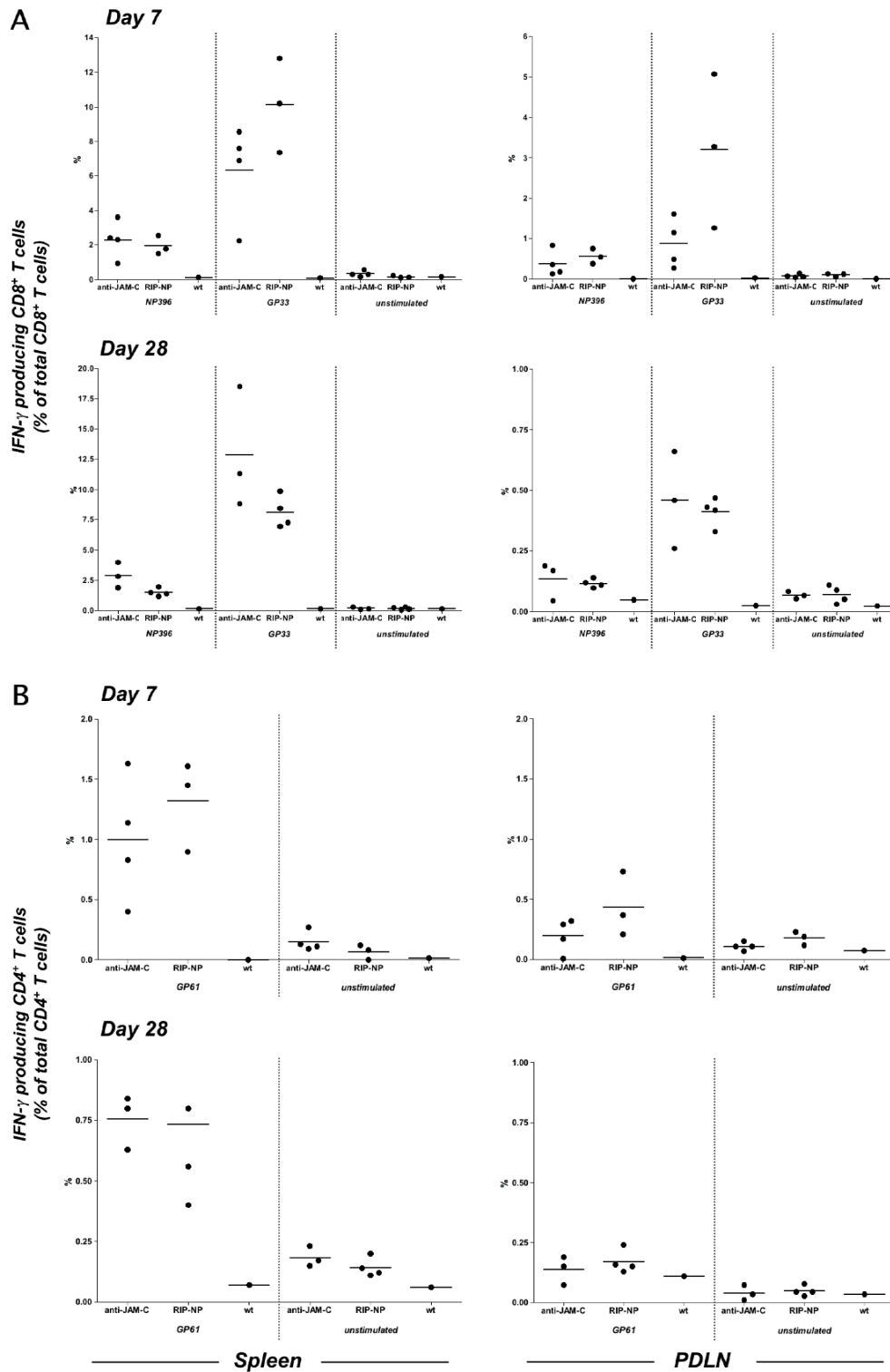
Figure 16: Neutralization of JAM-C has no significant influence on the functional activity of LCMV-specific T cells.

The presence of GP_{33}-, NP_{396}- and GP_{61}-specific CD8+ (A) and CD4+ (B) T cells on day 7 and 28 after LCMV-infection in the spleen and PDLN of anti-JAM-C antibody-treated and untreated RIP-LCMV-NP mice was analyzed by ICCS (IFN-γ) after o/n *in vitro* stimulation with GP_{33}, NP_{396} or GP_{61} peptide. Data are the mean of 3-4 mice per group. (A) GP_{33}-, NP_{396}- specific CD8+ T cells. (B) GP_{61}-specific CD4+ T cells. As internal controls unstimulated cells as well as lymphocytes from a wildtype C57BL/6 mouse (wt) were used.

8.2.4 JAM-C blockade: *In vivo* assessment of CD8+ T cell extravasation and ß cell-killing in a peptide/adjuvant transfer model

Due to the fact that after LCMV-infection expression of JAM-C is increased at the peak of islet infiltration and that blocking of JAM-C leads to a reduction of T1D we tried to visualize by two-photon microscopy the involvement of JAM-C in the real-time kinetics of cellular migration of diabetogenic T cells around the islets. The model used for our investigations employs the RIP-LCMV-GP x MIP-GFP mice that are expressing the green fluorescent protein (GFP) under the control of the mouse insulin promoter (MIP) specifically in the ß cells of Langerhans. To visualize the autoreactive T cells 1.5×10^7 naïve splenocytes of DsRed+ TCR-transgenic P14 mice, which harbor CD8+ T cells specific for the GP_{33} epitope, were transferred intravenously into RIP-LCMV-GP x MIP-GFP mice on day 0. One and 3 days later the mice were immunized i.p. with 2 mg GP_{33} peptide and additionally with 50 μg of Toll-like receptor (TLR) 9-binding CpG to initiate proinflammatory reactions. Six days after adoptive transfer of P14 splenocytes, 500 μg of TLR3-binding virus-related double stranded RNA-repeat polyinosinic-polycytidylic acid (Poly(I:C)) was administered i.p. to mimic a viral infection and to upregulate the MHC class I molecules. In this *in vivo* peptide/adjuvant stimulation model the DsRed+ GP_{33}-specific CD8+ T cells got activated and migrated to the pancreas where GP is expressed on pancreatic ß cells. This led to the destruction of ß cells followed by the development of diabetes in a highly synchronized fashion within 8 to 10 days after P14 transfer (Figure 18A). This migration into pancreas and the interaction between splenocytes and ß cells was further visualized by the two-photon microscopy, which

enabled the detection of red fluorescent splenocytes within green islets. To achieve this *in vivo* visualization of islet cells on cellular basis in real-time, a complex surgical preparation of the pancreas was performed. The mouse was first anesthetized with a ketamine (120 mg/kg) / xylazine (6 mg/kg) mixture (injected i.p.). After shaving the belly area the skin was cleaned with 70% isopropanol and an incision was made into the abdominal region to expose the spleen and the pancreatic tail region (Figure 17A). After removing of the spleen by cauterizing the splenic arteries, the pancreatic tail was gently exposed, fixed with glue on a custom-designed imaging stage and immersed in saline buffer (Figure 17B and C). To ensure an *in vivo* situation the vascular supply and oxygen pressure had to be kept intact and the body temperature had to be maintained during the whole imaging process. Therefore, the custom-designed imaging stage was surrounded with a basin filled with saline buffer that was continuously heated to 37°C by heating staves (Figure 17D). Finally, the mouse on the custom-designed imaging stage was carried to the two-photon microscopy for visualization of the infiltrated islets (Figure 17E and F). On a routine basis the mouse remained for 2-4 hours on the imaging stage for intra-vital microscopy and recording of cellular migration into the islets of Langerhans.

In our study two mice challenged with the peptide/adjuvant transfer model were repeatedly treated with anti-JAM-C antibody (100 μg) at days -1, 1, 3, 5 and 6. We found that the blockade of JAM-C did not alter the kinetics of diabetes onset, with both animals that were analyzed by two-photon microscopy turning hyperglycemic in the expected time-range between day 7 and 9 compared with peptide/adjuvant challenged but antibody untreated control mice (Figure 18B).
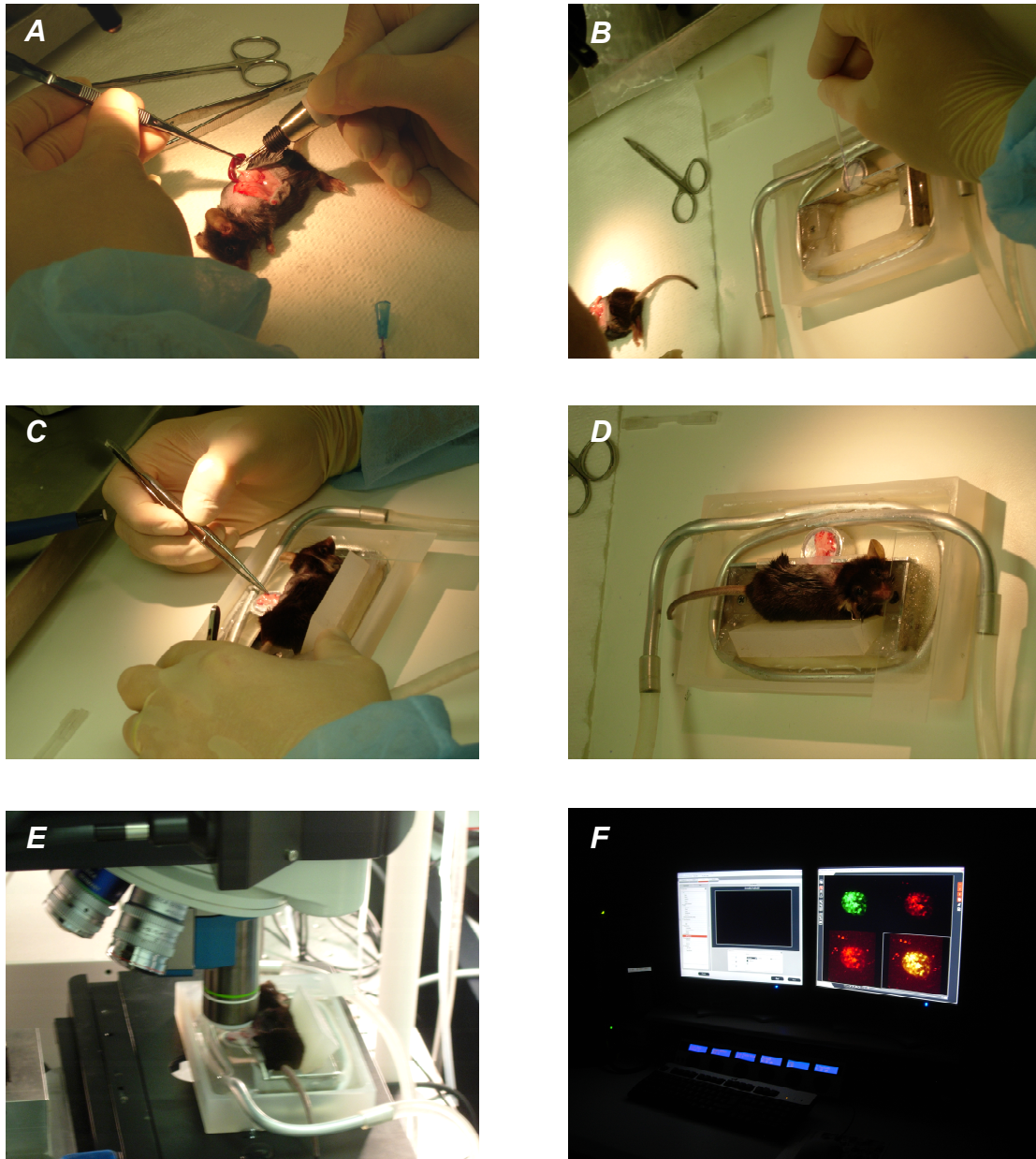
Figure 17: Surgical preparation of the pancreas for real-time imaging by two-photon microscopy.

(A) Before surgery, the mouse was anesthetized and belly area was cleaned and shaved. An incision was made in the belly region and after exposing the spleen and the pancreatic tail region the spleen was cauterized from the pancreas. (B and C) The pancreatic tail was fixed with glue on a custom-designed imaging stage and immersed in saline buffer. (D) The imaging stage was surrounded with a saline buffer filled basin that was continuously heated to 37°C. (E and F) The entire real-time imaging stage including the two-photon microscope.

Nevertheless, the extravasation and islet infiltration of aggressive P14-splenocytes might be affected by the anti-JAM-C antibody treatment. Therefore, the diabetogenic immune response at two distinct phases,

i.e. around the diabetic threshold in an animal that turned diabetic at day 8 post transfer with a blood glucose value marginally over 300 mg/dl and in a already severely diabetic one at day 7 post transfer, with blood glucose over 500 mg/dl, was analyzed. The relative contribution of CD4$^+$ T cells, CD8$^+$ T cells and B cells was determined by flow cytometry and it was found that the majority of infiltrated cells in the pancreas were CD8$^+$ T cells (Figure 18C). B cells and CD4$^+$ T cells represented only a minor component in mouse 2, whereas both subsets were virtually absent in mouse 1. Due to the GP$_{33}$-specific *in vivo* stimulation, CD8$^+$ T cells were generally overrepresented in the spleen.

ß cell decay was evident *in vivo* in both mice, and is best shown by presence of single ß cell clusters as observed in mouse 2 (Figure 18D, white arrows). In addition, real-time 3D monitoring of vascular stainings revealed extensive vasodilatation of the microvasculature surrounding the islets (Figure 18D). The fact that the blood flow was fully maintained also confirmed the physiologic conditions of our imaging approach. In mouse 1, an extensive DsRed$^+$ infiltrate was visualized in the immediate neighborhood of the ß cells (Figure 18D). In line with previous findings during the early diabetic phase of this model, the majority of the cells appeared to arrest in attachment to the ß cells for prolonged time periods. Such arrest was verified in 3 individual islets for approximately 5 minutes.

Finally, a 60 minutes 3D image series of the *in vivo* behavior of diabetogenic cells during the late stage of diabetes development in mouse 2 (Figure 19B) was compared with a peptide/adjuvant challenged RIP-LCMV-GP x MIP-GFP control mouse (Figure 19A). Continuous local circulation along the entire duration of the movie was

verified by the sporadic detection of rapidly moving DsRed+ cells in the blood flow (Figure 19B – first frame, red lines).
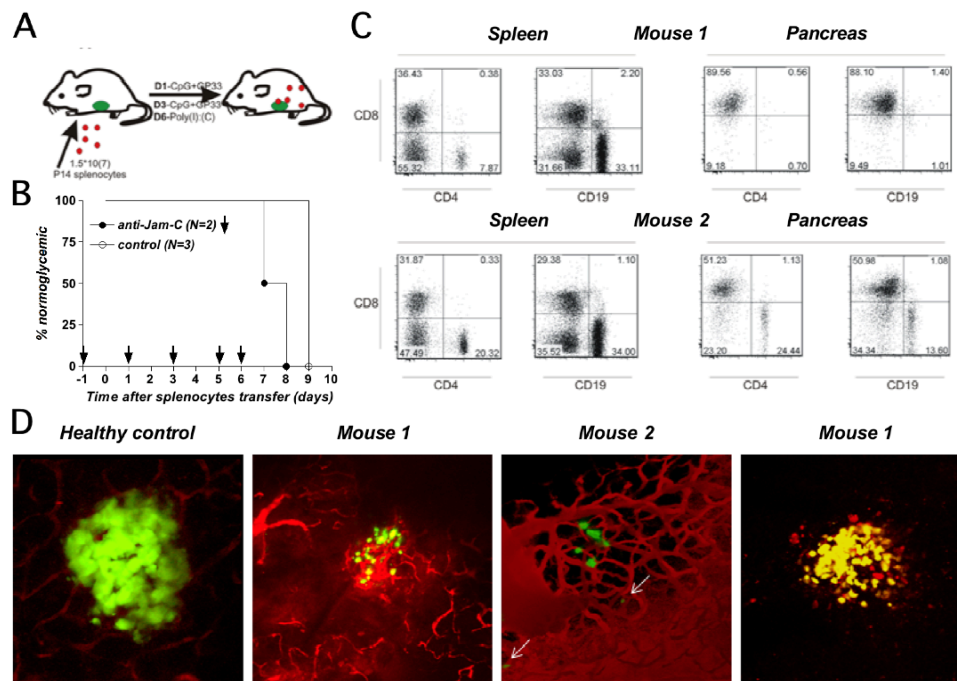
Figure 18: Jam-C blockade does not prevent CD8+ T cell extravasation and ß cell killing *in vivo* in the transfer model with peptide/adjuvant challenge.

(A) Schematic presentation of the peptide/adjuvant challenged model. 1.5×10^7 DsRed+ P14 splenocytes were transferred to RIP-LCMV-GP x MIP-GFP mice at day 0 and subsequently stimulated *in vivo* with 2 mg GP_{33} peptide and 50 µg CpG i.p. at day 1 and 3. Finally, 500 µg Poly(I:C) was injected i.p. at day 6. (B) Diabetes incidence in two groups of RIP-LCMV-GP mice challenged with peptide/adjuvant. Additionally one group was treated with 100 µg of anti-JAM-C mAb at days -1, 1, 3, 5 and 6 (as arrows indicated). (C) CD8+ T cell, CD4+ T cell and B cell populations in spleen and pancreas of anti-JAM-C mAb treated group. (D) Visualization of pancreatic islet cells by two photon-microscopy of an untreated healthy control and of two anti-JAM-C mAb treated and peptide/adjuvants challenged mice (red dots, DsRed+ P14 splenocytes; green, ß cells expressing GFP; red network, vascular system).

The final time frames of the Figure 19B show the real-time injection of fluorescently labeled dextran in order to provide accurate orientation of the vascular network. The islets had likely lost some of their ß cell mass as seen in their irregular shape but obviously still provided a significant source of MHC-presented antigen enabling a minority of the cells to arrest (Figure 19A and B, e.g. yellow arrowheads in the first

frame). There were different migration behaviors of individual cells observed during the whole imaging procedure. To visualize this migration pattern the DsRed+ cells had have been marked by red lines. Some DsRed+ cells just passed by, whereas some seemed to interact with remaining intact ß cells. One cell stuck out by moving to a ß cell, arresting there for several minutes, moving away and moving back once more before leaving the islet (Figure 19B).

Compared to the diabetogenic behavior of a peptide/adjuvant challenged RIP-LCMV-GP x MIP-GFP control mouse blocking of JAM-C did not prevent diabetogenic T cells extravasation, destruction of ß cells followed by the development of T1D in the P14-transfer RIP-LCMV model.

A *Untreated control*
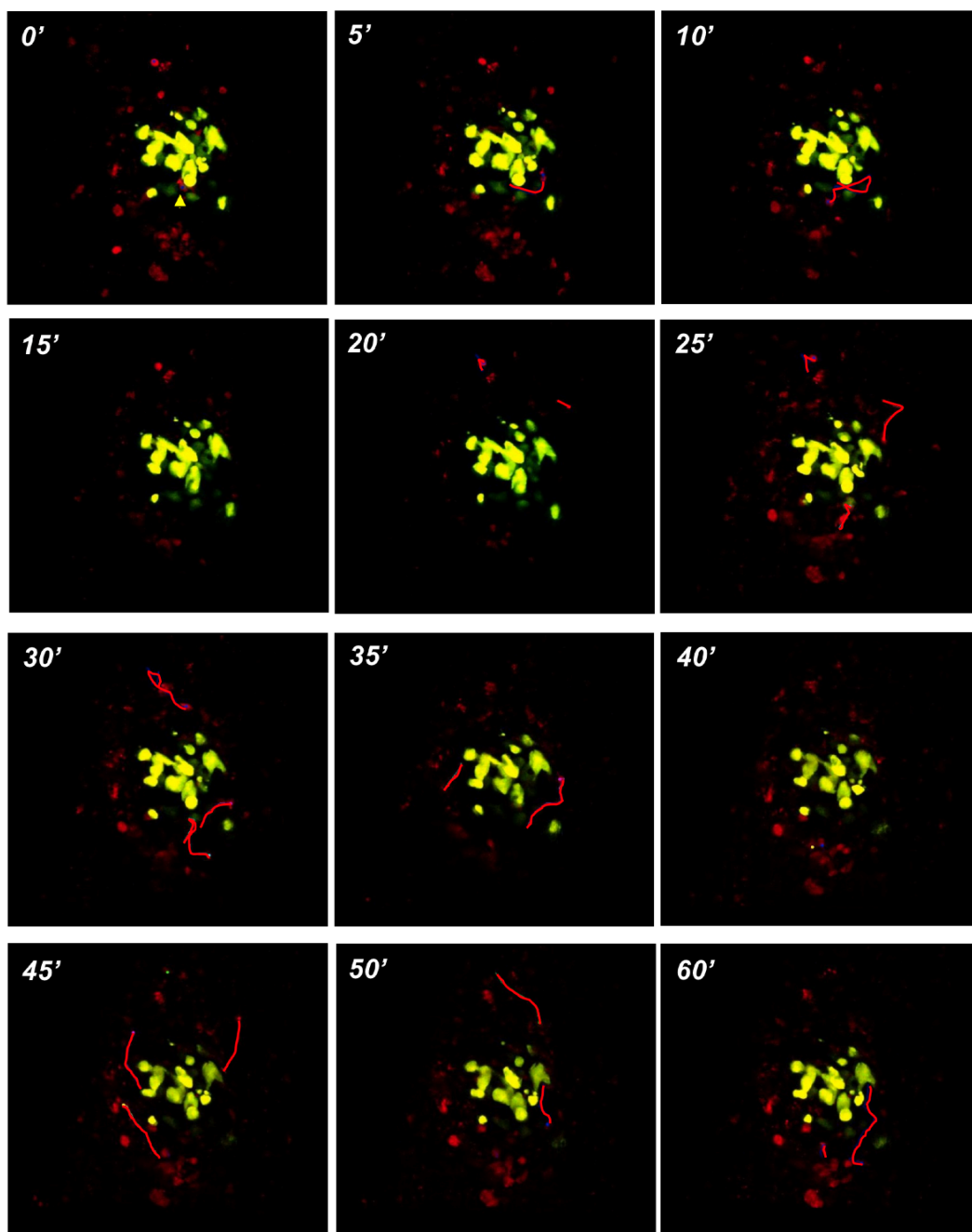
B *Anti-JAM-C antibody treated*
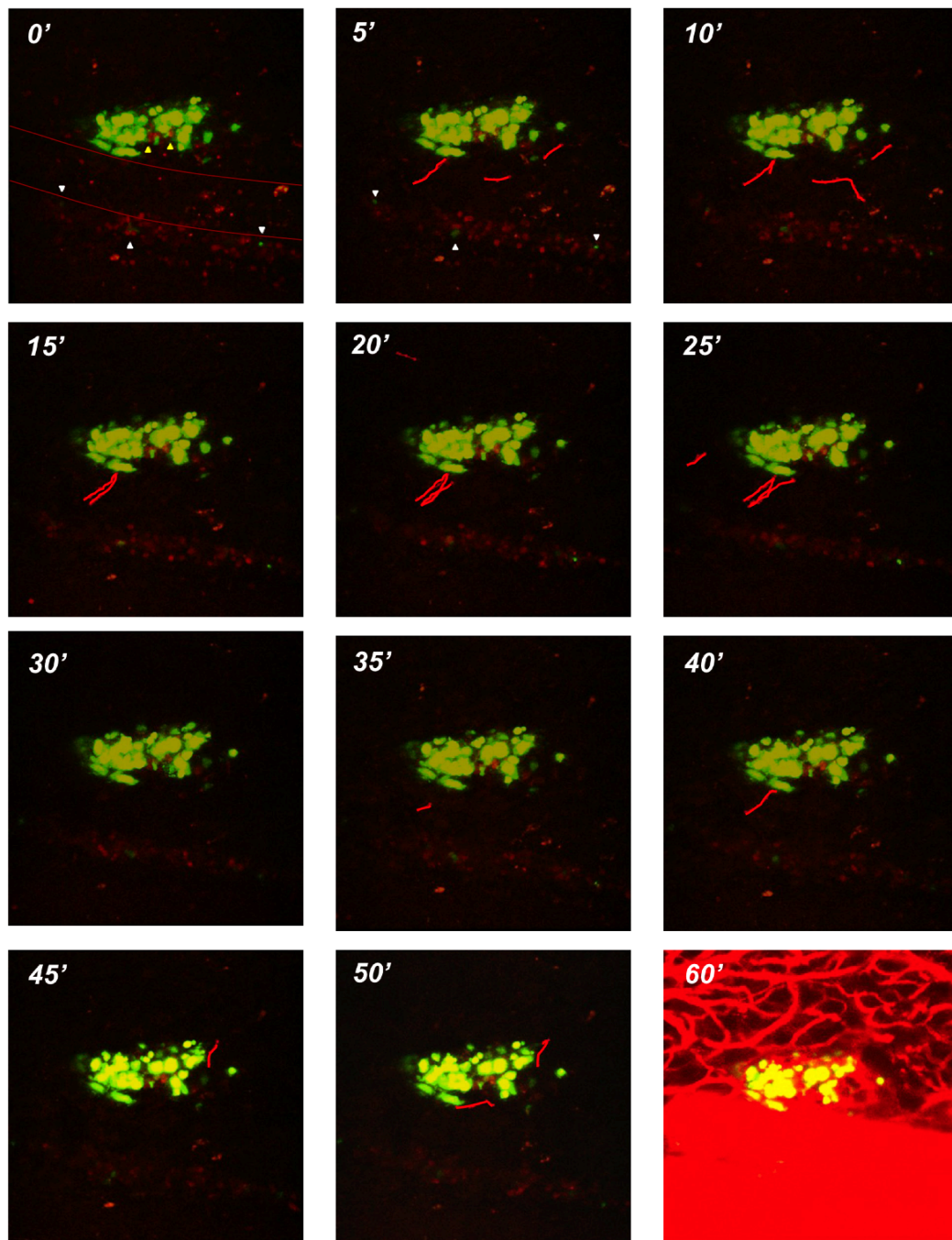
Figure 19: 60 minutes 3D image series of the *in vivo* behavior of diabetogenic cells during diabetes development.

Intravital/two-photon microscopy at day 8 after peptide/adjuvants challenge. 60 minutes 3D image series of the migration of DsRed[+] P14 splenocytes (red) to the islets of Langerhans of RIP-LCMV-GP x MIP-GFP mice (green) without (A) or with treatment of JAM-C neutralizing antibody (B). (A and B) Yellow arrowheads indicate ß cells with a significant source of MHC-presented antigen enabling a minority of the cells to arrest. (B) Red lines at time 0 mimic a pancreatic vessel. White arrowheads show phagocytic cells carrying ß cell-derived GFP locally engaging in interactions with T cells. Red marks visualize the migration behavior of some DsRed[+] splenocytes. After 60 minutes a fluorescently labeled dextran was injected to visualize the vascular network.

8.2.5 JAM-C overexpression: Characterization of JAM-C expression on pancreatic endothelial cells of transgenic pHHNS-JAM-C mice

Pancreatic JAM-C expression was characterized in transgenic mice overexpressing JAM-C under control of the Tie2-promotor specifically on endothelial cells (pHHNS-JAM-C mice) (92). Pancreas sections from pHHNS-JAM-C transgenic and wildtype mice were analyzed by immunofluorescence staining. In particular, pancreas tissue sections were double-stained with JAM-C and CD31, which was used as a specific endothelial cell marker. We found colocalization of JAM-C and CD31 on pancreatic blood vessels throughout the whole section and an increase in JAM-C expression in the pancreas of pHHNS-JAM-C transgenic mice compared with wildtype animals (Figure 20A). Western blotting using total tissue lysates of pHHNS-JAM-C transgenic mice compared to control mice revealed an increase in JAM-C expression predominantly in the lung and the liver. However, no JAM-C upregulation was detected in total tissue lysate of pancreata of uninfected pHHNS-JAM-C transgenic mice compared with control animals (Figure 20B). One observation for this discrepancy between the results obtained from immunohistochemistry and Western blotting might be that the observed increase of JAM-C expression in the immunofluorecence evaluations was restricted locally to pancreatic blood vessels. Therefore, the use of total tissue lysate might have resulted in a dilution of the JAM-C signal to a degree that did not allow for detection of the JAM-C upregulation by Western blot analysis. Even at day 10 after LCMV-infection no upregulation of JAM-C expression was found although our initial studies demonstrated that JAM-C expression is increased at day 10 to 14 after LCMV-infection (Figure

13 and Figure 20B). In contrast, we found a significant increase of JAM-C expression in the liver and the lung of pHHNS-JAM-C mice by Western blot (Figure 20B). However, in both organs the relative mass of endothelial cells is much higher than in the pancreas.

These results indicate that JAM-C seems to be upregulated in pHHNS-JAM-C transgenic mice compared with control mice as clearly demonstrated by immunohistochemistry. However, this increase is not detectable in whole pancreatic tissue lysates by Western blot analysis.
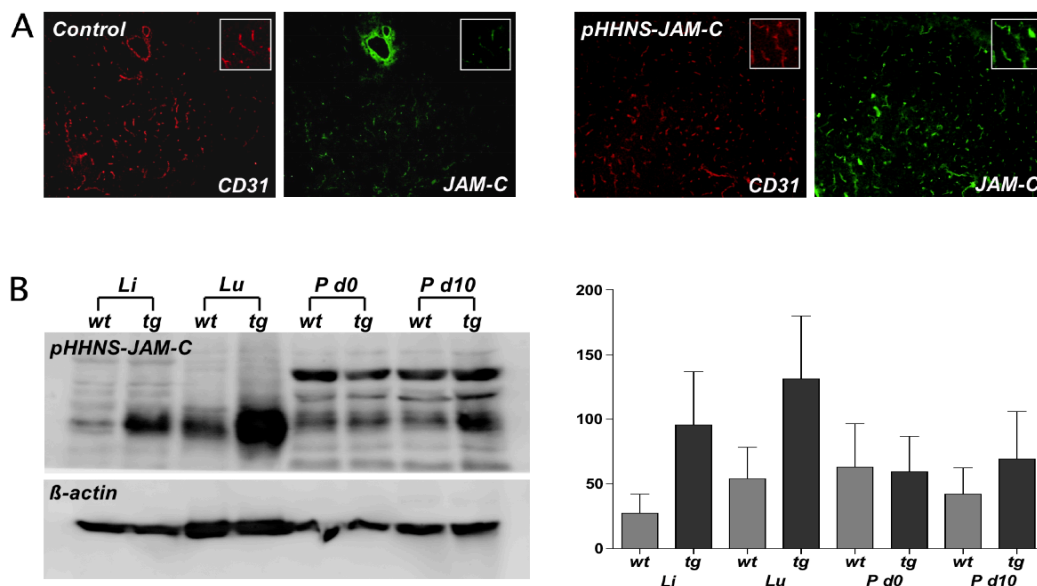
Figure 20: Characterization of JAM-C expression in the pancreas of pHHNS-JAM-C transgenic mice.

(A) Immmunofluorescence staining of pancreas sections of pHHNS-JAM-C transgenic mice (tg) compared to control mice (wt) (JAM-C, green; CD31, red). (B) Western blot analysis of JAM-C overexpression from total tissue lysates obtained from liver (Li), lung (Lu) and pancreas (P). Mean ± SEM of four different Western blot analysis of two mice each. Note that no significant upregulation of JAM-C expression was detectable even at day 10 after LCMV-infection.

8.2.6 JAM-C overexpression: Virus-induced diabetes is not accelerated

Previously we could show that blocking of JAM-C with a neutralizing antibody partially reduced T1D. To further analyze the influence of

JAM-C the pHHNS-JAM-C transgenic mice overexpressing JAM-C on endothelial cells were crossed with RIP-LCMV-GP and RIP-LCMV-NP mice. In the RIP-LCMV-GP lines all mice turned diabetic in a highly synchronized fashion between day 12 and 15 approximately 60 to 80% of all mice developed T1D regardless of the transgenic JAM-C expression (Figure 21A). The development of disease in male, single transgenic RIP-LCMV-NP mice followed a similar pattern as seen in RIP-LCMV-GP mice (Figure 21B), whereas the single transgenic RIP-LCMV-NP females turned diabetic within the expected time range of 2 to 5 months (Figure 21C). However, the kinetics and incidence of T1D was similar in double transgenic RIP-LCMV-NP x pHHNS-JAM-C mice (Figure 21C).

In summary, we observed that upregulated endothelial JAM-C expression did not have any effect on LCMV-induced T1D neither in the fast-onset RIP-LCMV-GP line (Figure 21A) nor in the slow-onset RIP-LCMV-NP line (Figure 21B and C). Thus, it appears that increased endothelial JAM-C expression cannot accelerate the severity of disease.

8.2.7 JAM-C overexpression: No influence on islet infiltration, viral clearance or the presence of LCMV-specific T cells

In order to confirm that increased JAM-C expression has only a minor effect on the immunopathology of virus-induced diabetes, mechanistic evaluations were performed. First, the cellular infiltration into islets of Langerhans was analyzed. Pancreata of RIP-LCMV-GP x pHHNS-JAM-C and RIP-LCMV-GP mice were harvested at day 6 after i.p. infection of 1 x 10^4 pfu LCMV and stained with Hämatoxylin.
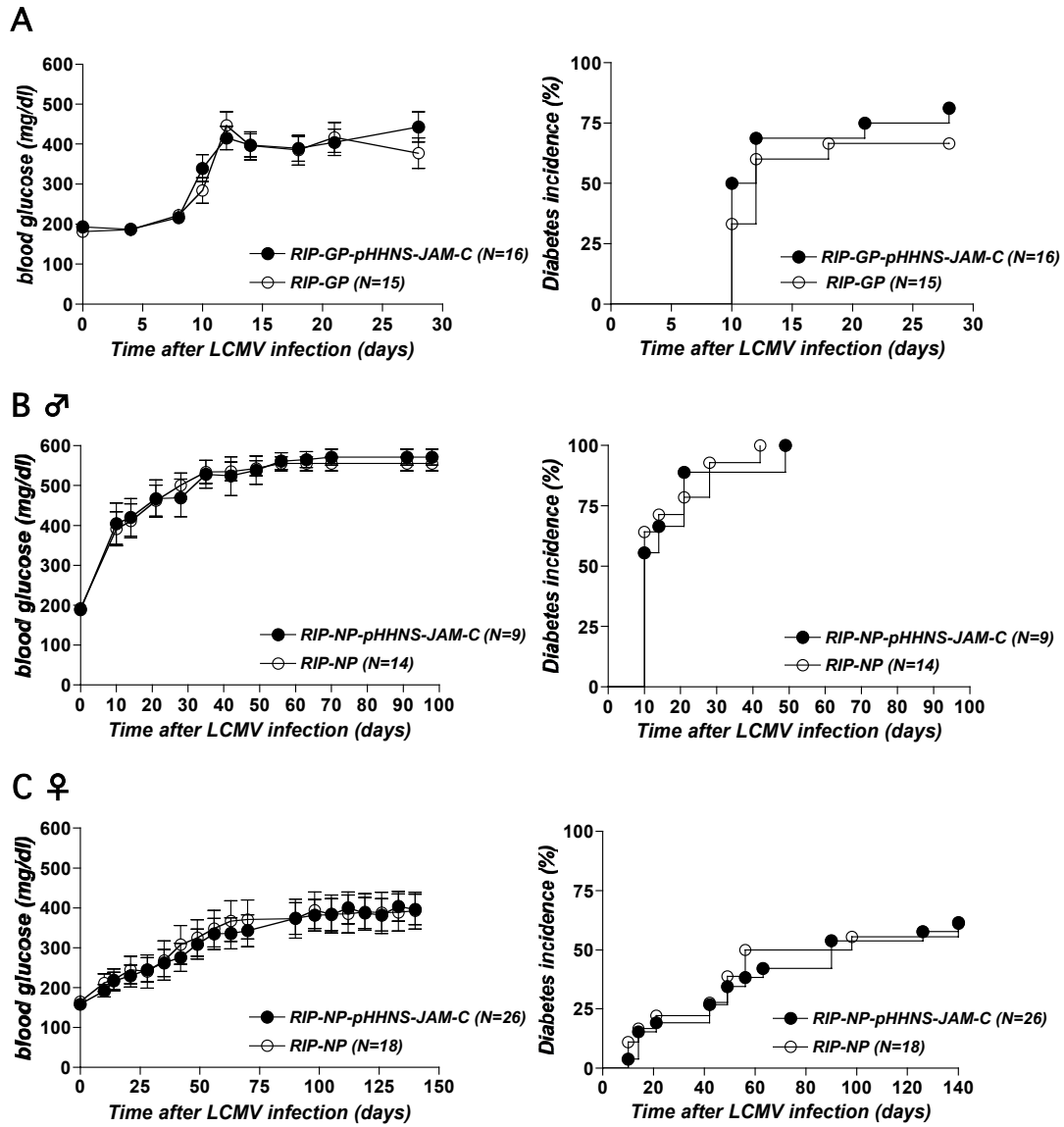
Figure 21: JAM-C overexpression does not influence the outcome of T1D.

(A-C) Mean blood glucose levels (left panels) and diabetes incidence (right panels) of single transgenic RIP-LCMV and double transgenic RIP-LCMV x pHHNS–JAM-C mice that were infected with a single dose of LCMV. Blood glucose was measured at weekly intervals (values >300 mg/dl were considered diabetic). Data are the mean ± SEM of 9-26 mice per group. (A) RIP-LCMV-GP x pHHNS–JAM-C transgenic mice. (B) Male RIP-LCMV-NP x pHHNS–JAM-C transgenic mice. (C) Female RIP-LCMV-NP x pHHNS–JAM-C transgenic mice.

At early time after infection, islets from both groups showed only small numbers of infiltrating lymphocytes and no significant differences were found between RIP-LCMV-GP x pHHNS-JAM-C and RIP-LCMV-GP mice (Figure 22A). Second, spleens as well as pancreata from RIP-LCMV-GP x pHHNS-JAM-C and RIP-LCMV-GP mice were harvested at day 3, 7, and

14 after i.p. infection of 1 x 10^4 pfu LCMV to analyze the influence of JAM-C overexpression on viral clearance. By LCMV-plaque assay the highest viral titer in the pancreas and the spleen was found at day 3 post-infection, whereas by day 14 after LCMV-infection no virus was detected in all organs analyzed. Importantly, no significant differences in clearance of LCMV in pancreas and spleen of RIP-LCMV-GP x pHHNS-JAM-C and RIP-LCMV-GP mice was found on days 3, 7 and 14 post LCMV-infection (Figure 22B). Third, Intracellular cytokine staining (ICCS) revealed no significant difference in IFN-γ positive CD8$^+$ T cells in the spleen or in the PDLN of RIP-LCMV-GP x pHHNS-JAM-C compared to RIP-LCMV-GP mice at day 10 after LCMV-infection (Figure 22C). In both mouse groups analyzed approximately 2% of all CD8$^+$ T cells isolated from the PDLN and approximately 10% of all CD8$^+$ T cells isolated from the spleen produced IFN-γ upon *ex vivo* stimulation with the GP$_{33}$ peptide. These results confirm the previous findings showing no acceleration in the development of T1D in RIP-LCMV x pHHNS-JAM-C mice. Thus, constitutive endothelial overexpression of JAM-C expression does not exacerbate the immunpathological mechanisms leading to virus-induced diabetes in RIP-LCMV mice.
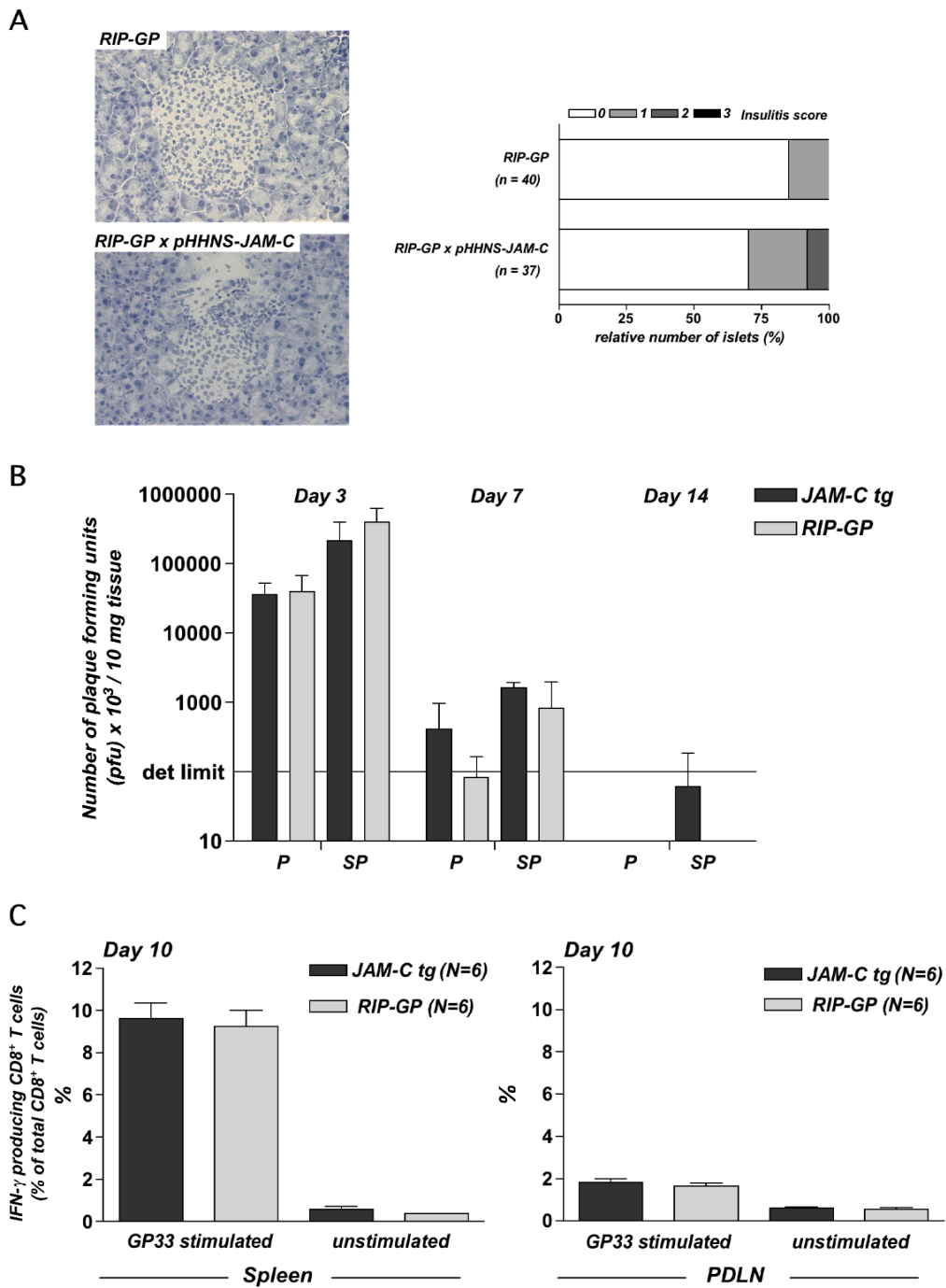
Figure 22: Increased JAM-C expression has no influence on islet infiltration, viral clearance or antigen specific immune response.

(A) Pancreas sections of RIP-LCMV-GP x pHHNS–JAM-C transgenic mice were probed for Hämatoxylin. Insulitis score obtained from sections of 3 mice per group (n=40, islets analyzed). Scoring system: 0, no infiltration; 1, some peri-insular infiltration; 2, heavy peri-insular infiltration with some intra-insular infiltrates; 3, heavy intra-insular infiltration and/or islet scars. (B) Virus titers in the pancreas (P) and spleen (SP) on days 3, 7 and 14 after infection are shown. Data are the mean ± SD of 3-4 mice per group. Det limit: Minimal number of plaques at highest tissue homogenate concentration required for statistical evaluation. (C) The presence of GP_{33}-specific $CD8^+$ T cells on day 10 after LCMV-infection in the spleen and PDLN of RIP-LCMV-GP or RIP-LCMV-GP x pHHNS-JAM-C mice was analyzed by ICCS (IFN-γ) after o/n in vitro stimulation with GP_{33} peptide. Data are the mean ± SEM of six mice per group.

DISCUSSION

9 Discussion

9.1 Attraction and transmigration in T1D

Type 1 diabetes is a chronic T cell-driven autoimmune disease that causes specific destruction of pancreatic ß cells in genetically predisposed individuals. The underlying mechanisms by which the antigen-specific T cells migrate, penetrate and transmigrate through the endothelial cells surrounding the islets is still not fully understood. In my project I have analyzed different factors involved in attraction and diabedesis of leukocytes and give new insights into the complex network of chemokines and their receptors and adhesion molecules expressed on endothelial cells.

9.2 Inhibition of CXCR3 receptor with an CXCR3 antagonist and its influence on T1D

Previous studies have reported the importance of the CXCR3 receptor in various animal models of chronic autoimmune diseases such as adjuvant arthritis in rats, murine lupus nephritis and experimental autoimmune encephalomyelitis (EAE) (93-95). Moreover, in another study from Frigerio et al., they have shown a delay in virus-induced T1D in CXCR3$^{-/-}$ RIP-LCMV-GP mice (60). In the present project we also used the RIP-LCMV mouse model as a model for human T1D that has been useful to help understand the pathogenic processes of the disease. In addition, we blocked the CXCR3 receptor with a CXCR3 antagonist called NIBR2130. Blocking with a low-molecular weight antagonist is of high pharmacological interest because of their high

bioavailability, their safety profile, their high stability and especially because of the possibility to apply them orally unlike antibodies that have to be administered by *i.v.* injection. The compound NIBR2130 that is related to lysergic acid diethylamine (LSD) is highly specific for the CXCR3 receptor and inhibits the receptor with an IC_{50} value of 54 nM (91). Moreover, NIBR2130 does not inhibit other chemokine receptors such as CCR5, CXCR4 and CXCR2. Contrary to LSD it only inhibits serotonin 5HT2A receptor with an IC_{50} value below 1 μM, whereas LSD efficiently binds to various serotonin, dopamine and adrenergic receptors (91). The CXCR3 antagonist NIBR2130 binds to the CXCR3 receptor without inducing functional activity. In a study from Zerwes et al., they illustrated by a CXCL11-induced CXCR3 receptor occupancy assay in rat whole blood that NIBR2130 indeed inhibited the CXCR3 receptor and that the receptor remained on the surface and was not internalized after binding of NIBR2130 (61). Due to these facts NIBR2130 is a highly selective and potent antagonist for the CXCR3 receptor and therefore a very promising structure useful as a drug to reduce leukocyte migration to the site of injury in several diseases.

In this part of my project we blocked the CXCR3 receptor with NIBR2130 by subcutaneously implanted osmotic pumps during the development of T1D in the fast-onset RIP-LCMV-GP as well as in the slow-onset RIP-LCMV-NP mouse model. We found that the delivery of the antagonist was fully maintained and the blood concentration was always kept 3 to 6 times higher than the IC_{50}-value during the first month, which includes the time of viral infection and first part of antigen-specific response development followed by autoimmune disease. Nevertheless, it seems that only a continuous delivery of the CXCR3 antagonist lead to the inhibition of the development of virus-

induced T1D. As soon as the administration was stopped after one month of treatment the mice rapidly caught up to the control animals in terms of their blood glucose levels and started to develop the disease. In particular, we found a significant delay in the development of T1D in the slow-onset RIP-LCMV-NP strain but not in the fast-onset RIP-LCMV-GP strain. The data suggest that the inhibition of CXCR3 leads to a significant delay in the onset of disease but is not that efficient to fully reduce T1D. Further, the more aggressive progress of T1D in the fast-onset RIP-LCMV-GP mice seems to be more resistant to CXCR3-blockade. Unexpectedly, the pathogenic processes of T1D, as reflected by islet infiltration of different T cell subsets did not differ in antagonist-treated compared to buffer treated RIP-LCMV-NP mice infected with LCMV. We have only detected a tendency of more activated antigen-specific T cells during viral response in the control mice compared to NIBR2130-treated animals, whereas during the development of autoimmunity equal amounts of antigen-specific T cells regardless of the inhibition of the CXCR3/CXCL10 interaction was found. The distinct outcome of disease in the different mouse strains could be due to the fact that RIP-LCMV-GP mice develop T1D in a very rapid fashion with the presence of high affinity, autoaggressive CD8$^+$ T cells independently of CD4$^+$ T cell help. Although it is known that CXCR3 is predominantly expressed on T$_H$1-polarized activated/memory T cells (58) it has been shown that 95% of LCMV-specific CD8$^+$ T cells are CXCR3$^+$ after LCMV-infection (57). Different outcome of T1D in these two mouse strains was observed in other studies as well where CXCL10 was specifically overexpressed by ß cells of Langerhans. In this study only in the RIP-LCMV-NP mice the development of disease was massively accelerated whereas in the more aggressive RIP-LCMV-GP mouse model no influence of CXCL10 overexpression was found (57).

The delay in the onset of T1D could not be confirmed by the pathogenic mechanisms analyzed at day 28 after LCMV-infection. Islet infiltration was similar and the functional impairment of ß cells was comparable between NIBR2130-treated and untreated mice. Although the CXCR3-receptor was blocked in NIBR2130-treated mice similar numbers of CXCR3^{+} leukocytes infiltrating islets were found when compared to control animals. Since no difference in the infiltration rate of aggressive T cells within the pancreas was observed the islet infiltration of T_{regs} was analyzed. However, we did not find any increase of infiltrating T_{regs}, whose could favor the immunomodulatory processes and finally delaying the onset of T1D.

Thus the only difference that was found between LCMV-infected RIP-LCMV-NP mice that have been treated with NIBR2130 or not was a minimal reduction in LCMV-specific CD8^{+} T cells at day 7 but not at day 28 post-infection. Previously, it has been shown that the CXCR3-ligand, CXCL10 is upregulated at days 1 to 4 after LCMV-infection (56). Moreover, neutralization of CXCL10 resulted in decreased islet infiltration, preserved insulin production and abrogated the development of T1D. Among the expression of several chemokines analyzed at different time points after LCMV-infection, CCL5 in contrast to CXCL10 peaked at day 7 and 10 post-infection (56). CCL5 has been shown to interact with CCR5 and play an active role in recruiting leukocytes into inflammatory sites of injury (96). Since CCL5 expression is upregulated after the peak of CXCL10 one could assume that the role of CXCR3/CXCL10 interaction could be overtaken by other chemokine receptor/ligand interaction at later time points after LCMV-infection. Therefore, a slight reduction in LCMV-specific T cells was observed at day 7 but not at day 28 after infection.

For blood glucose values to reach diabetic levels up to 80%-90% of all ß cells would have to be destroyed. Thus, at day 28 after LCMV-infection the discordance between islet infiltration and blood glucose values may be due to the fact that in control mice the β-cell destruction threshold has already been reached. In the NIBR2130-treated mice only 60%-70% of all ß cells might be destroyed and therefore the mice range marginal underneath the threshold needed to develop T1D.

In the study from Frigerio et al., besides the delay of T1D in CXCR3^{-/-} RIP-LCMV-GP mice they also observed more CD3^{+} T cells infiltrating islets of control mice compared to CXCR3^{-/-} mice at day 6 and 8 after LCMV-infection (60), which is in discordance to our findings. However, they used the fast-onset RIP-LCMV-GP mouse line developed in the lab of Hengartner and Zinkernagel (38) and a different LCMV strain for disease initiation.

Nevertheless, the fact that there were still some infiltrations observed in absence of this CXCR3 receptor indicates that alternative routes of migration might lead to islet infiltrations. In another study the blockade of CXCR3 by NIBR2130 in a rat model of cardiac allograft rejection was analyzed. They found that the pharmacologic blockade did not result in prolonged cardiac allograft survival (61). Moreover, in another study antagonists to CXCR3 and CXCR4 were used in the experimental autoimmune encephalomyelitis. There the blockade of both receptors simultaneously significantly inhibited clinical EAE and were more beneficial than blocking both separately (95). Such data indicate that treatment of more than one critical player involved in the pathogenic processes of T1D would possibly be more successful in reducing the outcome of disease. One of such possible critical players might be the adhesion molecule JAM-C (see chapter: JAM-C and its role in T1D).
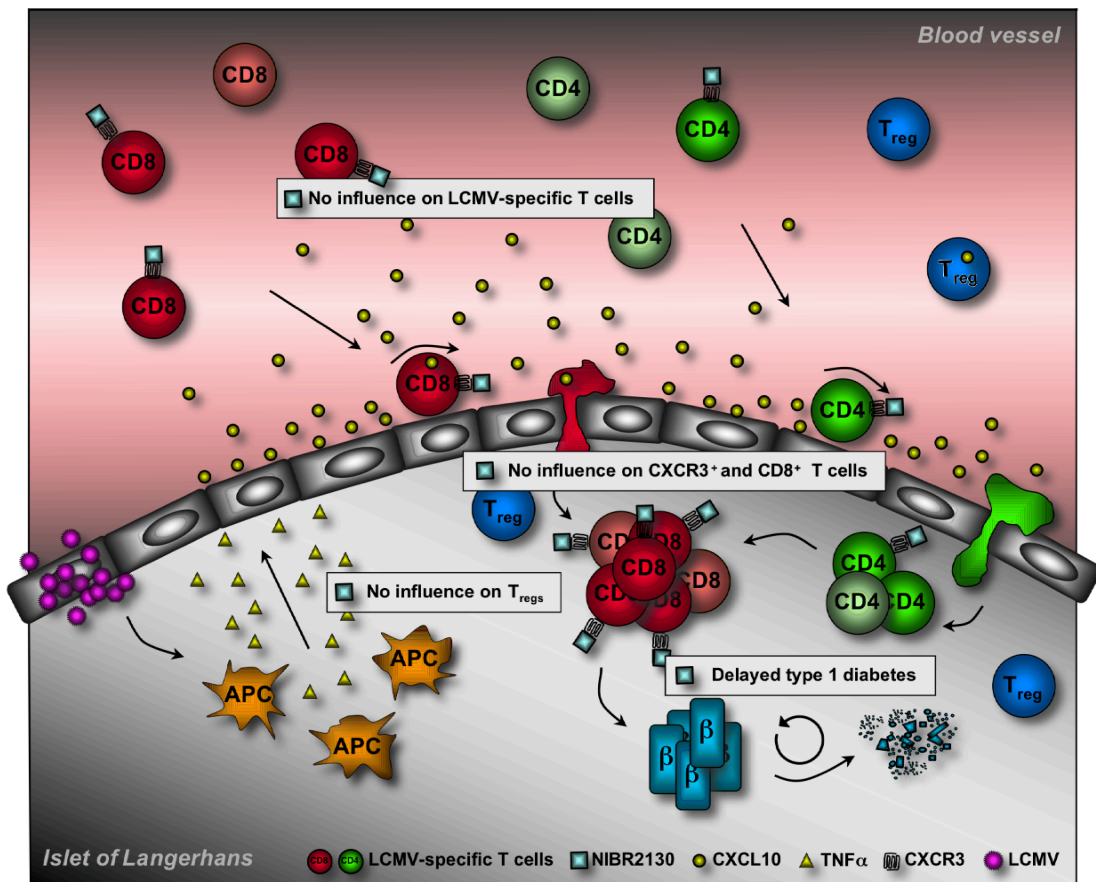
Figure 23: Influence of NIBR2130 on the immunological mechanisms in the RIP-LCMV mouse model.

The neutralization of CXCR3 with NIBR2130 delays the development of T1D in the slow-onset of T1D mouse model. However, the blockade of CXCR3 has no influence on islet infiltration of CXCR3+ T cells, CD8+ T cells as well as T_{regs} after one month of LCMV-infection. Moreover, NIBR2130-treatment has no impact on LCMV-specific T cells and the functional impairment of ß cells.

Conclusion – Project 1:

In summary, I have found that pharmacologic blockade of CXCR3 during development of virus-induced T1D results in a moderate but significant delay of overt disease as long as CXCR3 remains blocked. However, the immunopathogenesis of T1D seems not be blocked since neither the frequency nor the migratory properties of islet-specific T cells was significantly changed during CXCR3 blockade. These results suggest that it might need therapeutic interference that targets more than just one factor in the complex network of chemokine and cytokine signaling

to prevent aggressive T cells to reach their target. The moderate differences in the onset of clinical disease during CXCR3 blockade reflect the complex pathogenesis of T1D. Further, our findings underline the importance of possible thresholds in the number of aggressive T cells and in the degree of β-cell destruction that have to be reached for the occurrence of overt disease.

9.3 JAM-C and its role in T1D

In this part of my project we addressed the question whether JAM-C is involved in leukocyte transmigration to the site of injury in T1D. For this purpose, we blocked or overexpressed JAM-C in the RIP-LCMV mouse model. The blockade of JAM-C with a neutralizing antibody resulted in a slight reversion or delay of the development of virus-induced diabetes whereas the overexpression of JAM-C had no influence on the trafficking and transmigration of leukocytes to the ß cells of Langerhans.

Leukocyte migration from the blood into tissue involves several steps of molecular interactions between leukocyte and endothelial cells. These interactions allow the leukocytes to role, adhere and finally transmigrate through the endothelial cells to the site of injury (66). JAM-C, localized in endothelial-cell tight junctions, was shown to be involved in the final steps, namely transmigration. Previous studies have shown that JAM-C plays an important role in inflammatory pathologies such as peritonitis, arthritis and pancreatitis. Blockade of JAM-C with a neutralizing antibody reduced the accumulation of leukocytes at the site of inflammation (85, 86, 89).

As shown in cerulein-induced pancreatitis in mice JAM-C is expressed within the pancreas and upregulated after cerulein treatment (89). In

our investigations we found JAM-C expression around the islets of Langerhans as well as throughout the whole pancreas. Moreover, after LCMV-infection JAM-C expression was significantly upregulated at day 10 to 14 and correlated with the islet infiltration and functional impairment that prompt to the assumption that JAM-C may play an important role in T1D.

The anti-JAM-C antibody used inhibits both JAM-C homophilic interactions as well as JAM-C/JAM-B heterophilic interactions (79). The blockade of JAM-C with this neutralizing antibody resulted in a slight delay in RIP-LCMV-NP mice. However, neither the infiltration rate nor the presence of antigen-specific T cells was reduced in anti-JAM-C antibody-treated mice at day 7 and 28 after LCMV-infection. These results are consistent with a previous study using neutrophils, which demonstrated adhesion and transmigration on cultured HUVECs under flow was JAM-C independent (97). It has to be mentioned that this was an *in vitro* study and that in different experimental models of inflammation in mice an influence of JAM-C on leukocyte extravasation was shown (84, 86, 92).

Further, in the more aggressive fast-onset RIP-LCMV-GP mouse model a reversion of the outcome of T1D was observed. As assessed in a previous study blocking JAM-C with the same JAM-C neutralizing antibody did not affect monocyte transendothelial migration under flow, but led to increased monocyte reverse transmigration and return to the circulation (88). This observation raises the possibility that the disruption of the JAM-B/JAM-C interaction might lead to a shift in the leukocyte entry/exit equilibrium at endothelial junctions. Thus, an increase of T cells with a reverse-transmigratory behavior might result in the observed reversion of T1D in some RIP-LCMV-GP mice.

The influence of the neutralization of JAM-C in a peptide/adjuvant transfer model was analyzed. In this model highly reactive P14 splenocytes including GP_{33}-specific CD8^{+} T cells were transferred prior diabetes induction with the stimulation of the immunodominant LCMV peptide GP_{33} and Poly(I:C). In this model JAM-C blockade did not diminish CD8^{+} T cell extravasation *in vivo* as analyzed by two-photon microscopy at day 7 to 9 after adoptive transfer of P14 splenocytes. Visualization of the interaction of infiltrating cells and ß cells within islets demonstrated a highly diverse migration behavior of individual cells. However, no difference between anti-JAM-C antibody-treated and control animals could be observed. This finding is possibly due to the overwhelming number of transferred highly aggressive GP_{33}-specific CD8^{+} T cells. JAM-C blockade might therefore not be efficient enough to influence T1D in such an aggressive P14-transfer RIP-LCMV model. In comparison to the LCMV-infected RIP-LCMV-GP mice, in the P14-transfer RIP-LCMV model the immune response was characterized at day 7-8 after adoptive transfer. It is possible that the neutralization of JAM-C has similar effect after the initial inflammation as in the RIP-LCMV-GP mice. In those mice the neutralization of JAM-C resulted in a reversion of the development of T1D after two months of LCMV-infection (Figure 24).

JAM-C overexpression on mouse endothelial cells has been shown to increase the early influx of inflammatory cells into lungs after i.p. LPS challenge (92) and upregulate leukocyte infiltrate and tissue damage in cerulein-induced pancreatitis (89). In contrast, in our mouse model for T1D JAM-C overexpression had no influence on the development of disease. Early infiltration, viral clearance as well as presence of antigen-specific T cells were similar in double transgenic JAM-C x RIP-LCMV and in single transgenic RIP-LCMV mice.
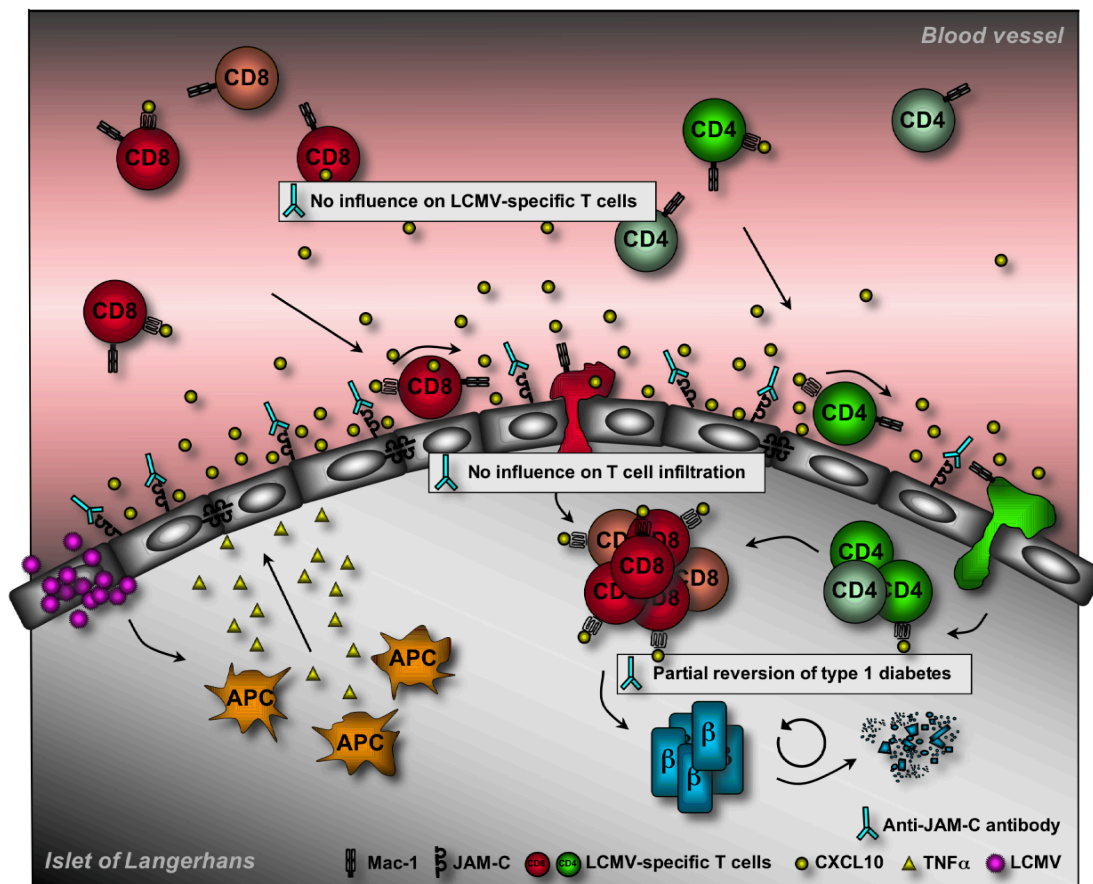
Figure 24: Influence of anti-JAM-C antibody treatment on the immunopathological mechanisms in the RIP-LCMV mouse model.

The blockade of JAM-C with a neutralizing antibody results in a slight reversion of the development of T1D in RIP-LCMV-GP mice and slightly delays the onset of disease in the RIP-LCMV-NP mice. However, the neutralization of JAM-C has no influence on islet infiltration and insulin production nor on LCMV-specific T cells.

One reason for the contrary findings might be the nature of the different disease model used. In the cerulein-induced pancreatitic model an inflammation within the acinar part of the pancreas was induced by the administration of the chemical compound, cerulein that finally resulted in pancreatitis. Hence, the cerulein model is rather different than the virus-induced RIP-LCMV model and its immunopathogenic processes involved in the destruction of ß cells. An alternative explanation would be that JAM-C overexpression does not have any influence on virus-induced T1D because unlike to antibody treatment JAM-C is overexpressed from the beginning of the

development and therefore the immune system might adapt to this exceptional condition. Further, we found that in contrast to cerulein-administration infection with LCMV by itself induces JAM-C upregulation in the pancreas at the time of peak lymphocyte infiltration. Therefore, the additional transgenic overexpression might not have an accelerating effect on the migration of aggressive, islet-specific T cells into the islets. In consideration of the fact that JAM-C overexpression has an influence on leukocyte infiltration in different inflammatory models such as the peritonitis model and the model of pulmonary leukocyte recruitment (92), JAM-C may not play such an important role during the development of T1D. Moreover, JAM-C expression is strong in the respiratory tract, which is heavily vascularized and has a high endothelial cell content. Thus, in the lung JAM-C plays a more crucial role in the transmigration of leukocytes through the endothelial cell layer to penetrate the site of inflammation (Figure 25).

There is evidence from several studies that adhesion molecules other than JAM-C indeed have an impact on the development of T1D. In an adoptive transfer model of diabetes in NOD mice the neutralization of L-selectin or VLA-4 that are expressed on migrating leukocytes and interact with adhesion molecules expressed on the endothelial cells resulted in a reduction of T1D (68, 69). Moreover, the treatment with an antibody neutralizing VCAM-1 delayed the onset of disease, whereas blocking antibody against ICAM-1 had only a marginal effect on the onset of T1D (71). ICAM-1 is constitutively expressed in low concentrations on endothelial cells, however upon inflammation it is highly upregulated, can bind LFA-1 and MAC-1. VCAM-1 plays an important role in rolling arrest and firm adhesion. In contrast to ICAM-1, VCAM-1 is only expressed on endothelial cells after cytokine

stimulation, binds to VLA-4 and mediates adhesion of leukocytes to the endothelium (63, 67, 70).
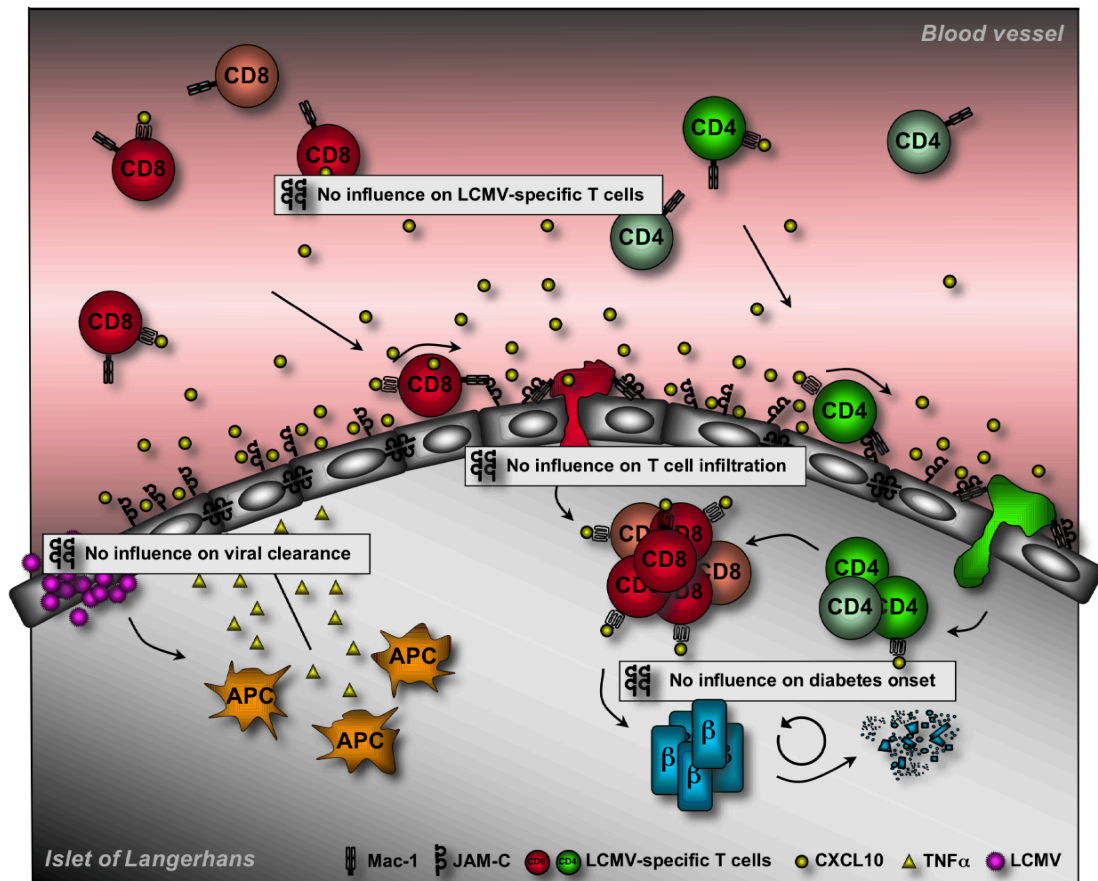
Figure 25: Influence of JAM-C overexpression on the immunopathological mechanisms in the RIP-LCMV mouse model.

The overexpression of JAM-C has no influence on the development of T1D in the RIP-LCMV mouse model. Moreover, the JAM-C overexpression has no impact on islet infiltration and viral clearance nor on LCMV-specific T cells.

These data indicate that the interaction of VLA-4/VCAM-1 seems to be crucial for the rolling and adhesion of leukocytes to the site of injury in this adoptive transfer model of diabetes in NOD mice and the MAC-1 or LFA-1 interaction with ICAM-1 has less impact in this mouse model. Other than the adhesion molecules previously described JAM-C seems to play a minor role in rolling and adhesion of leukocytes. JAM-C is rather crucial in transmigration of leukocytes through the endothelial cell layer to enter the site of inflammation (84). JAM-C interacts with

MAC-1 and CD11c mediating extravasation of leukocytes (62, 79). Collectively these data and our findings in the RIP-LCMV model suggest that JAM-C/MAC-1 interaction plays only a minor role in the pathogenesis of T1D.

Conclusion – Project 2:

Various studies have shown that JAM-C plays a pivotal role in several inflammatory pathologies. In this part of my project I investigated the influence of JAM-C in virus-induced T1D by several approaches such as neutralization and overexpression of JAM-C in the RIP-LCMV model as well as blockade of JAM-C in a peptide/adjuvant transfer model. Although LCMV-infection causes a significant increase of JAM-C expression and JAM-C neutralization resulted in a decrease and partial reversal of disease, we detected only a minor impact of JAM-C on frequency and migration of islet-specific T cells. Therefore, we conclude that JAM-C expression plays a minor role in this model of T1D and other adhesion molecules are likely to compensate for the lack of JAM-C availability during the pathogenesis of the disease.

APPENDIX

10 Material and Methods

10.1 Source of Materials

10.1.1 Plastic ware

70 μm nylon cell strainer	BD Falcon; 352350
One touch Ultra	Life Scan Inc.; 060-213-10A
96-well V-bottom plates	Anicrin; 3911924
Cell culture flasks (25, 75, 175 cm2)	Cellstar
Coverslip	Menzel-gläser
Cryomolds	Electron Microscopy science; 62352-30
Cryotubes	Sarstedt; 72.379.002
Eppendorf tubes	Eppendorf
FACS-tubes	Biorad; 223-9390
FACS-tubes	BD Falcon; 352052
Falcon tubes (15, 50 ml)	Cellstar
Heparin coated capillary	Fisher scientific; 02-668-10
Mini-Osmotic-Pump (Model 2002)	Alzet; 10165-07
Needles (23G, 27G, 30G)	BD Microlance
Plastic pipets (5, 10, 25, 50 ml)	Corning INC
PVDF Transfer Membrane	PolyScreen; NEF1002
Sialin coated slides	Menzel-gläser; J1800AMN/
Sterile Filter (50, 250, 500 ml)	Millipore; SCGPU05RE
Syringes (1 ml)	Terumo; BS-01T
Syringes (3, 5, 10, 20 ml)	Braun
Teststrips	Life Scan Inc.; 2943903
Tissue culture dishes	Cellstar
Tissue culture plates (6, 12, 24, 48, 96 well)	Cellstar

10.1.2 Chemicals

Acetic Acid	J.T. Baker; 6052
Agarose	Sigma; A9539

Ammonium sulfate	Merck; 101211
APS	Sigma; A3678
Aquamount	Merck; 1.08562.0050
Brefeldin A	Sigma; B6542
Bromophenol blue	Roth; 512.1
Chloroform	Riedel-de Haën; 32211
Citrate acid	Applichem; 77-92-9
Dc Protein assay Reagent A Reagent B Reagent S	BioRad 500-0113 500-0114 500-0115
DEPC (Diethylpyrocarbonate)	Sigma; D5758
Dextran, Texas Red, 70 kDa	Invitrogen; D-1864
DMSO (Dimethylsulfoxide)	Sigma; D5879
pBR328-Marker	Roth; X902.1
DTT (1,4-Dithiothreit)	Roth; 6908.1
ECF substrate	Amersham Bioscience; RPN 5785
EDTA	AppliChem; A1103.1000
Ethanol absolut	Riedel-de Haën; 24102
Ethidium bromide	Sigma; E8751
Ficoll-Paque PLUS	GE Healthcare; 17-1440-02
Formaldehyde	Redel-de Haën; 33220
Glucose	Merck; 104074
Glycerol	Roth; 3783.1
H2O2	Roth; 8070.1
HCl	Riedel-de Haën; 30721
Hematoxylin	AppliChem A4840.1000
HEPES	Gibco; 15630
Hyflo Super Cel medium	Sigma; 56678
Immunofluore mounting Medium	ICN; 622701
Isofluran	Abbott; B506
Iso-Propanol	Prolabo; R11-36-67
Ketamine/xylazine hydrochloride solution	Sigma; K113
Kwik-Stop Styptic Powder	ARC laboratories 106012
Methanol	Fluka; 65543

NaCl	J.T. Baker; 0278
Na-N3	Roth; K305.1
NH4Cl	Merck; 1.01145.0500
N-Methyl-2-pyrrolidinon	Aldrich; 32,863-4
Paraformaldehyde	Merck; 1.04005.1000
Pen/Strep	Gibco; 15140
Peroxidase substrate	Vector; SK-4100
Polyethylene glycol 200 (PEG200)	Sigma; P3015-500G
Potassium acetate	Merck; 1.04820.1000
Protein Assay Standard 1	BioRad 500-0005
Protein G Sepharose 4 Fast Flow	GE Healthcare; 17-0618-01
Protease inhibitor tablet	Roche
Rotiphorese Gel 30 (30% Acrylamide/0.8% bis-acrylamide)	Roth; 3029.1
Saponin	Sigma; S7900
SDS	Roth; 2326.2
Skim milk powder	Töpfer Allgäu; 60226
Sodium Pyruvate	Gibco; 11360
TEMED	Roth; 2367.3
Tissue-Tek OCT	Sakura; 4583
Triethanolamine	Sigma; 90278
Tri-Reagent	Sigma; T9424
Tris-HCl	Roth; 4855.2
Tris	Usb; 77514
Triton X-100	Sigma; T8787
Trypan blue	Sigma; T8154
Tween-20	Sigma; P7949
Ultroser HY and Ultroser SF	Life Sciences; 66029
Xylene	Riedel-de Haën; 16446

10.1.3 Composition of buffers, solutions and culture media

0.5% Trypsin-EDTA	Gibco; 25300
2x Laemmli sample buffer	20% v/v Upper gel buffer

	20% v/v Glycerol
	4% SDS
	1.54% DTT
	bromophenol blue
ABC reagent solution (Peroxidase Substrate Kit DAB)	5 ml ddH2O
	4 drops of DAB Stock solution
	2 drops of Hydrogen Peroxide Solution
DEPC H2O	1% DEPC in ddH2O
	stir over night and autoclave
DMEM + GlutaMax I	Gibco; 61965
FACS fixation buffer	PBS
	0.1% PFA
FACS PBS/saponin buffer	PBS
	1% FBS
	0.1% NaN3
	0.1% Saponin
FACS PBS/staining buffer	PBS
	1% FBS
	0.1% NaN3
FACS PFA/saponin buffer	PBS
	0.1% Saponin
	10 mM HEPES
	4% PFA
FBS (Foetal bovine serum)	Biochrom AG; S0115
Lower gel buffer	1.5 M Tris-HCl (pH 8.8)
	Autoclave
NIBR2130 buffer	418 μl N-Methyl-2-pyrrolidinon
	418 μl 0.1 M HCl
	5.43 ml PEG200
	2.93 ml 0.9% NaCl-solution
PBS	Gibco; 14190
Proteinase K	10 mg/ml Proteinase K
	10 mM Tris-HCl (pH 7.5)
Proteinase K buffer	ddH2O
	0.5% SDS
	10 mM NaCl
	50 mM Tris (pH 8)
	3 mM EDTA
Red blood cell lysis buffer	0.83% NH4Cl in ddH2O

	Sterile filtrated
RIPA buffer	ddH2O
	40 mM Tris (pH 7.5)
	150 mM NaCl
	1% Triton X-100
	6 mM EDTA
	10% Glycerol
	1% Na-deoxycholate
	0.1% SDS
RPMI 1640 + GlutaMax I	Gibco; 61870
Running buffer	25 mM Tris
	192 mM Glycine
	0.1% SDS
	pH 8.3
TAE buffer	40 mM Tris-Acetate
	1 mM EDTA
Transfer buffer	1.44% Glycine
	0.3% Tris
	80% v/v ddH2O
	20% v/v MeOH
Upper gel buffer	0.5 M Tris-HCl (pH 6.8)
	Autoclave

10.1.4 Enzymes and proteins

Collagenase P	Roche; 11 213 857 001
DNase	Sigma; DN25
M-MLV-reverse transcriptase	Promega; M1705
Protease inhibitor cocktail tablets	Roche; 11 873 580 001
Proteinase K	Carl Roth; 7528.1
RNase OUT	Invitrogen; 10777-019
RQ1 RNase-free DNase	Promega; M6101
Superscript II reverse transcriptase	Invitrogen; 18064-022
Taq-polimerase	Peqlab Biotechnologie GmbH; 01-1030

10.1.5 Nucleotides and nucleic acids

GP_{33} peptide	KAVYNFATM
NP_{396} peptide	FQPQNGQFI

GP$_{61}$ peptide	GLKGPDIYKGVYQFKSVEFD
CpG	IDT; ODN1826
GP F Primer	5' GGG AAA GGA GAA TCC TGG AC 3'
GP R Primer	5' GCA ATC TGA CCT CTG CCT TC 3'
NP F Primer	5' AAT CCA TGT AGG AGC GTT GG 3'
NP R Primer	5' AAC AGC GAG GAC CTC TTG AA 3'
JAM-C F Primer	5' GGG AAG TCG CAA AGT TGT GAG TT 3'
JAM-C R Primer	5' TGC AGT GTT GCC GTC TTG CCT ACA G 3'
dNTP	Peqlab; 20-2011
Poly(I:C)	Sigma; P9582
Random Primers	Fermentas; S0142

10.1.6 Antibodies

Antibodies used for FACS-staining	
APC-anti-mouse CD8a/Lyt-2 (Clone 53-6.7)	Southern Biotech; 1550-11
APC-anti-mouse CD4/L3T4 (Clone GK 1.5)	Southern Biotech; 1540-11
FITC-anti-mouse CD4/L3T4 (Clone GK 1.5)	Southern Biotech; 1540-02
FITC-anti-mouse CD45R/B220 (RA3-6B2)	BD Pharmingen; 553088
FITC-anti-mouse CD8a/Lyt-2 (Clone 53-6.7)	Southern Biotech; 1550-02
PE-anti-mouse CD8 alpha (Clone KT15)	Serotec; MCA609PEB
PE-anti-mouse CD4 (Clone YTS191.1)	Serotec; MCA1767PEB
PE-anti-mouse CD11c (p150/90)	eBiosience; 12-0114-82
PE-anti-mouse IFN-γ	BD Pharmingen; 5544412
PE-Cy5-anti-mouse CD8a/Lyt-2 (Clone 53-6.7)	Southern Biotech; 1550-16
Streptavidin-APC	Southern Biotech; 7100-11M
Antibodies used for Western Blot	
Goat anti-mouse IgG (H+L)-AP Conjugate	Bio-Rad; 170-6520
Swine anti-goat IgG (H+L) Alk. Phos. conjugate	Invitrogen; G50008
Goat anti-mouse JAM-C IgG	R&D Systems; AF1213
Mouse anti-ß-actin	Sigma; A5441
Antibodies used for Histology	
Rat anti-mouse CD4/L3T4 (Clone GK 1.5)	BD Pharmingen; 553043
Rat anti-mouse CD45R/B220 (RA3-6B2)	BD Pharmingen; 553084
Rat anti-mouse CD8a/Lyt-2 (Clone 53-6.7)	BD Pharmingen; 553027

Rat anti-mouse Foxp3	eBioscience; 14-5773
Rat anti-mouse F4/80	Serotec; MCAP497
Polyclonal guinea pig anti-swine insulin	DakoCytomation; A0564
Rat anti-mouse CD31	BD Pharmingen; 557355
Goat anti-mouse NKp46/NCR1	R&D Systems; AF2225
Biotinylated anti-goat IgG (H+L)	Vector; BA-5000
Biotinylated anti-guinea Pig IgG (H+L)	Vector; BA-7000
Biotinylated anti-hamster IgG (H+L)	Vector; BA-9100
Biotinylated anti-rabbit IgG (H+L)	Vector; BA-1000
Biotinylated anti-rat IgG (H+L)	Vector; BA-4001
Antibodies used for Plaque assay	
Rat antibody specific for LCMV (VLA-4)	(98)
Peroxidase-conj. AffiniPure goat anti-rat IgG (H+L)	Jackson ImmunoResearch Laboratories, Inc.; 112-035-033

10.1.7 Kits

Avidin/Biotin blocking Kit	Vector; SP-2001
Peroxidase Substrate Kit DAB	Vector; SK-4100
Quantitec SYBR Green PCR	Qiagen; 204143
RNeasy Mini Kit	Quiagen; 74104
Roti-Histokit	Roth; 6638.1
Roti-Quant Protein assay	Roth;
SlowFade Antifade Kit	Molecular Probs; S2828

10.1.8 Cell lines

Rat hybridoma cells for anti-JAM-C antibody production

Rat hybridoma cells are Sp2/0 cells that were fused with splenocytes from JAM-C antibody immunized male Fisher rats (78) and were originally received from Prof. Beat A. Imhof from the University of Geneva. The cells were grown in DMEM, 1% Ultroser HY and 0.1% FBS.

MC57 (mus musculus) cells for plaque assay

MC57 cells are a methylcholanthrene-induced fibrosacroma cell line. The cells were maintained in RPMI 1640 medium. All media were supplemented with 2 mM L-glutamine and 7% (vol/vol) fetal calf serum.

10.1.9 Virus

LCMV-Armstrong (Arm)

The Armstrong strain of LCMV, clone 53b, was used for all experiments. LCMV was plaque purified three times on Vero cells (ATCC CCL-81), and stocks were prepared by a single passage on hamster kidney fibroblast cell line BHK-21 (ATCC CCL-10, American Type Culture Collection, Manassas, VA).

10.1.10 Mouse strains

Transgenic mice (H-2b x H-2d [bxd]) with rat insulin promoter (RIP) fused to cDNA encoding the NP or GP of LCMV-Arm were made for direct expression of LCMV viral proteins by pancreatic ß cells. The transgenic mice were generated by standard microinjection of C57BL/6J fertilized eggs with the construct containing hybrid DNA molecules (37, 99).

The transgenic pHHNS-JAM-C mice were generated under the control of the endothelial specific promotor Tie-2. The coding region for murine JAM-C was inserted in place of *lacZ*-SV40pA into pBSIISK-HHNS construct (92).

RIP-LCMV-GP x pHHNS-JAM-C and RIP-LCMV-NP x pHHNS-JAM-C double-transgenic mouse lines were generated by crossing pHHNS-JAM-C single-transgenic mice to RIP-LCMV-GP or RIP-LCMV-NP single-transgenic lines.

The DsRed[+] P14 double-transgenic mouse line was generated by crossing DsRed[+] single-transgenic mice to P14-TCR specific for LCMV-H-2D[b] single-transgenic line (100, 101).

RIP-LCMV-GP x MIP-GFP double-transgenic mouse line was generated by crossing RIP-LCMV-GP single-transgenic mice to MIP-GFP single-transgenic line that has ß cells genetically tagged with the green fluorescence protein (36, 38, 102).

Wild-type C57BL/6 mice were purchased from the breeding colony of Harlan Netherlands.

Experiments were carried out with age- and sex-matched animals kept under specific pathogen free (SPF) conditions and in accordance with German regulations. All animal experiments were approved by the local Ethics Animal Review Board (Darmstadt, Germany).

10.2 Methods

10.2.1 Cell biological methods

10.2.1.1 Cultivation of cells

Cells were cultured in plastic cell culture flasks (25, 75 or 175 cm^2) at 37°C (5% CO2, relative humidity 95%) with appropriate medium.

Adherent cells were split when confluent. Medium was removed from the culture flask, the cellular monolayer was rinsed with 10 ml sterile PBS and the cells were incubated for 5–10 minutes at 37°C in 3 ml of trypsin-EDTA solution to detach the cells from the plastic. The detached cells were collected, and spun at 250 x g for five minutes. Finally the cells were resuspended in appropriate medium and split.

10.2.1.2 Freezing of cells

A freezing container was pre-cooled for 30 minutes at 4°C. The freezing medium was prepared containing 90% FBS and 10% DMSO. Cells were trypsinized, washed with PBS and centrifuged at 250 x g for five minutes. Cells were resuspended in 1 ml of pre-cooled freezing medium and 1 ml aliquots were transferred into cryotubes. The aliquots were placed into the freezing container and transferred to -70°C. The freezing containers ensure that the cell samples are cooled down to –70°C at a rate of 1°C/min. After 48 hours, the cryotubes were transferred to the liquid nitrogen tank (–196°C).

10.2.1.3 Thawing of cells

Cell aliquots were taken out of the liquid nitrogen tank and warmed immediately in a water bath (37°C) until cells started to thaw. 1 ml of warm medium was added and liquefied cells were transferred into a 15 ml tube. This step was repeated until all cells were thawed. Cells were step-wise thawed to dilute the liquefied DMSO as fast as possible to avoid cell damage. After spun cells at 250 x g for five minutes fresh culture medium was added and the cells were checked for their viability by trypan blue stain. Cells were cultured in appropriate conditions and the following day the cells were evaluated for viability and density.

10.2.1.4 Determining the density of a cell suspension

The cellular density of a suspension was determined by mixing 10-20 μl of the cell suspension with an equal volume of Trypan blue solution. The cells in the resulting suspension were counted directly in a Neubauer chamber using a microscope. Dead cells were identified by cytoplasmic staining with Trypan blue. A grid at the bottom of the

chamber was used to count the cells and the cell density (cells per ml) was calculated with the following formula:

Cellular density (cells/ml) = number of cells on the grid x dilution factor x 10^4 ml^{-1}

10.2.1.5 Isolation of pancreatic islet cells

Islet cells were isolated by injecting 3 ml of collagenase P solution ((1.2 U/ml) in RPMI w/o) into the pancreas. After 30 minutes incubation at 37°C the warm RPMI were removed and 10 ml of cold RPMI was added. The pancreas was disaggregated by shaking the tube for one minute and passed through a kitchen sieve into fresh 50 ml tube. Two pancreata were pooled and filled up with RPMI to 50 ml. The cells were settled down for 5 minutes on ice and then the medium was sucked off leaving 20 ml in the bottom of the tube. This step was repeated once but the cells were settled down for 10 minutes and the medium was sucked off to 15 ml. After refilling the tube with PRMI the cell suspension was centrifuged at 1000 rpm for two minutes at room temperature (RT). The pellet was resuspended in 10 ml Ficoll-Paque Plus and overlaid with 5 ml RPMI. The gradient was centrifuged at 2000 rpm for 15 minutes at RT. After spin the islets were transferred in a new 50 ml tube, once washed and handpicked for further use.

10.2.1.6 Isolation of splenocytes

Spleen cells were isolated by squeezing the spleen through a 70 μm nylon cell strainer with a syringe plunger in 10 ml RPMI. With a pipette a single cell suspension was prepared in 10 ml RPMI. The supernatant was centrifuged at 1600 rpm for five minutes at 4°C. To eliminate the red blood cells the pellet was resuspended in 5 ml 0.83% NH_4Cl in PBS and incubated for one to two minutes at RT. To stop the reaction 5 ml RPMI was added and the cells were centrifuged at 1600 rpm for five

minutes at 4℃. The cell pellet was resuspended in RPMI 10% FBS, P/S and the cells were kept at 4℃ until use.

10.2.1.7 Isolation of pancreatic lymphocytes

Pancreatic lymphocytes were isolated by mashing the pancreas between two slides and further squeezing the remaining tissue through a 70 μm nylon cell strainer with a syringe plunger in 10 ml RPMI supplemented with 0.1 mg/ml DNase. With a pipette a single cell suspension was prepared in 10 ml RPMI. The cell suspension was centrifuged at 1600 rpm for five minutes at 4℃. The cell pellet was resuspended in RPMI 10% FBS, P/S and the cells were kept at 4℃ until use.

10.2.1.8 Isolation of lymphocytes from pancreatic draining lymph nodes

The lymphocytes from the pancreatic draining lymph nodes were isolated by squeezing the lymph nodes through a 70 μm nylon cell strainer with a syringe plunger in 10 ml RPMI. With a pipette a single cell suspension was prepared in 10 ml RPMI. The cell suspension was centrifuged at 1600 rpm for five minutes at 4℃. The cell pellet was resuspended in RPMI 10% FBS, P/S and the cells were kept at 4℃ until use.

10.2.1.9 Preparation of protein extraction from liver, lung and pancreas homogenates

Organs were harvested and homogenized with a tissue homogenizer in 5 ml RIPA-buffer containing protease inhibitor.

10.2.1.10 Flow cytometry

FACS staining of blood, spleen, pancreatic draining lymph nodes and pancreas

Cells were harvested and centrifuged at 1600 rpm for five minutes. Erythrocytes were lysed by resuspending the cell pellet with 5 ml 0.83% NH_4Cl, wait for two minutes and adding 5 ml RPMI containing 10% FBS to stop the reaction. Around 10^6 cells were transferred to a V-bottom 96-well plate. The cells were washed once by spinning the plate at 1600 rpm for five minutes at 4°C, resuspending with 150 μl FACS PBS/staining buffer and spinning again for five minutes. The cells were stained with fluorocrome labeled antibody of choice in 50 μl PBS/staining buffer for at least 20 minutes at 4°C in the dark. After two additional washes with 150 μl PBS/staining buffer the cells were fixed in 200 μl FACS-fixation buffer and transferred to FACS-tubes and analyzed by flow cytometry at a BD FACS Calibur or BD FACS Canto II.

10.2.1.11 Intracellular cytokine stain (ICCS)

Restimulation of lymphocytes

Cytotoxic T lymphocytes (CTLs) produce Interferon-γ (IFN-γ) after stimulation; therefore intracellular staining for IFN-γ was used to quantify specific and functionally competent CTLs.

100 μl lymphocytes at 10^7 cells/ml in RPMI 10% FBS, P/S, 50 μl of the specific stimulant (2 μg/ml GP_{33}, NP_{396}, or 4 μg/ml GP_{61}) and 50 μl RPMI 10% FBS containing 2 μg/ml Brefeldin A (to block secretion of IFN-γ) were added per well of a flat-bottom 96-well plate. Negative and positive controls were included adding 50 μl of medium or 50 μl of peptides added to splenocytes harvested at day 7 post LCMV-infection. The plate was incubated for six hours or overnight at 37°C,

5% CO_2. The cells were resuspended and transferred to a 96-well V-bottom plate and were ready for staining.

Staining

After the cells were washed twice by resuspending with 150 μl PBS/staining buffer and spinning at 1600 rpm for five minutes at 4°C the cells were stained with fluorocrome labeled anti-CD8 and/or anti-CD4 antibody in 50 μl PBS/staining buffer for at least 20 minutes at 4°C in the dark. After two additional washes with 150 μl PBS/staining buffer the cells were fixed and permeabilised with 100 μl of PFA/saponin solution for 10 minutes at RT. After the cells were washed twice by resuspending with 150 μl PBS/saponin buffer and spinning at 1600 rpm for seven minutes at 4°C the cells were stained with PE-conjugated anti-mouse-IFN-γ antibody in 50 μl PBS/saponin buffer for 30 minutes at 4°C in the dark. After washing the cells two times with PBS/saponin buffer and once with PBS/staining buffer the cells were resuspended in 200 μl FACS fixation buffer, transferred to FACS-tubes analyzed by flow cytometry.

10.2.1.12 LCMV Plaque assay

MC57 cells were grown in RPMI 1640, 7% FBS and were split 1:1 one day before starting the assay to have the cells in their expansion phase. A cell suspension at a concentration of $8 * 10^5$/ml was used. 5 ml of this cell suspension was needed for each 24-well plate. The organs used were weighed prior freezing in liquid nitrogen. The organs were kept frozen at – 80°C until further use. Organs were put into 1 ml MEM with 2% FBS per 0.1 g of tissue. After grinding the organs with a homogenizer the samples were centrifuged for 5 minutes at 300 x g and kept on ice until further use. 130 μl MEM with 2% FBS were added to rows 2-12 of a round bottom 96-well plate. After adding 200 μl of

sample in duplicate to the first row a 1:10 dilution was performed. 200 μl of the MC57 cells were added to a 24-well plate and 200 μl of diluted samples were transferred to the MC57 cells. After four hours incubation at 37°C, 5% CO_2 400 μl of a 1:1 mixture of 2x DMEM and 2% methyl cellulose was overlaid onto the cell – organ sample mixture. After 2 days incubation at 37°C, 5% CO_2 plates were stained with DAB substrate. After flicking of the overlay form the cells the cells were fixed with 4% formalin-PBS for 30 minutes at RT. Then 240 μl 1% Triton X solution was added to each well and incubated for 20 minutes at RT. To block unspecific binding 240 μl 10% FBS in PBS was added and incubated for 1 hour at RT. 240 μl of 1:4 diluted VL-4 rat anti-LCMV antibody in 1% FBS in PBS was added to the samples and incubated for 60 minutes at RT. After washing the plate twice with PBS 240 μl 1:400 diluted second antibody in 1% FBS in PBS was added to each sample. After 60 minutes incubation at RT plates were washed twice with PBS and 300-400 μl of the DAB substrate was added to each sample, incubated for 5-10 minutes, until a good color was produced. The coloring was stopped by washing the plates with tap water. Finally, to let the plates dry they were inverted placed on a paper towel. The virus titer was calculated with the following formula (two adjacent wells were counted):

Titer = ((m x 10) + n) /2 x (dilutionfactor of lower dilution) x 5 [pfu/ml]

m = number of foci in the well with higher dilution (less foci)
n = number of foci in the well with lower dilution (more foci)

10.2.1.13 Anti-JAM-C antibody production and purification

Rat hybridoma cells were grown in DMEM, 1% Ultroser HY and 0.1% FBS. The collected supernatants were filtered on Hyflo super cel and 0.45 μm polycarbonate filter.

Then the supernatants were precipitated with 45% (277g/l) of ammonium sulphate by adding the salt progressively over a period of two hours minimum at 4°C with agitation. After the precipitation the solution was centrifuged at 3'000 x g for 30 minutes at 4°C. The supernatant was discarded and the precipitate was resuspended in 1/50 of the initial volume in PBS. After dialyses against PBS for 4-6 hours the solution was centrifuged in Eppendorf tubes at 14'000 rpm in a micro-centrifuge to remove Transferrin. The supernatants were collected and filtered on 0.22 μm filter.

For the purification of the antibody Protein G sepharose 4 fast flow was used. Because the binding capacity of the resin is reduced for rat IgG, approximately 2 mg/ml of gel was necessary. The amount of needed Sepharose G slurry was washed once with PBS and centrifuged at 500 x g for five minutes and then the beads were settled down for 10 minutes more. After removing the supernatant the antibody solution was added to the beads and incubated over night at 4°C on an end-over-end rotation. The beads with bound antibody were washed twice with PBS, centrifuged at 500 x g for five minutes and settled down for ten minutes more. The antibodies were eluted with 0.1 M Triethanolamine (pH 10.5). After removing the supernatant the same volume of Triethanolamine as the bead volume was added and incubated for two minutes at RT and centrifuged at 500 x g for five minutes. After collecting the eluted antibody the solution was immediately neutralized with 2 M Tris pH 7.5. The elution step was repeated seven times. After the protein concentration was determined on a Nano-drop (ND-1000 Spectrometer), the fractions of interest were pooled and salt exchanged against PBS for 4-6 hours. At the end the antibody concentration was measured by Nano-drop, filtered on 0.22 μm filter and stored at 4 or – 20°C until use.

10.2.1.14 Determination of NIBR2130 in mouse whole blood

Before analysis whole blood samples were prepared by a protein precipitation step. Calibrations and quality control samples were prepared in mouse whole blood. For each calibration a 50 μl aliquot of unknown whole blood samples or control samples was transferred to 0.5 ml Eppendorf tubes. 20 μl internal standard (a structurally related compound with similar behavior) at a concentration of 1 μg/ml was added to each sample, except blank samples. After short mixing by vortex 100 μl of 0.04 mol/l $ZnSO_4$ in 90% methanol was added to each sample. After the samples were ultrasonicated for 10 minutes and vortexed for 15 minutes they were centrifuged at 16'000 x g for 5 minutes. A 60 μl aliquot of the supernatant of each sample was diluted with 30 μl water in HPLC-μ Vials and stored at 10°C until analysis. For the chromatography 10 μl of each sample were directly injected on a Kromasil 100-C18 0.5 x 50 mm column with 3.5 μm particles (G&T Septech AS, Norway). The column was heated at 50°C. For separation a linear gradient was applied (Table 1). Solvent A was 0.2% formic acid, solvent B 0.2% formic acid in acetonitrile and the flow of the capillary pump was hold at 20 μl/min.

Time (minutes)	Solvent B (%)	
0	5	
3.0	5	Switch to mass spectrometry
10.0	95	
12.0	95	Switch to waste
12.1	5	
15.0	5	Stop time

Table 1: Gradient conditions for separation.

For detection, the column effluent was directly injected into the atmospheric pressure electrospray source (AP-ESI) of the linear trap

mass spectrometry with a capillary temperature of 250°C a sheet gas flow of 20 l/h and a auxiliary gas flow set to 10 l/h. Compound and internal standard were detected as their $[MH]^+$ ions in MRM mode with a spray voltage of 3.5 V and the collision energy set to 20%. For detection parameters were optimized for NIBR2130 and the mass transition 498.2 m/z → 379.2 + 405.2 m/z, applying an isolation window of 2 m/z, was used.

10.2.1.15 Immunohistological stainings

Immunohistochemical stainings

Organs were harvested at the times indicated, immersed in Tissue-Tek OCT, and quick-frozen on dry ice. 6 - 7 μm tissue sections were cut using a cryomicrotome and mounted on sialin-coated slides.

Three different fixing types were used: Sections were fixed in 95% ethanol or 1:1 diluted ethanol/acetone at -20°C for 15 minutes and after drying the slides on a paper towel for ten minutes circles were drawn around the specimen with a wax pencil. In the third fixing type the circles were drawn around the specimen before fixation with 4% PFA at RT for 10 minutes.

The sections were washed two times in PBS for two minutes and incubated in 0.3% H_2O_2/0.1% Na-azid in PBS for 15 minutes at RT. After washing two times in PBS for two minutes one drop of avidin was placed on each specimen and incubated for 10 minutes at RT. The sections were washed and one drop of biotin was placed on each specimen and incubated for 10 minutes at RT. After an additional washing step, a few drops of 10% FBS in PBS was added and incubated for 15 minutes at RT. The 10% FBS in PBS was tapped off, the sections were washed quickly in PBS and ~ 60 μl of the first antibody diluted 1:200 – 1:1000 in 10% FBS in PBS was added on each

specimen and incubated for one hour at RT in a humidified chamber. After tapping off the first antibody solution, the sections were washed two times in PBS for four minutes and 100 μl of biotinylated secondary antibody diluted 1:200 – 1:1000 in 10% FBS in PBS was added on each specimen and incubated for 45 minutes at RT in a humidified chamber. The secondary antibody solution was tapped off and sections were washed two times for four minutes in PBS. One drop of ABC reagent solution was added on each specimen and incubated for 30 minutes at RT. After tapping off the remaining ABC reagent and two washes in PBS for four minutes 60 μl peroxidase substrate was added on each specimen and incubated for five minutes at RT. The reaction was stopped by washing in PBS and the sections were counterstained in hematoxylin solution for five minutes at RT and washed two times in PBS. After adding two drops of aquamount onto each section a coverslip was placed onto each slide. The sections were then incubated at RT for more than two hours and pictures were made at a Microscope (Biozero BZ-8000, Keyence).

Immunofluorescence stainings

Organs were harvested at the times indicated, immersed in Tissue-Tek OCT, and quick-frozen on dry ice. 6-7 μm tissue sections were cut using a cryomicrotome and mounted on sialin-coated slides. After fixing the sections in 95% ethanol at -20°C for 15 minutes, or with 4% PFA, the sections were washed two times in PBS for two minutes and incubated for 30 minutes with PBS containing 10% FBS in PBS at RT. After tapping off the FBS in PBS blocking solution the sections were washed in PBS and the first antibody diluted 1:200 – 1:1000 in FBS in PBS was added to the sections and incubated for two hours at RT in a humified chamber in the dark. After washing three times in PBS for

four minutes the fluorescent-labeled secondary antibody diluted 1:200 – 1:400 in FBS in PBS was added and the sections were incubated for one hour at RT in a humidified chamber in the dark. The secondary antibody solution was tapped off and the sections were washed three times in PBS for four minutes and then mounted in immunofluore mounting medium.

10.2.2 Molecular biological methods

10.2.2.1 Mouse tail DNA isolation

Tail biopsies (0.3 cm) were digested overnight with 5 μl of proteinase K (10 mg/ml) in 500 μl of proteinase K buffer at 55℃. 75 μl of 8M KOAc and 500 μl chloroform were added and the tubes were inverted several times, incubated at -70℃ for 15 minutes and centrifuged for five minutes at 14'000 rpm in a micro-centrifuge. Then the supernatant was transferred to new tubes, 1 ml of ethanol was added and the tubes were inverted several times. After centrifugation at 14'000 rpm for 10 minutes the supernatant was removed and the DNA pellet was washed with 1 ml of 70% ethanol. DNA was air dried for 10 to 30 minutes and then re-dissolved in 100 μl TE buffer and stored at 4℃.

10.2.2.2 RNA extraction from tissues

Tissues were harvested and homogenized in 1 ml TRI reagent per 50-100 mg tissue with a tissue homogenizer. Per 50-100 mg tissue 0.2 ml chloroform was added and the homogenate was vortexed for 15-20 seconds. After 2-15 minutes incubation at RT the homogenate was centrifuged at 12'000 x g for 15 minutes at 4℃. After centrifugation the upper aqueous phase was transferred into a new tube and 0.5 ml isopropanol was added. The tubes were inverted several times and

after an incubation of 5-10 minutes centrifuged at 12'000 x g for eight minutes. The supernatant was removed and the RNA pellet was washed with 1 ml 75% ethanol. After centrifugation at 7'500 x g for five minutes the RNA pellet was air dried for 5-10 minutes and then re-dissolved in an appropriate volume of H_2O_{DEPC} and incubated at 56°C for ten minutes. The RNA concentration was determined on a Nano-drop (ND-1000 Spectrometer) and the RNA was stored at -80°C for further usage.

10.2.2.3 Polymerase chain reaction (PCR)

PCR was used to amplify the transgenic insert of the RIP-LCMV-GP, RIP-LCMV-NP, and JAM-C mice for screening.

The components of the PCR reaction:

	NP, JAM-C	GP
ddH$_2$O	19.9 μl	14.3 μl
10x PCR buffer	2.5 μl	2 μl
10 mM dNTP-Mix	0.5 μl	1.6 μl
10 μM reverse Primer	0.5 μl	0.5 μl
10 μM forward Primer	0.5 μl	0.5 μl
TAQ-Polymerase	0.1 μl	0.1 μl
DNA	1 μl	1 μl

Cycling:

	GP	NP	JAM-C
initial denaturation at	94°C > 3 min	94°C > 5 min	95°C > 1:30 min
	35 cycles:	35 cycles:	40 cycles:
denaturation at	94°C > 45 sec	94°C > 30 sec	95°C > 30 sec
primer annealing at	56°C > 45 sec	56°C > 30 sec	63°C > 30 sec
elongation at	72°C > 1 min	72°C > 1 min	72°C > 1 min
additional elongation at	72°C > 3 min	72°C > 3 min	72°C > 7 min

Cool to	4°C	4°C	4°C

For all reactions a water sample was included as negative control to confirm the viability of the PCR result. PCR products were analyzed by agarose gel electrophoresis.

10.2.2.4 DNA agarose gel electrophoresis

Separation of DNA fragments of different sizes was achieved by agarose gel electrophoresis. A 1% agarose gel was routinely used and the expected size of the fragments was between 0.5 and 10 kb. Agarose was dissolved in TAE buffer by boiling. After cooling to hand temperature 1 μg/ml Ethidium bromide was added while stirring. The solution was poured into an appropriate gel tray with inserted combs. Following cooling and solidification the combs were removed and the gel was placed into an electrophoresis container containing 1x TAE as running buffer. The slots were loaded with DNA samples to which 16% of 6x DNA loading dye was added. An appropriate DNA molecular weight marker was run in parallel in order to evaluate molecular weights of the DNA fragments. The voltage applied for the separation was 5V per cm space between the two electrodes. The gels were run for 20-30 minutes and the separated DNA bands were visualized and pictures were taken under UV irradiation (300 nm).

10.2.2.5 Quantification of DNA, RNA and proteins

DNA and RNA concentrations were measured on a Nano-drop (ND-1000 Spectrometer).

Protein concentrations were measured with two different assays dependent on the protein solution: First, the Bio-rad Protein assay and the standard protocol followed. In brief, 50 μl PBS and 50 μl protein sample were mixed and 2-fold serial diluted with PBS over 11 steps of

a 96-well flat bottom plate. The standard solution (2 mg/ml) was serial diluted 2-fold with PBS in duplicates and two wells were filled with 100 μl PBS as blank controls. Color developer was diluted 1:5 in PBS, 200 μl were added to all wells and the plate was measured at 595 nm with an ELISA microplate reader (Sunrise, Tecan).

Second, the Lowry assay (Bio-Rad DC Protein Assay), a colorimetric assay was used for protein concentration in detergent solution. In brief, 20 μl of samples and standards (0.2-1 mg/ml) were mixed with 100 μl of reagent A' (20 μl of reagent S to each ml of reagent A). 800 μl of reagent B was added to each sample, mixed and 250 μl of each mix were transferred to a 96-well flat bottom plate. RIPA-buffer was used as blank controls. After 15 minutes at RT absorbance was measured at 650-750 nm with an ELISA microplate reader (Sunrise, Tecan).

10.2.2.6 SDS PAGE

For the separation of proteins, first an appropriate separating gel was prepared using a 0.75 mm spacer:

	10% one gel	two gels	12% one gel	two gels
Acrylamide	3.33 ml	5 ml	4 ml	6 ml
Lower gel buffer	2.5 ml	3.75 ml	2.5 ml	3.75 ml
Distilled water	4.07 ml	6.1 ml	3.4 ml	5.1 ml
SDS (20% w/v)	50 μl	75 μl	50 μl	75 μl
TEMED	5 μl	7.5 μl	5 μl	7.5 μl
APS (10% w/v)	50 μl	75 μl	50 μl	75 μl

Just after adding the TEMED and APS, the acrylamide solution was poured to about 5.3 cm from the bottom. During polymerisation an isopropanol or water overlay was added. After ~ one hour of

polymerisation the overlay was removed and a 3% stacking gel was prepared:

	3% one gel	two gels
Acrylamide	0.5 ml	0.75 ml
Upper gel buffer	1.25 ml	1.875 ml
Distilled water	3.25 ml	4.875 ml
SDS (20% w/v)	25 μl	37.5 μl
TEMED	5 μl	7.5 μl
APS (10% w/v)	25 μl	37.5 μl

Immediately after pouring, the comb was added. Samples were heated for 5 minutes to 95°C in 2x or 4x Laemmli sample buffer. After polymerization, the comb was removed and the wells were washed with 1x Running buffer to remove any unpolymerised acrylamide. The gels were mounted in the electrophoresis apparatus and the inner chamber was filled with 1x Running buffer. The samples were loaded and the outer chamber was also filled with 1x Running buffer. Electrophoresis was performed at 125–140 V until the front reached the bottom of the gel (1-1.5 hours).

10.2.2.7 Western blotting

A PVDF membrane (5.2 x 8.5 cm) was prepared and put into methanol for five seconds. The membrane and four pieces of Whatman paper (6 x 9 cm) were equilibrated in transfer buffer for five minutes. The gel and the membrane were put into the blotting apparatus together with the Whatman paper in the following order: 2 Whatman paper – membrane – gel – 2 Whatman paper. Air bubbles in between were removed by rolling a glass pipette over the stock. The proteins were blotted onto the membrane at constant 125 mA per gel, thus set at 250 mA if transferred two gels. It was run for one and a half hours.

For blocking, the membrane was incubated for two hours at RT in PBS 5% milk containing 0.1% Tween-20 on a shaker. The primary antibody was diluted 1:100-1:10'000 in PBS 5% milk containing 0.1% Tween-20. The membrane was incubated over night at 4°C together with 10 ml of the antibody solution. After washing six times with PBS 5% milk containing 0.1% Tween-20 for five minutes, the second stage antibody, IgG was added at a dilution of 1:1000-1:20'000 in 10 ml PBS 5% milk containing 0.1% Tween-20. The membrane was incubated together with this solution at RT for two hours, washed three times with PBS 5% milk containing 0.1% Tween-20 and another three times with PBS for five minutes. The separated protein bands were visualized with 1 ml ECF reagent and pictures were taken on a Pharos (Pharos FX Plus Molecular Imager, Bio Rad)

10.2.3 Experiments with mice

10.2.3.1 Blood collection

Mice were anesthetized with isofluran and blood samples were taken retro-orbitally with a heparin coated capillary. In an eppendorf tube 100 μl blood was collected in 0.05 M EDTA to inhibit blood coagulation and stored at -80°C. Blood was collected at various time points as indicated.

10.2.3.2 Injections

LCMV-Arm intraperitoneal injections (i.p.)

Unless described otherwise, mice were injected with a total of 1 x 10^4 particles of LCMV-Arm (*i.p.*). Mice were held in one hand and 100 μl virus were injected with a syringe intra peritoneal.

Anti-JAM-C antibody intraperitoneal injections (i.p.)

Mice were injected with 100 µg anti-JAM-C antibody (*i.p.*). Mice were held in one hand and 100 µl antibody was injected with a syringe intra peritoneal one day before and then at days 1, 2, 5, 8, 11, and 14 after LCMV-infection in RIP-LCMV-GP mice and one day before and then at days 1, 3, 7, 11, 14, 18, 22, 26, 29, and 34 post LCMV-infection in RIP-LCMV-NP mice.

TCR-transgenic P14 splenocytes intravenous injection (i.v.)

Mice were injected with a total of 1.5×10^7 DsRed$^+$ TCR-transgenic P14 splenocytes (*i.v.*). Mice were anesthetized with isofluran and 200 µl of DsRed$^+$ TCR-transgenic P14 splenocytes were injected with a syringe retro-orbitally.

GP$_{33}$ peptide, CpG and Poly(I:C) intraperitoneal injections (i.p.)

One and 3 days after adoptive transfer of DsRed$^+$ P14 splenocytes the mice were stimulated in vivo with 2 mg GP$_{33}$ peptide in 900 µl H$_2$O with 50 µg CpG and on day six 500 µg of Poly(I:C) was administered (*i.p.*).

10.2.3.3 Glucose challenge

Mice were fasted for 12-16 hours and than received a single intra peritoneal injection of 1.5 mg/g body weight glucose. Blood glucose was measured immediately before injection and then at 10, 20, 30, 40, 60, 120, 240, and 450 minutes after infection.

10.2.3.4 Liver and lung perfusions

Liver

Mice were anesthetized with isofluran and killed by cervical dislocation. After the abdomen had been opened the hepatic vein and hepatic artery were cut and the liver was perfused with ~ 5 ml PBS through

the hepatic portal vein. The liver was removed and appropriately stored for further processing.

Lung

Mice were anesthetized with isofluran. After the abdomen had been opened the hepatic vein and hepatic artery were cut and the lung was perfused by injecting ~ 5 ml PBS through the right heart chamber. The lung was removed and appropriately stored for further processing.

10.2.3.5 Surgical preparation of the pancreas for real-time imaging by two-photon microscopy

Before surgery, Mice were anesthetized with an appropriate dose of ketamin/xylazine. After cleaning and shaving the belly area an incision was made in the belly region to expose the spleen and the pancreatic tail region. After cauterization of the splenic arteries, the spleen was removed from the pancreas and the exposed pancreatic tail was fixed with glue on a custom-designed imaging stage and immersed in saline buffer. To maintain the body temperature of the mice during the whole image period the imaging stage was surrounded with a saline buffer filled basin that was continuously heated to 37°C. At the end of the movies an intravenous injection of 70 kDA, Texas Red-labeled dextran was used to visualize vascular networks.

10.2.3.6 Alzet mini-osmotic pump implantation

The pumps were filled with a CXCR3 antagonist (NIBR2130) and subcutaneous implanted in mice. After two weeks of implantation the pumps were changed for two weeks more.

The pumps were filled under sterile conditions. The empty pumps together with the flow moderator were weighed for the calculation of the solution loaded. The pumps were carefully filled with a 1 ml syringe

attached a blunt-tipped 27 gauge filling tube. The subcutaneous implantation of the pumps followed the insertion of the flow moderation into the body of the pump. After anesthetizing the mice the skin at the back slightly posterior to the capsulae was shaved, washed and a suitable incision was made. The subcutaneous tissue was spread to a pocket, the pump was inserted and the wound was closed with sutures. After implantation 1 ml 0.9% NaCl solution preheated to 37°C was injected next to the pump to provide movement of the pump. Either the following one to two days or every second day the NaCl injection was repeated.

11 References

1. Kennneth Murphy, P.T., Mark Walport. 2008. *Janeway's Immuno Biology*.
2. Pietropaolo, M., Surhigh, J.M., Nelson, P.W., and Eisenbarth, G.S. 2008. Primer: immunity and autoimmunity. *Diabetes* 57:2872-2882.
3. Podojil, J.R., and Miller, S.D. 2009. Molecular mechanisms of T-cell receptor and costimulatory molecule ligation/blockade in autoimmune disease therapy. *Immunol Rev* 229:337-355.
4. Zhou, L., Chong, M.M., and Littman, D.R. 2009. Plasticity of CD4+ T cell lineage differentiation. *Immunity* 30:646-655.
5. Zinkernagel, R.M., and Doherty, P.C. 1974. Restriction of in vitro T cell-mediated cytotoxicity in lymphocytic choriomeningitis within a syngeneic or semiallogeneic system. *Nature* 248:701-702.
6. Gavanescu, I., Kessler, B., Ploegh, H., Benoist, C., and Mathis, D. 2007. Loss of Aire-dependent thymic expression of a peripheral tissue antigen renders it a target of autoimmunity. *Proc Natl Acad Sci U S A* 104:4583-4587.
7. Ueda, H., Howson, J.M., Esposito, L., Heward, J., Snook, H., Chamberlain, G., Rainbow, D.B., Hunter, K.M., Smith, A.N., Di Genova, G., et al. 2003. Association of the T-cell regulatory gene CTLA4 with susceptibility to autoimmune disease. *Nature* 423:506-511.
8. Christen, U., and von Herrath, M.G. 2005. Infections and autoimmunity--good or bad? *J Immunol* 174:7481-7486.
9. von Herrath, M.G., Fujinami, R.S., and Whitton, J.L. 2003. Microorganisms and autoimmunity: making the barren field fertile? *Nat Rev Microbiol* 1:151-157.
10. Christen, U., and von Herrath, M.G. 2004. Initiation of autoimmunity. *Curr Opin Immunol* 16:759-767.
11. Christen, U., and von Herrath, M.G. 2004. Induction, acceleration or prevention of autoimmunity by molecular mimicry. *Mol Immunol* 40:1113-1120.
12. Kirvan, C.A., Swedo, S.E., Heuser, J.S., and Cunningham, M.W. 2003. Mimicry and autoantibody-mediated neuronal cell signaling in Sydenham chorea. *Nat Med* 9:914-920.
13. Ang, C.W., Jacobs, B.C., and Laman, J.D. 2004. The Guillain-Barre syndrome: a true case of molecular mimicry. *Trends Immunol* 25:61-66.

14. Christen, U., Edelmann, K.H., McGavern, D.B., Wolfe, T., Coon, B., Teague, M.K., Miller, S.D., Oldstone, M.B., and von Herrath, M.G. 2004. A viral epitope that mimics a self antigen can accelerate but not initiate autoimmune diabetes. *J Clin Invest* 114:1290-1298.

15. Fujinami, R.S., von Herrath, M.G., Christen, U., and Whitton, J.L. 2006. Molecular mimicry, bystander activation, or viral persistence: infections and autoimmune disease. *Clin Microbiol Rev* 19:80-94.

16. Fowler, M.J. 2007. Diabetes: Magnitude and Mechanisms. *Clinical Diabetes* 25.

17. Martinic, M.M., and von Herrath, M.G. 2008. Real-time imaging of the pancreas during development of diabetes. *Immunol Rev* 221:200-213.

18. Langerhans, P. 1937. Contributions to the microscopic anatomy of the pancreas. *Bull Inst History Med* 5:1-39.

19. Weir, G.C., and Bonner-Weir, S. 1990. Islets of Langerhans: the puzzle of intraislet interactions and their relevance to diabetes. *J Clin Invest* 85:983-987.

20. Gillespie, K.M. 2006. Type 1 diabetes: pathogenesis and prevention. *CMAJ* 175:165-170.

21. Zipris, D. 2009. Epidemiology of type 1 diabetes and what animal models teach us about the role of viruses in disease mechanisms. *Clin Immunol* 131:11-23.

22. Greenbaum, C.J., Schatz, D.A., Cuthbertson, D., Zeidler, A., Eisenbarth, G.S., and Krischer, J.P. 2000. Islet cell antibody-positive relatives with human leukocyte antigen DQA1*0102, DQB1*0602: identification by the Diabetes Prevention Trial-type 1. *J Clin Endocrinol Metab* 85:1255-1260.

23. Atkinson, M.A., and Eisenbarth, G.S. 2001. Type 1 diabetes: new perspectives on disease pathogenesis and treatment. *Lancet* 358:221-229.

24. Richer, M.J., and Horwitz, M.S. 2009. Preventing viral-induced type 1 diabetes. *Ann N Y Acad Sci* 1173:487-492.

25. Fronczak, C.M., Baron, A.E., Chase, H.P., Ross, C., Brady, H.L., Hoffman, M., Eisenbarth, G.S., Rewers, M., and Norris, J.M. 2003. In utero dietary exposures and risk of islet autoimmunity in children. *Diabetes Care* 26:3237-3242.

26. Baekkeskov, S., Aanstoot, H.J., Christgau, S., Reetz, A., Solimena, M., Cascalho, M., Folli, F., Richter-Olesen, H., and De Camilli, P. 1990. Identification of the 64K autoantigen in insulin-dependent diabetes as the GABA-synthesizing enzyme glutamic acid decarboxylase. *Nature* 347:151-156.

27. Palmer, J.P., Asplin, C.M., Clemons, P., Lyen, K., Tatpati, O., Raghu, P.K., and Paquette, T.L. 1983. Insulin antibodies in insulin-dependent diabetics before insulin treatment. *Science* 222:1337-1339.

28. Bonifacio, E., Lampasona, V., Genovese, S., Ferrari, M., and Bosi, E. 1995. Identification of protein tyrosine phosphatase-like IA2 (islet cell antigen 512) as the insulin-dependent diabetes-related 37/40K autoantigen and a target of islet-cell antibodies. *J Immunol* 155:5419-5426.

29. Gianani, R., and Eisenbarth, G.S. 2005. The stages of type 1A diabetes: 2005. *Immunol Rev* 204:232-249.

30. Keymeulen, B., Vandemeulebroucke, E., Ziegler, A.G., Mathieu, C., Kaufman, L., Hale, G., Gorus, F., Goldman, M., Walter, M., Candon, S., et al. 2005. Insulin needs after CD3-antibody therapy in new-onset type 1 diabetes. *N Engl J Med* 352:2598-2608.

31. Herold, K.C., Hagopian, W., Auger, J.A., Poumian-Ruiz, E., Taylor, L., Donaldson, D., Gitelman, S.E., Harlan, D.M., Xu, D., Zivin, R.A., et al. 2002. Anti-CD3 monoclonal antibody in new-onset type 1 diabetes mellitus. *N Engl J Med* 346:1692-1698.

32. Staeva-Vieira, T., Peakman, M., and von Herrath, M. 2007. Translational mini-review series on type 1 diabetes: Immune-based therapeutic approaches for type 1 diabetes. *Clin Exp Immunol* 148:17-31.

33. Bresson, D., Togher, L., Rodrigo, E., Chen, Y., Bluestone, J.A., Herold, K.C., and von Herrath, M. 2006. Anti-CD3 and nasal proinsulin combination therapy enhances remission from recent-onset autoimmune diabetes by inducing Tregs. *J Clin Invest* 116:1371-1381.

34. Shapiro, A.M., Lakey, J.R., Ryan, E.A., Korbutt, G.S., Toth, E., Warnock, G.L., Kneteman, N.M., and Rajotte, R.V. 2000. Islet transplantation in seven patients with type 1 diabetes mellitus using a glucocorticoid-free immunosuppressive regimen. *N Engl J Med* 343:230-238.

35. Onaca, N., Naziruddin, B., Matsumoto, S., Noguchi, H., Klintmalm, G.B., and Levy, M.F. 2007. Pancreatic islet cell transplantation: update and new developments. *Nutr Clin Pract* 22:485-493.

36. Makino, S., Kunimoto, K., Muraoka, Y., Mizushima, Y., Katagiri, K., and Tochino, Y. 1980. Breeding of a non-obese, diabetic strain of mice. *Jikken Dobutsu* 29:1-13.

37. Oldstone, M.B., Nerenberg, M., Southern, P., Price, J., and Lewicki, H. 1991. Virus infection triggers insulin-dependent diabetes mellitus in a transgenic model: role of anti-self (virus) immune response. *Cell* 65:319-331.

38. Ohashi, P.S., Oehen, S., Buerki, K., Pircher, H., Ohashi, C.T., Odermatt, B., Malissen, B., Zinkernagel, R.M., and Hengartner, H. 1991. Ablation of "tolerance" and induction of diabetes by virus infection in viral antigen transgenic mice. *Cell* 65:305-317.

39. Harnish, D.G., Dimock, K., Bishop, D.H., and Rawls, W.E. 1983. Gene mapping in Pichinde virus: assignment of viral polypeptides to genomic L and S RNAs. *J Virol* 46:638-641.

40. Cornu, T.I., and de la Torre, J.C. 2001. RING finger Z protein of lymphocytic choriomeningitis virus (LCMV) inhibits transcription and RNA replication of an LCMV S-segment minigenome. *J Virol* 75:9415-9426.

41. Salvato, M.S., and Shimomaye, E.M. 1989. The completed sequence of lymphocytic choriomeningitis virus reveals a unique RNA structure and a gene for a zinc finger protein. *Virology* 173:1-10.

42. Oxenius, A., Bachmann, M.F., Zinkernagel, R.M., and Hengartner, H. 1998. Virus-specific MHC-class II-restricted TCR-transgenic mice: effects on humoral and cellular immune responses after viral infection. *Eur J Immunol* 28:390-400.

43. Kotturi, M.F., Peters, B., Buendia-Laysa, F., Jr., Sidney, J., Oseroff, C., Botten, J., Grey, H., Buchmeier, M.J., and Sette, A. 2007. The CD8+ T-cell response to lymphocytic choriomeningitis virus involves the L antigen: uncovering new tricks for an old virus. *J Virol* 81:4928-4940.

44. Christen, U., and von Herrath, M.G. 2004. Manipulating the type 1 vs type 2 balance in type 1 diabetes. *Immunol Res* 30:309-325.

45. Christen, U., and von Herrath, M.G. 2003. Cytokines and chemokines in virus-induced autoimmunity. *Adv Exp Med Biol* 520:203-220.

46. von Herrath, M.G., Dockter, J., and Oldstone, M.B. 1994. How virus induces a rapid or slow onset insulin-dependent diabetes mellitus in a transgenic model. *Immunity* 1:231-242.

47. McGavern, D.B., Christen, U., and Oldstone, M.B. 2002. Molecular anatomy of antigen-specific CD8(+) T cell engagement and synapse formation in vivo. *Nat Immunol* 3:918-925.

48. Zlotnik, A., and Yoshie, O. 2000. Chemokines: a new classification system and their role in immunity. *Immunity* 12:121-127.

49. Baggiolini, M. 1998. Chemokines and leukocyte traffic. *Nature* 392:565-568.

50. Christen, U., and Von Herrath, M.G. 2004. IP-10 and type 1 diabetes: a question of time and location. *Autoimmunity* 37:273-282.

51. Honkanen, J., Nieminen, J.K., Gao, R., Luopajarvi, K., Salo, H.M., Ilonen, J., Knip, M., Otonkoski, T., and Vaarala, O. IL-17 Immunity in Human Type 1 Diabetes. *J Immunol.*

52. Seewaldt, S., Thomas, H.E., Ejrnaes, M., Christen, U., Wolfe, T., Rodrigo, E., Coon, B., Michelsen, B., Kay, T.W., and von Herrath, M.G. 2000. Virus-induced autoimmune diabetes: most beta-cells die through inflammatory cytokines and not perforin from autoreactive (anti-viral) cytotoxic T-lymphocytes. *Diabetes* 49:1801-1809.

53. Christen, U., Wolfe, T., Mohrle, U., Hughes, A.C., Rodrigo, E., Green, E.A., Flavell, R.A., and von Herrath, M.G. 2001. A dual role for TNF-alpha in type 1 diabetes: islet-specific expression abrogates the ongoing autoimmune process when induced late but not early during pathogenesis. *J Immunol* 166:7023-7032.

54. Ejrnaes, M., von Herrath, M.G., and Christen, U. 2006. Cure of chronic viral infection and virus-induced type 1 diabetes by neutralizing antibodies. *Clin Dev Immunol* 13:337-347.

55. Liu, M.T., Chen, B.P., Oertel, P., Buchmeier, M.J., Armstrong, D., Hamilton, T.A., and Lane, T.E. 2000. The T cell chemoattractant IFN-inducible protein 10 is essential in host defense against viral-induced neurologic disease. *J Immunol* 165:2327-2330.

56. Christen, U., McGavern, D.B., Luster, A.D., von Herrath, M.G., and Oldstone, M.B. 2003. Among CXCR3 chemokines, IFN-gamma-inducible protein of 10 kDa (CXC chemokine ligand (CXCL) 10) but not monokine induced by IFN-gamma (CXCL9) imprints a pattern for the subsequent development of autoimmune disease. *J Immunol* 171:6838-6845.

57. Rhode, A., Pauza, M.E., Barral, A.M., Rodrigo, E., Oldstone, M.B., von Herrath, M.G., and Christen, U. 2005. Islet-specific expression of CXCL10 causes spontaneous islet infiltration and accelerates diabetes development. *J Immunol* 175:3516-3524.

58. Sallusto, F., Lenig, D., Mackay, C.R., and Lanzavecchia, A. 1998. Flexible programs of chemokine receptor expression on human polarized T helper 1 and 2 lymphocytes. *J Exp Med* 187:875-883.

59. Lacotte, S., Brun, S., Muller, S., and Dumortier, H. 2009. CXCR3, inflammation, and autoimmune diseases. *Ann N Y Acad Sci* 1173:310-317.

60. Frigerio, S., Junt, T., Lu, B., Gerard, C., Zumsteg, U., Hollander, G.A., and Piali, L. 2002. Beta cells are responsible for CXCR3-mediated T-cell infiltration in insulitis. *Nat Med* 8:1414-1420.

61. Zerwes, H.G., Li, J., Kovarik, J., Streiff, M., Hofmann, M., Roth, L., Luyten, M., Pally, C., Loewe, R.P., Wieczorek, G., et al. 2008. The chemokine receptor Cxcr3 is not essential for acute cardiac allograft rejection in mice and rats. *Am J Transplant* 8:1604-1613.

62. Weber, C., Fraemohs, L., and Dejana, E. 2007. The role of junctional adhesion molecules in vascular inflammation. *Nat Rev Immunol* 7:467-477.

63. Petri, B., and Bixel, M.G. 2006. Molecular events during leukocyte diapedesis. *FEBS J* 273:4399-4407.

64. Vestweber, D. 2007. Adhesion and signaling molecules controlling the transmigration of leukocytes through endothelium. *Immunol Rev* 218:178-196.

65. Springer, T.A. 1990. Adhesion receptors of the immune system. *Nature* 346:425-434.

66. Ley, K., Laudanna, C., Cybulsky, M.I., and Nourshargh, S. 2007. Getting to the site of inflammation: the leukocyte adhesion cascade updated. *Nat Rev Immunol* 7:678-689.

67. Elangbam, C.S., Qualls, C.W., Jr., and Dahlgren, R.R. 1997. Cell adhesion molecules--update. *Vet Pathol* 34:61-73.

68. Yang, X.D., Karin, N., Tisch, R., Steinman, L., and McDevitt, H.O. 1993. Inhibition of insulitis and prevention of diabetes in nonobese diabetic mice by blocking L-selectin and very late antigen 4 adhesion receptors. *Proc Natl Acad Sci U S A* 90:10494-10498.

69. Yang, X.D., Michie, S.A., Tisch, R., Karin, N., Steinman, L., and McDevitt, H.O. 1994. A predominant role of integrin alpha 4 in the spontaneous development of autoimmune diabetes in nonobese diabetic mice. *Proc Natl Acad Sci U S A* 91:12604-12608.

70. Vonlaufen, A., Apte, M.V., Imhof, B.A., and Frossard, J.L. 2007. The role of inflammatory and parenchymal cells in acute pancreatitis. *J Pathol* 213:239-248.

71. Baron, J.L., Reich, E.P., Visintin, I., and Janeway, C.A., Jr. 1994. The pathogenesis of adoptive murine autoimmune diabetes requires an interaction between alpha 4-integrins and vascular cell adhesion molecule-1. *J Clin Invest* 93:1700-1708.

72. Garrido-Urbani, S., Bradfield, P.F., Lee, B.P., and Imhof, B.A. 2008. Vascular and epithelial junctions: a barrier for leucocyte migration. *Biochem Soc Trans* 36:203-211.

73. Mandell, K.J., and Parkos, C.A. 2005. The JAM family of proteins. *Adv Drug Deliv Rev* 57:857-867.

74. Bradfield, P.F., Nourshargh, S., Aurrand-Lions, M., and Imhof, B.A. 2007. JAM family and related proteins in leukocyte migration (Vestweber series). *Arterioscler Thromb Vasc Biol* 27:2104-2112.

75. Aurrand-Lions, M., Johnson-Leger, C., Wong, C., Du Pasquier, L., and Imhof, B.A. 2001. Heterogeneity of endothelial junctions is reflected by differential expression and specific subcellular localization of the three JAM family members. *Blood* 98:3699-3707.

76. Zimmerli, C., Lee, B.P., Palmer, G., Gabay, C., Adams, R., Aurrand-Lions, M., and Imhof, B.A. 2009. Adaptive immune response in JAM-C-deficient mice: normal initiation but reduced IgG memory. *J Immunol* 182:4728-4736.

77. Johnson-Leger, C.A., Aurrand-Lions, M., Beltraminelli, N., Fasel, N., and Imhof, B.A. 2002. Junctional adhesion molecule-2 (JAM-2) promotes lymphocyte transendothelial migration. *Blood* 100:2479-2486.

78. Aurrand-Lions, M., Duncan, L., Ballestrem, C., and Imhof, B.A. 2001. JAM-2, a novel immunoglobulin superfamily molecule, expressed by endothelial and lymphatic cells. *J Biol Chem* 276:2733-2741.

79. Lamagna, C., Meda, P., Mandicourt, G., Brown, J., Gilbert, R.J., Jones, E.Y., Kiefer, F., Ruga, P., Imhof, B.A., and Aurrand-Lions, M. 2005. Dual interaction of JAM-C with JAM-B and alpha(M)beta2 integrin: function in junctional complexes and leukocyte adhesion. *Mol Biol Cell* 16:4992-5003.

80. Scheiermann, C., Meda, P., Aurrand-Lions, M., Madani, R., Yiangou, Y., Coffey, P., Salt, T.E., Ducrest-Gay, D., Caille, D., Howell, O., et al. 2007. Expression and function of junctional adhesion molecule-C in myelinated peripheral nerves. *Science* 318:1472-1475.

81. Gliki, G., Ebnet, K., Aurrand-Lions, M., Imhof, B.A., and Adams, R.H. 2004. Spermatid differentiation requires the assembly of a cell polarity complex downstream of junctional adhesion molecule-C. *Nature* 431:320-324.

82. Lamagna, C., Hodivala-Dilke, K.M., Imhof, B.A., and Aurrand-Lions, M. 2005. Antibody against junctional adhesion molecule-C inhibits angiogenesis and tumor growth. *Cancer Res* 65:5703-5710.

83. Orlova, V.V., Economopoulou, M., Lupu, F., Santoso, S., and Chavakis, T. 2006. Junctional adhesion molecule-C regulates

vascular endothelial permeability by modulating VE-cadherin-mediated cell-cell contacts. *J Exp Med* 203:2703-2714.

84. Ludwig, R.J., Zollner, T.M., Santoso, S., Hardt, K., Gille, J., Baatz, H., Johann, P.S., Pfeffer, J., Radeke, H.H., Schon, M.P., et al. 2005. Junctional adhesion molecules (JAM)-B and -C contribute to leukocyte extravasation to the skin and mediate cutaneous inflammation. *J Invest Dermatol* 125:969-976.

85. Rabquer, B.J., Pakozdi, A., Michel, J.E., Gujar, B.S., Haines, G.K., 3rd, Imhof, B.A., and Koch, A.E. 2008. Junctional adhesion molecule C mediates leukocyte adhesion to rheumatoid arthritis synovium. *Arthritis Rheum* 58:3020-3029.

86. Chavakis, T., Keiper, T., Matz-Westphal, R., Hersemeyer, K., Sachs, U.J., Nawroth, P.P., Preissner, K.T., and Santoso, S. 2004. The junctional adhesion molecule-C promotes neutrophil transendothelial migration in vitro and in vivo. *J Biol Chem* 279:55602-55608.

87. Imhof, B.A., Zimmerli, C., Gliki, G., Ducrest-Gay, D., Juillard, P., Hammel, P., Adams, R., and Aurrand-Lions, M. 2007. Pulmonary dysfunction and impaired granulocyte homeostasis result in poor survival of Jam-C-deficient mice. *J Pathol* 212:198-208.

88. Bradfield, P.F., Scheiermann, C., Nourshargh, S., Ody, C., Luscinskas, F.W., Rainger, G.E., Nash, G.B., Miljkovic-Licina, M., Aurrand-Lions, M., and Imhof, B.A. 2007. JAM-C regulates unidirectional monocyte transendothelial migration in inflammation. *Blood* 110:2545-2555.

89. Vonlaufen, A., Aurrand-Lions, M., Pastor, C.M., Lamagna, C., Hadengue, A., Imhof, B.A., and Frossard, J.L. 2006. The role of junctional adhesion molecule C (JAM-C) in acute pancreatitis. *J Pathol* 209:540-548.

90. Skowera, A., Ellis, R.J., Varela-Calvino, R., Arif, S., Huang, G.C., Van-Krinks, C., Zaremba, A., Rackham, C., Allen, J.S., Tree, T.I., et al. 2008. CTLs are targeted to kill beta cells in patients with type 1 diabetes through recognition of a glucose-regulated preproinsulin epitope. *J Clin Invest* 118:3390-3402.

91. Thoma, G., Baenteli, R., Lewis, I., Wagner, T., Oberer, L., Blum, W., Glickman, F., Streiff, M.B., and Zerwes, H.G. 2009. Special ergolines are highly selective, potent antagonists of the chemokine receptor CXCR3: discovery, characterization and preliminary SAR of a promising lead. *Bioorg Med Chem Lett* 19:6185-6188.

92. Aurrand-Lions, M., Lamagna, C., Dangerfield, J.P., Wang, S., Herrera, P., Nourshargh, S., and Imhof, B.A. 2005. Junctional

adhesion molecule-C regulates the early influx of leukocytes into tissues during inflammation. *J Immunol* 174:6406-6415.

93. Mohan, K., and Issekutz, T.B. 2007. Blockade of chemokine receptor CXCR3 inhibits T cell recruitment to inflamed joints and decreases the severity of adjuvant arthritis. *J Immunol* 179:8463-8469.

94. Steinmetz, O.M., Turner, J.E., Paust, H.J., Lindner, M., Peters, A., Heiss, K., Velden, J., Hopfer, H., Fehr, S., Krieger, T., et al. 2009. CXCR3 mediates renal Th1 and Th17 immune response in murine lupus nephritis. *J Immunol* 183:4693-4704.

95. Kohler, R.E., Comerford, I., Townley, S., Haylock-Jacobs, S., Clark-Lewis, I., and McColl, S.R. 2008. Antagonism of the chemokine receptors CXCR3 and CXCR4 reduces the pathology of experimental autoimmune encephalomyelitis. *Brain Pathol* 18:504-516.

96. Appay, V., and Rowland-Jones, S.L. 2001. RANTES: a versatile and controversial chemokine. *Trends Immunol* 22:83-87.

97. Sircar, M., Bradfield, P.F., Aurrand-Lions, M., Fish, R.J., Alcaide, P., Yang, L., Newton, G., Lamont, D., Sehrawat, S., Mayadas, T., et al. 2007. Neutrophil transmigration under shear flow conditions in vitro is junctional adhesion molecule-C independent. *J Immunol* 178:5879-5887.

98. Battegay, M., Cooper, S., Althage, A., Banziger, J., Hengartner, H., and Zinkernagel, R.M. 1991. Quantification of lymphocytic choriomeningitis virus with an immunological focus assay in 24- or 96-well plates. *J Virol Methods* 33:191-198.

99. von Herrath, M.G., Dockter, J., Nerenberg, M., Gairin, J.E., and Oldstone, M.B. 1994. Thymic selection and adaptability of cytotoxic T lymphocyte responses in transgenic mice expressing a viral protein in the thymus. *J Exp Med* 180:1901-1910.

100. Vintersten, K., Monetti, C., Gertsenstein, M., Zhang, P., Laszlo, L., Biechele, S., and Nagy, A. 2004. Mouse in red: red fluorescent protein expression in mouse ES cells, embryos, and adult animals. *Genesis* 40:241-246.

101. Pircher, H., Burki, K., Lang, R., Hengartner, H., and Zinkernagel, R.M. 1989. Tolerance induction in double specific T-cell receptor transgenic mice varies with antigen. *Nature* 342:559-561.

102. Hara, M., Wang, X., Kawamura, T., Bindokas, V.P., Dizon, R.F., Alcoser, S.Y., Magnuson, M.A., and Bell, G.I. 2003. Transgenic mice with green fluorescent protein-labeled pancreatic beta - cells. *Am J Physiol Endocrinol Metab* 284:E177-183.

12 Acknowledgements

13 Curriculum vitae

Personal data

Name	Christen Selina
Date of birth	8. Mai 1979 in Chur, Switzerland

Education

1986 – 1990	Primarschule Frutigen
1991 – 1996	Sekundarschule Thun
1996 – 2000	Freies Gymnasium Bern/Typus Mathematik
	Certificate: Maturität

University

2001 – 2003	Basic studies of Biology at the University in Bern
	1. Vordiplom
2003 – 2004	Advanced study period in cell biology at the University in Bern with focus on cell biology and medical microbiology
	2. Vordiplom
2004 – 2005	MSc Thesis by Prof. Dr. Norbert Müller at the Institute for Parasitology at the Veterinary Medicine and Medicine Faculty of the University Bern (IPVM)
	Certificate for master of science in biology with major in cell biology

Doctoral degree	
2006 – 2010	Klinikum der J.W. Goethe - Universität Frankfurt/Main, Institut für allgemeine Pharmakologie und Toxikologie, supervised by PD Dr. phil. nat. Dr. med. habil. U. Christen

Internship	
2001	Social work experience for six months in an asylum for poor and malnourished children in Guayaquil, Ecuador
10.-12.2009	Collaboration work with Dr. M.G. von Herrath and Dr. K. Coppieters at the La Jolla Institute for Allergy and Immunology, La Jolla, California, USA

Academic teacher	
	Prof. Dr. N. Müller, Dr. N. von Allmen, PD Dr. U. Christen, Dr. E. Hintermann, Dr. M.G. von Herrath, Dr. K. Coppieters, Prof. Dr. H. H. Radeke, Prof. Dr. Th. Dingermann, Prof. Dr. J. Pfeilschifter

14 Publications

Publications

Selina Christen, Martin Holdener, Monika Bayer, Josef Pfeilschifter, Edith Hintermann, Hans-Guenther Zerwes and Urs Christen (2010). Small molecule CXCR3 antagonist NIBR2130 blocks type 1 diabetes in a virus-induced mouse model. (*manuscript submitted*)

Selina Christen, Kerstin Rose, Martin Holdener, Monika Bayer, Josef Pfeilschifter, Edith Hintermann, Michel Aurand-Lions, Beat Imhof and Urs Christen (2010). Limited effect of junctional adhesion molecule C on islet infiltration and incidence of virus-induced diabetes. (*manuscript in preparation*)

Selina Christen, Monika Bayer, Josef Pfeilschifter, Edith Hintermann, and Urs Christen (2010). Islet-specific overexpression of CXCL10 causes specific beta-cell killing and type 1 diabetes in mice treated with a sub-diabetic dose of streptozotocin. (*manuscript in preparation*)

Von Allmen N, Christen S, Forster U, Gottstein B, Welle M, Müller N (2006). Acute trichinellosis increases susceptibility to *Giardia lamblia* infection in the mouse model. *Parasitology* 1-11.

Presentation/Poster

Christen S., Hintermann E., Holdener M., Bayer M., Christen U. JAM-C and its influence on the pathogenesis of type 1 diabetes.
2009 poster presentation at the 10th International Congress of the Immunology of Diabetes Society (IDS), Malmö, Sweden.

Christen S., Hintermann E., Holdener M., Bayer M., Christen U. JAM-C and its influence on the pathogenesis of type 1 diabetes.
2007 poster presentation at the Annual Meeting of the Swiss Society of Pharmacology and Toxicology, Bern, Switzerland.

Christen S., Hintermann E., Holdener M., Bayer M., Christen U. JAM-C and its influence on the pathogenesis of type 1 diabetes.
2007 poster presentation at the 37th Annual Meeting of the German Society for Immunology, Heidelberg, Germany.

Christen, S., Hintermann, E., Bayer, M. and *Christen, U. *. JAM-C and its influence on the pathogenesis of type 1 diabetes.
2007 poster presentation at the 48. Frühjahrstagung der Deutschen Gesellschaft für experimentelle und klinische Pharmakologie und Toxikologie (DGPT) – Mainz, Germany/ [Abstract published in */Naunyn-Schmiedeberg's Archives of Pharmacology/* 375-Suppl 1: Abstract #236]

Christen S. Investigation of the influence of the intestinal inflammatory processes on *Giardia lamblia* infections in the murine host.
2005 MSc Thesis, University of Bern, Monograph.